Sun-synchronous Spacecraft Compliance with International Space Debris Guidelines

M.S. Schild

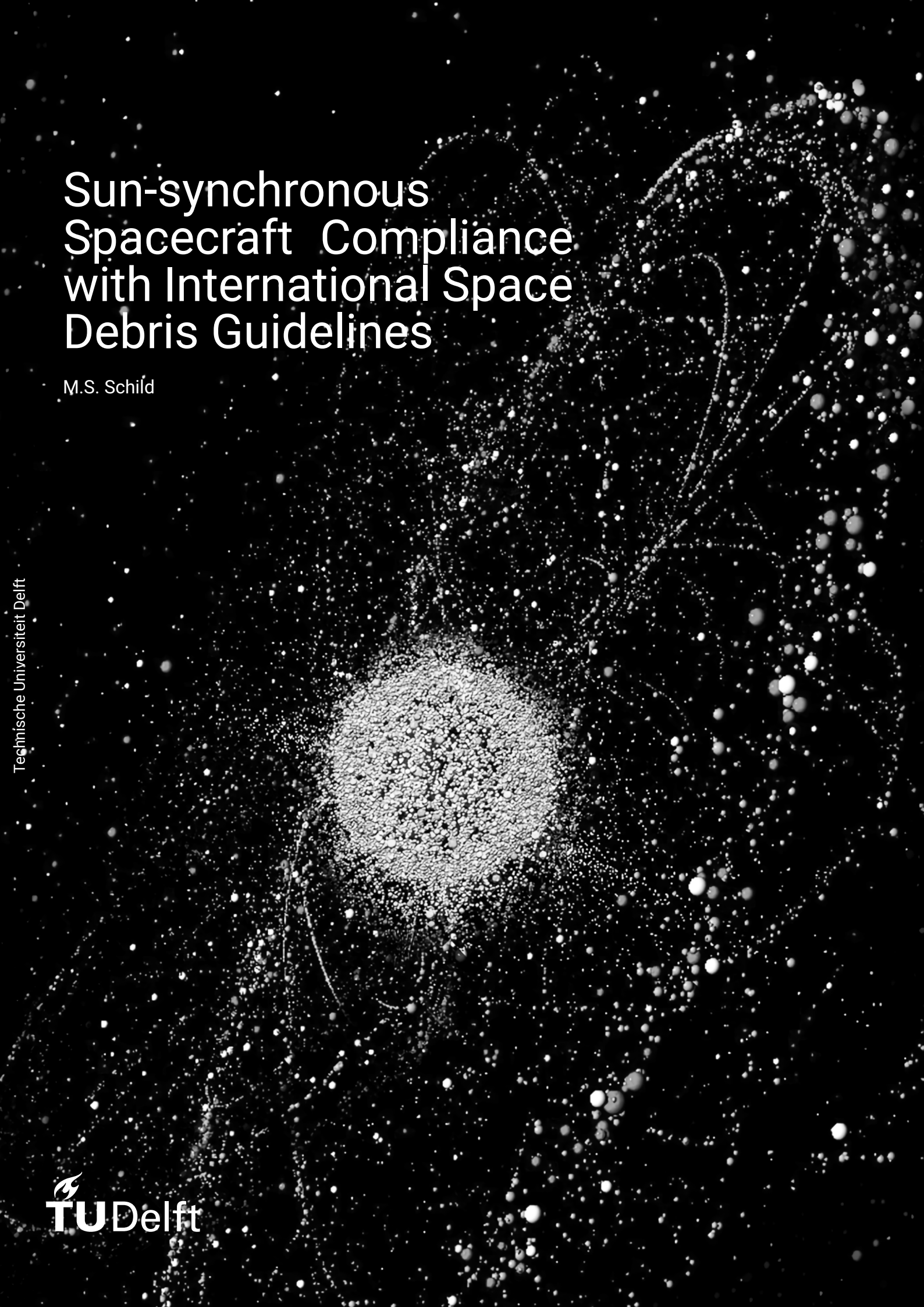

Technische Universiteit Delft

TU Delft

Cover image obtained from Studio Roosegaarde

Sun-synchronous Spacecraft Compliance with International Space Debris Guidelines

by

Maarten Sybe Schild

to obtain the degree of Master of Science
at Delft University of Technology,
to be defended publicly on Thursday March 11, 2021 at 14:00.

Student number:	4158474	
Project duration:	June 3, 2020 – February 21, 2021	
Thesis committee:	Ir. R. Noomen,	TU Delft, supervisor
	Dr. ir. E. Mooij,	TU Delft, chair
	Dr. ir. L.E. Meester,	TU Delft, examiner

An electronic version of this thesis is available at `http://repository.tudelft.nl/`.

TU Delft

Abstract

Due to ever increasing accessibility, recent years have seen a fast growing number of launches to space, especially to Sun-synchronous orbit. The spent rocket parts, payload fairings and eventually non-functioning payloads of these launches remain in orbit. It is well-established that this accumulation of space debris over time is quickly making this the most severe threat to future spaceflight operations. To address and mitigate this problem a set of internationally agreed guidelines were established including a maximum of 25-year remaining orbital lifetime in this region after end-of-life. This study evaluates if Sun-synchronous satellite operators adhere to this guideline.

To determine this compliance, the operational status of the satellites with orbital control capabilities is established using a maneuver detection algorithm. For satellites without the capability to maneuver a model is created based on mass and design lifetime to determine the duration of the operational phase. Using a semi-analytic propagation method the remaining orbital lifetimes is determined.

The results show an overall compliance of 59% with an increasing trend starting around 2014, before which compliance was 20 to 40 %, to approximately 95% in 2017 and 2018. A large difference is observed for different mass categories, where satellites with a mass lower than 10 kg have a compliance of 86.4% compared to approximately 35% for heavier satellites. Analysis shows that this is mainly due to the lower orbits the former satellites were launched in. No large differences are observed between satellites with or without orbital control capabilities.

These results reveal that compliance with the guidelines has been poor in the past but is increasing in recent years. This is mostly a result of operators choosing an orbit with a low altitude to have sufficient natural decay, and less of operators choosing to perform altitude lowering maneuvers at the end of operational phase to achieve compliance.

Preface

Looking up to the night sky one can only wonder in awe. The incomprehensible scale of space, visualised by the stark contrast of the empty darkness and the countless number of small stars, commands humbleness of every observer. With the launch of the first satellites, followed by the first manned spaceflights and ultimately the moon landings, mankind has entered a completely new chapter in its history. A chapter transcending national borders and communities, and one of international cooperation aimed at discovering our place in the universe. This is currently best exemplified by the almost two-decade long multi-lateral operation of the International Space Station.

This rapid innovation has come at a cost however: the increasing number of objects in space near Earth are a major cause of concern for the future of spaceflight. To guarantee the safe launch and operation of satellites and manned missions in the decades to come the international community will have to act swiftly and decisively to take the required actions. This research topic was chosen to support those efforts and provide insight in the current mitigation strategies and their effectiveness.

As of writing, the world is currently facing its greatest crisis I have witnessed, with a pandemic wreaking havoc indiscriminately in many countries across the world. Especially in these times international cooperation and solidarity will prove its merit. It is precisely these values that we will need if we want to prosper in the face of the challenges to come.

I would like to thank my parents and brothers for their encouragements and support. I am grateful for the welcoming distractions and interesting discussions with my roommates, friends and fellow students. I would also like to thank the staff of the faculty of Aerospace Engineering at Delft University of Technology for their continued assistance, education and inspiration. Finally, a special thanks to my supervisor Ir. R. Noomen for his input and guidance during this study.

M.S. Schild
Delft, February 2021

Contents

1 Introduction **1**

2 Background Information **3**
2.1 Space Debris . . . 3
2.1.1 Initial Work . . . 3
2.1.2 Modern Regulations . . . 4
2.1.3 25 Year Lifetime Rule . . . 6
2.2 Inventory of Satellites . . . 7
2.2.1 General Overview . . . 7
2.2.2 Low Earth Orbit . . . 10
2.2.3 Sun-synchronous Orbit . . . 12

3 Orbital Mechanics **15**
3.1 Reference Frames . . . 15
3.1.1 Earth-centered Earth-fixed . . . 15
3.1.2 Earth-centered Inertial . . . 16
3.1.3 Normal Tangent Cross-track . . . 17
3.2 Orbital Elements . . . 17
3.2.1 Keplerian elements . . . 17
3.2.2 Two-Line Elements . . . 18
3.2.3 Alternative Representations . . . 18
3.3 Orbital Perturbations . . . 18
3.3.1 Aerodynamic Drag . . . 19
3.3.2 Gravity Field . . . 20
3.3.3 Solar Radiation Pressure . . . 21
3.3.4 Third-Body Gravity . . . 21

4 Methodology **23**
4.1 Heritage . . . 23
4.1.1 Compliance of Italian LEO satellites . . . 23
4.1.2 CNES LEO Compliance Study . . . 24
4.1.3 ESA Studies . . . 25
4.2 Research Questions . . . 25
4.3 Method . . . 26
4.3.1 Operational Status . . . 26
4.3.2 Orbital Lifetime . . . 26
4.3.3 Algorithm . . . 27
4.4 Development Cases . . . 28
4.5 Data sources . . . 30
4.5.1 Two Line Element Data . . . 30
4.5.2 Maneuver Data . . . 31
4.5.3 Satellite Property Data . . . 31

5 Maneuver Detection **33**
5.1 Linear Slope Correction . . . 34
5.1.1 Theil-Sen-Siegel Estimator . . . 34
5.1.2 Corrected Series . . . 35
5.2 Threshold Generation . . . 36
5.2.1 Interquartile Range . . . 36
5.2.2 Harmonic Analysis . . . 37

5.3 Event Detection . . . 39
5.4 Performance with parameter tuning . . . 40
5.5 Validation . . . 41
5.5.1 Test Cases . . . 41

6 Operational Status Determination **43**
6.1 Maneuver Based . . . 43
6.2 Non Maneuver Based . . . 45
6.2.1 Mass based model . . . 46
6.3 Combined Population. . . . 47

7 Orbital Lifetime Estimation **49**
7.1 Estimation Methods . . . 49
7.1.1 Analytical . . . 49
7.1.2 Numerical Integration . . . 50
7.1.3 Semi-Analytic . . . 51
7.1.4 Selection . . . 51
7.2 STELA Implementation . . . 52
7.2.1 Semi-analytic extrapolation method . . . 52
7.2.2 Model Settings . . . 52
7.2.3 Inputs . . . 54
7.2.4 Validation . . . 54
7.3 Orbital lifetime . . . 56

8 Compliance **59**
8.1 Results . . . 59
8.2 Sensitivity Study . . . 64
8.3 Comparison. . . . 67
8.4 Discussion . . . 68

9 Conclusions and Recommendations **71**
9.1 Conclusions. . . . 71
9.2 Recommendations . . . 73

Bibliography **75**

Nomenclature

The next list describes the abbreviations, constants and symbols that will later be used within the body of the document.

Abbreviations

AOP	After Operational Phase
API	Application Programming Interface
ASI	Italian Space Agency
BC	Ballistic Coefficient
BNSC	British National Space Centre
CD	Compliant With Direct Re-entry
CNES	Centre National d'Etudes Spatiales (French for National Centre for Space Studies)
CNSA	China National Space Administration
COPUOS	Committee on the Peaceful Uses of Outer Space
COSPAR	Committee on Space Research
CSA	Canadian Space Agency
CWFB	Compliant With Attempt False Before
CWO	Compliant Without Attempt
CWTB	Compliant With Attempt True Before
DISCOS	Database and Information System Characterising Objects in Space
DLR	German Aerospace Center
DORIS	Doppler Orbitography and Radiopositioning Integrated by Satellite
DSST	Draper Semi-analytic Satellite Theory
ECEF	Earth-centered Earth-fixed
ECI	Earth-centered Inertial
ECSS	European Cooperation for Space Standardisation
ENU	East North Up
EOL	End-of-Life
EOP	End of Operational Phase
ESA	European Space Agency
GEO	Geostationary Orbit
IADC	Inter-Agency Space Debris Coordination Committee
IDS	International DORIS Service

ILRS	International Laser Ranging Service
IQR	Interquartile Range
ISO	International Organization for Standardization
ISRO	Indian Space Research Organisation
JAXA	Japan Aerospace Exploration Agency
KARI	Korea Aerospace Research Institute
LEO	Low Earth Orbit
MEO	Medium Earth Orbit
NASA	National Aeronautics and Space Administration
NASDA	National Space Development Agency of Japan
NCWFB	Not Compliant With Attempt False Before
NCWO	Not Compliant Without Attempt
NCWTB	Not Compliant With Attempt True Before
NED	North East Down
RAAN	Right Ascension of Ascending Node
ROSCOSMOS	Russian Federal Space Agency
SATCAT	Satellite Catalog
SDP	Simplified Deep Space Perturbations
SGP	Simplified General Perturbations
SRP	Solar Radiation Pressure
SSAU	State Space Agency of Ukraine
SSO	Sun-synchronous Orbit
SST	Semi-analytic Satellite Theory
STELA	Semi-analytic Tool for End of Life Analysis
TCC	Two-Line Element Consistency Check
TDB	Barycentric Dynamical Time
TLE	Two-Line Element
TTSA	Two-Line Element Time Series Analysis
TU Delft	Delft University of Technology
TUDAT	TU Delft Astrodynamics Toolbox
UKSA	United Kingdom Space Agency
UN	United Nations
USSPACECOM	United States Space Command
USSTRATCOM	United States Strategic Command

Constants

c	Speed of light [62]	299 792 458 m/s
R	Mean equatorial radius [62]	6.3781×10^6 m

Symbols

Λ	Geographic Longitude	rad
μ	Gravitational parameter	m^3/s^2
Ω	Longitude of the ascending node	rad
ω	Argument of periapsis	rad
ϕ	Geocentric latitude	rad
ρ	Atmospheric density	kg/m^3
θ	True anomaly	rad
A	Area	m^2
a	Semi-major axis	m
C_D	Drag coefficient	-
Cr	Solar radiation pressure coefficient	-
e	Eccentricity	-
H	Scale height	m
h	Altitude	m
h_a	Apogee height	m
h_p	Perigee height	m
i	Inclination	rad
L	Lifetime	s
M_0	Mean anomaly	rad
n	Mean motion	rad/s
r	Distance	m
S	Cross-Sectional Area	m^2
W	Energy flux	W/m^2
Z_a	Apogee radius	m

1

Introduction

From the very first endeavours of space flight to the most recent modern spacecraft launches, all have come with a negative consequence. Their spent rocket parts and eventually non-functioning payloads remain in orbit around Earth. Due to their low numbers, this space debris was not considered to be a problem at first but its accumulation over time and the ever increasing accessibility to space is quickly making this the most severe threat to future spaceflight operations. Being uncontrollable, these space debris parts are risking collisions with operational satellites and other space debris. Such a collision would then result in even more debris objects thereby increasing the likelihood of even more collisions, a cascading effect known as the Kessler syndrome which could lead to entire orbits rendered completely unusable. To address and mitigate this problem a set of internationally agreed regulations and guidelines were set and signed where satellites have to limit their time in certain regions in space around Earth after end-of-life.

The purpose of this study is to investigate the state of the space environment in Sun-synchronous orbit and to develop and implement a method to be able to answer the research question:

Do satellite operators adhere to the international guidelines regarding the 25-year time limit after end-of-life for satellites in Sun-synchronous Orbit?

The study will be done by first looking at the exact space debris guidelines and regulations in Chapter 2, together with an overview of the satellites orbiting Earth. Following this the relevant orbital mechanics will briefly be discussed in Chapter 3. Thereafter existing compliance studies will be researched and their results and methods will be described in Chapter 4, together with the chosen approach and data sources. In order to determine the compliance of a satellite, the operational status has to be determined. To do so use is made of a maneuver detection algorithm as discussed in Chapter 5. This is combined with a design lifetime study to be able to determine the operational status for both satellites with and without orbital control capabilities in Chapter 6. The second major part in compliance determination is the orbital lifetime estimation which can be found in Chapter 7. These parts were combined to determine the compliance in Chapter 8. Finally, conclusions regarding the aforementioned aspects of the study and their outcomes, as well as recommendations on improvements and future studies will be given in Chapter 9.

2

Background Information

With increasing accessibility and affordability to get satellites into space, orbits around the Earth are becoming more and more densely populated. This growth, not only of functioning and non-functioning satellites, but also spent rocket stages, and particles resulting from collisions and explosions, has raised concerns regarding the future use of these orbits. This chapter will give a broad overview of this space debris problem.

This is done by first giving a brief history of the research done, and the regulations that aim to mitigate the problem in Section 2.1. The current state of the space environment will be analysed in Section 2.2. In this last section it will also be shown why the Sun-synchronous regime was chosen as the focus of this study.

2.1. Space Debris

Space debris is the term used to describe non-functioning man-made material in orbit around Earth. It should be noted that sometimes micro meteorites are also considered to be space debris but in this study only man-made material is considered. The size of this material ranges from very large spent rocket stages to very small metal flakes or paint chips. Due to their very large relative velocity, even these small particles pose a significant risk to other spacecraft or manned missions.

As early as 1974 concerns were raised regarding the impact of this debris on spaceflight in the future [8]. Since then a large amount of research was done on this subject and recommendations and guidelines were established by multiple bodies, agencies and research groups to remedy this problem. This section aims to provide a brief history and overview of this work, it combines information from the space agencies itself as well as the timeline as given by Bonnal [6] [7] and Johnson [30]. For a more in-depth history the reader is referred to the works of these authors respectively. This timeline was established to later on be able to compare possible trend changes in the generation of space debris or guideline compliance with the dates of these events.

2.1.1. Initial Work

As stated, the earliest research done on the effects of space debris was done in the early to mid 70's, where the focus was mainly on the modelling of space debris [4] and the risk for individual satellites [8], not on prevention or mitigation.

However, this would quickly change as researchers realised the potential consequences of the cascading effect of this problem. In the work done by Kessler and Cour-Palais [32] recommendations are given to study different methods of stopping or slowing down the formation of a debris belt by deorbiting large objects once their usefulness is over and that the production of fragments due to collisions or explosions should be prevented.

National and Agency Standards

The first international standard involving space debris was created by the European Space Agency (ESA) mentioning the need to avoid creating space debris in orbits that intersect with orbits used by space systems as well as the desire to deorbit spent stages [23]. Bonnal [6] mentions however that this standard was not really applicable because it was too theoretical. The first concrete guideline regarding the limitation of orbital lifetime was established by NASA in 1995 stating that the lifetime of a space system should be limited to 25 years

after the completion of the mission or that the system should be moved to a designated disposal orbit [43]. To achieve this deorbit within 25 years, required area-to-mass contours are given for different low Earth orbit (LEO) apogee and perigee altitudes, as shown in Figures 2.1 and 2.2.

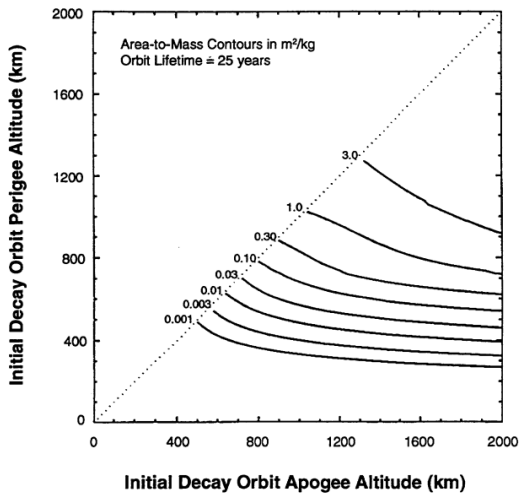

Figure 2.1: Area-to-mass contours for 25-year orbit lifetime for low-eccentricity orbits [43].

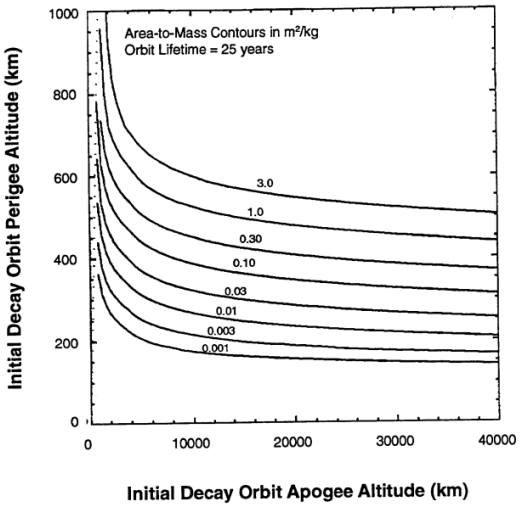

Figure 2.2: Area-to-mass contours for 25-year orbit lifetime for high-eccentricity orbits [43].

This was followed by many countries and national space agencies establishing their own guidelines and standards such as:

- National Space Development Agency of Japan (NASDA) standard NASDA-STD-18 (1996) [44]
- RNC-Q-40-512 from the Centre National d'Etudes Spatiales (CNES) in France (1999) [11]
- The Russian Federation GOST–P-52925-2008 (2008) [47]
- The German Aerospace Center (DLR) RF-0S-001 standard (Issue 7. 2012) [19]

Many more countries have adopted individual laws and regulations, usually with good coherence with respect to each other [7]. A full overview of these national regulations was made by the Committee on the Peaceful Uses of Outer Space (COPUOS) [14]. Due to the scale and global implications of the problem however, it was desired to establish more internationally oriented guidelines.

Early Global Cooperation
The Inter-Agency Space Debris Coordination Committee (IADC) had its initial meetings between ESA and NASA starting in 1987, with the official 1st IADC meeting happening in Moscow in 1993. It has one Steering Group and four Working Groups: Measurements, Database and Environment, Protection and Mitigation.

Five European agencies (the Italian Space Agency (ASI), the British National Space Centre (BNSC), CNES, DLR and ESA) prepared their combined European Space Debris Mitigation Standard in the early 2000's [1].

These two works form the base of the modern international guidelines on space debris.

2.1.2. Modern Regulations

As of writing there are four major guidelines in effect internationally: the European Code of Conduct for Space debris Mitigation, the IADC Space Debris Mitigation Guidelines, the United Nations guidelines and the International Organization for Standardization ISO 24113. Once again it was found that these four have good coherence with respect to each other and are highly similar.

European Code of Conduct for Space Debris Mitigation
The European Code of Conduct for Space Debris Mitigation is heavily based on the guidelines as established in the previously mentioned European Space Debris Mitigation Standard (EDMS). It was developed and subsequently formally adopted by ASI, BNSC, CNES, DLR and ESA.

Within this Code of Conduct, in Section 5.2.2, two protected regions around the Earth are designated, one in LEO and one in GEO. Following this, end-of-life measures are defined to avoid or reduce the generation

of space debris [2]. Code SD-OP-03 states that the operator of a space system should perform disposal manoeuvres at the end of the operational phase to limit the presence in the protected regions to a maximum of 25 years. Three methods of achieving this are given, in decreasing order of preference:

1. Direct re-entry.
2. Limit orbital lifetime to less than 25 years after the operational phase of the mission.
3. Transfer to a designated disposal orbit.

For satellites operating in medium Earth orbit (MEO), no concrete guidelines are given, as this region is not considered to possess a unique nature and is therefore not protected. Space systems operating in the geostationary orbit should be transfered at the end of their operational phase to a disposal orbit with a minimum perigee altitude above geostationary according to:

$$\Delta H = 235 + 1000 \cdot Cr \cdot \frac{S}{m} \tag{2.1}$$

where ΔH is the difference in altitude in kilometers, Cr is the solar radiation pressure coefficient and $\frac{S}{m}$ the ratio of the cross-sectional area in m^2 over the space systems dry mass in kilogram.

Inter-Agency Space Debris Coordination Committee Guidelines
Currently there are 13 members of the Inter-Agency Space Debris Coordination Committee: ISA, CNES, the China National Space Administration (CNSA), the Canadian Space Agency (CSA), DLR, the Indian Space Research Organisation (ISRO), the Japan Aerospace Exploration Agency (JAXA), the Korea Aerospace Research Institute (KARI), NASA, the Russian Federal Space Agency (ROSCOSMOS), the State Space Agency of Ukraine (SSAU), the United Kingdom Space Agency (UKSA) and ESA.

With these 13 agencies, a very large part of the nationalities operating in space are covered, as can be seen in the satellite inventory given in Section 2.2. The guidelines [28], first issued in 2002 with a revision in 2007, state the same two protected regions as the European Code of Conduct as described in the previous section and are based on three fundamental principles:

1. Prevent on-orbit break-ups.
2. Remove spacecraft and stages that reached the end of their operational phase from popular regions.
3. Limit the number of objects released during nominal operations.

Furthermore, the guidelines state the same 25-year orbital lifetime rule for LEO and the re-orbit rule for GEO space systems as described in the previous section. These, as can be derived from the agencies involved very well internationally supported guidelines are the base of the guidelines as established by the United Nations Committee on the Peaceful Uses of Outer Space (COPUOS).

United Nations Guidelines
The United Nations (UN) involvement in space can mainly be attributed to the desire of the international community to not weaponize space platforms. For this purpose the Committee on the Peaceful Uses of Outer Space (COPUOS) was established in 1958 and has currently over 95 member states. Over time this committee has extended its scope and now also oversees the exploration and use of outer space, international liability for damage caused by space systems, planetary protection and space debris mitigation. On the basis of the guidelines of the IADC, COPUOS published their own guidelines in 2007 [56]:

1. Limit debris released during normal operations.
2. Minimize the potential for break-ups during operational phases.
3. Limit the probability of accidental collision in orbit.
4. Avoid intentional destruction and other harmful activities.
5. Minimize potential for post-mission break-ups resulting from stored energy.
6. Limit the long-term presence of spacecraft and launch vehicle orbital stages in the low Earth orbit region after the end of their mission .
7. Limit the long-term interference of spacecraft and launch vehicle orbital stages with the geosynchronous Earth orbit region after the end of their mission.

These guidelines were formally endorsed by the General Assembly of the UN in their 62nd Session in 2007 [55]. Although overall it is very coherent with the recommendations and the sentiment of the previous work done by the IADC and in the European Code of Conduct, there is no explicit mention of the protected regions, the 25-year rule for the LEO region or the disposal orbit rule.

International Organization for Standardization
Whereas the previously mentioned guidelines mainly involve governments and national space agencies, the International Organization for Standardization (ISO) aims to promote space debris mitigation and prevention design in the global space industry [31]. Formally first issued in 2010, this top level standard ISO 24113 involves multiple lower-level standards applicable to space debris mitigation. In general, ISO 24113 agrees with and elaborates on the guidelines that were established earlier by the IADC and follows most of the work previously done including the protected regions in LEO and GEO as well as the designated disposal orbits and 25-year lifetime rule for LEO space systems. Of interest for this study are the lower level standards ISO 16164, regarding the disposal of spacecraft in LEO, and ISO 27852 regarding orbit lifetime estimation.

This last document provides guidance on acceptable modelling techniques to predict orbit lifetime and their applicability. These established modelling standards will be used and discussed later in Chapter 7.

2.1.3. 25 Year Lifetime Rule

It can be seen that most of the guidelines such as the one published by the United Nations are not very directly worded. In this way it leaves room for interpretation and no clearly defined points where compliance can be determined. The major exceptions are the guidelines regarding the limiting of the orbital lifetime, in either of the two protected regions, after the operational phase of the mission to a maximum of 25 years. This guideline shows up in all modern major treaties regarding space debris. These two protected regions are LEO and GEO as visualised in Figure 2.3.

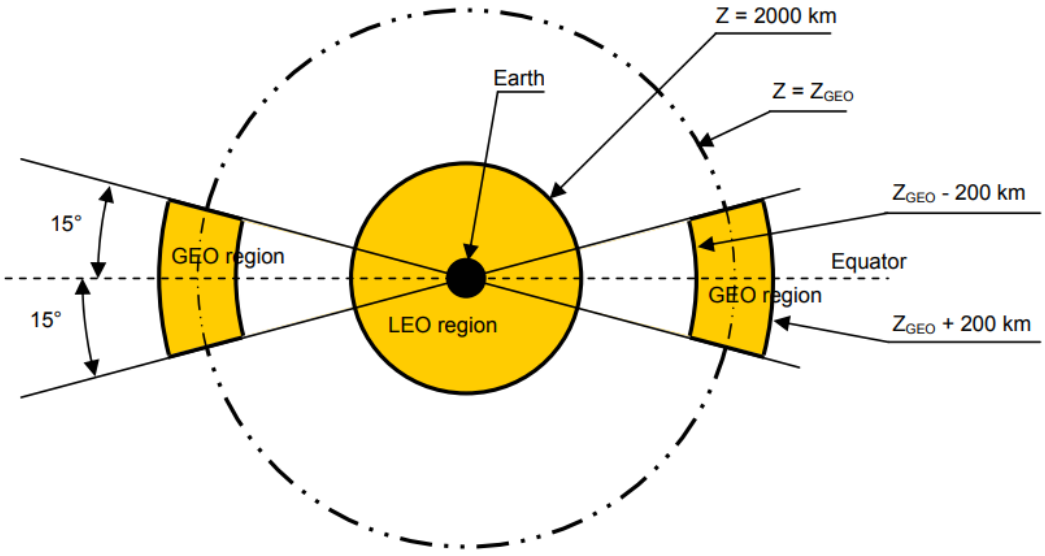

Figure 2.3: Protected regions as defined in the European Code of Conduct for Space Debris Mitigation [2].

Within the previously mentioned Code of Conduct, in Section 5.2.2, the exact definition of these two protected regions around the Earth are given, one in LEO and one in GEO as [2]:

1. The protected low Earth orbit region (LEO region) is a spherical shell extending from the surface of Earth up to an altitude of 2000 km.
2. The protected geosynchronous region (GEO region) is a segment of a spherical shell defined by:
    - A lower altitude equal to the geosynchronous altitude minus 200 km.
    - An upper altitude equal to the geosynchronous altitude plus 200 km.
    - -15 degrees ≤ latitude ≤ +15 degrees.
    - Where the geosynchronous altitude is defined as having an altitude of 35,786 km.

This altitude is defined with respect to a spherical Earth with a radius of 6378 km. The so-called 25 year lifetime rule therefore states that satellites operating within either of these regions will have to leave it within 25 years after the operational phase of the mission is over.

This study will be regarding the compliance rate with this 25 year lifetime rule of satellites operating in the Sun-synchronous orbit regime, which lies within the LEO protected region. Why this exact group of satellites was chosen as the focus of the study will be discussed in the next section.

2.2. Inventory of Satellites

The launch of Sputnik I by the Soviet Union in 1957 marked the beginning of Earth orbiting satellites. Since then numerous more have been launched, first only by governmental and (inter)national agencies, but more recently space is becoming increasingly accessible. This has allowed smaller countries, universities and companies to launch their own spacecraft, take more risk and has kicked-off rapid innovation. However, due to their relative popularity, some of the regions have seen a huge increase in spatial density and are at risk of becoming overpopulated. This section aims to identify those regions and what type of objects are currently in it.

2.2.1. General Overview

To give a general overview of these objects currently residing in orbit around Earth, use is made of the Space Environment Report by ESA [21]. In order to classify their results ESA uses the following definitions for objects given in Table 2.1.

Table 2.1: Object Classification. Adapted from ESA [21].

Type	Description
PL	Payload
PF	Payload Fragmentation Debris
PD	Payload Debris
PM	Payload Mission Related Object
RB	Rocket Body
RF	Rocket Fragmentation Debris
RD	Rocket Debris
RM	Rocket Mission Related Object
UI	Unidentified

For completeness, objects that could not be traced to their origin are classified as unidentified. Using this definition it can be concluded that all objects except those classified as payload and still operational can be considered space debris, as they currently serve no purpose anymore.

In Figure 2.4 it can be seen that the number of objects in orbit around Earth is increasing quickly, with the majority of the objects made up of the actual payload and payload fragmentation debris, followed by rocket bodies and rocket body fragmentation. Two clear jumps can be observed, corresponding to the Chinese anti-satellite missile test in January 2007 and the collision of the Iridium 33 satellite with the defunct Russian Kosmos-2251 satellite on February 2009. These two events are responsible for a large number of the fragmentation objects and with that a large fraction of the total object count.

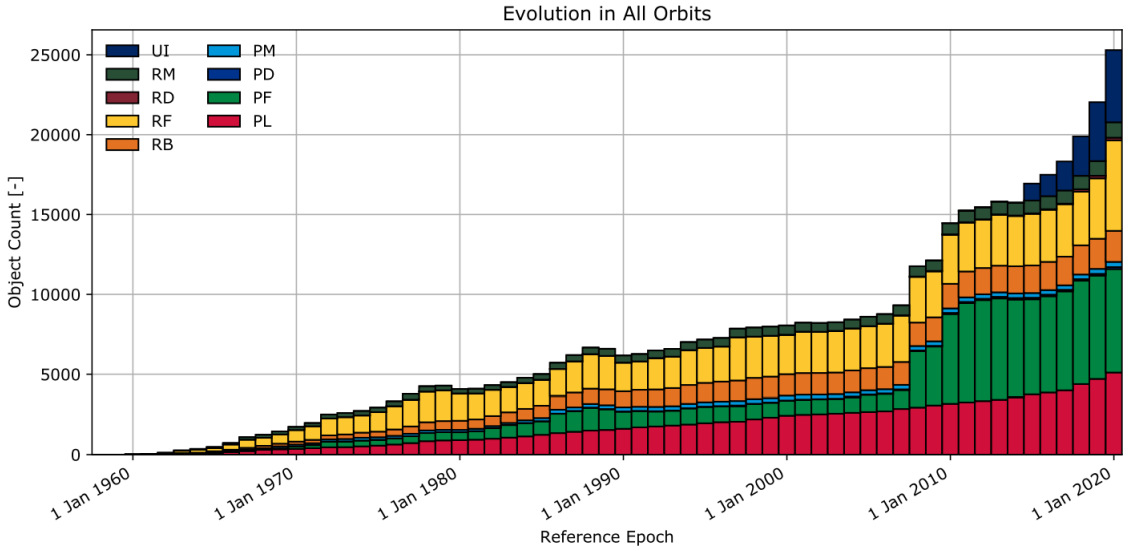

Figure 2.4: Number of objects in orbit around Earth over time [21].

With increasing sensor performance, objects are detected that can generally not be traced back anymore to a launch or source. This results in the increasing number of unidentified objects over time. Simply using the object count does not give a complete picture however, as all objects are treated equally regardless of their parameters and properties. Therefore, Figure 2.5 shows the total area of objects in orbit over time. It can immediately be seen that with this metric the payload and rocket body objects dominate and although the fragmentation objects are numerous, they are very small. A similar distribution is obtained when using the mass of the object instead of the area [21].

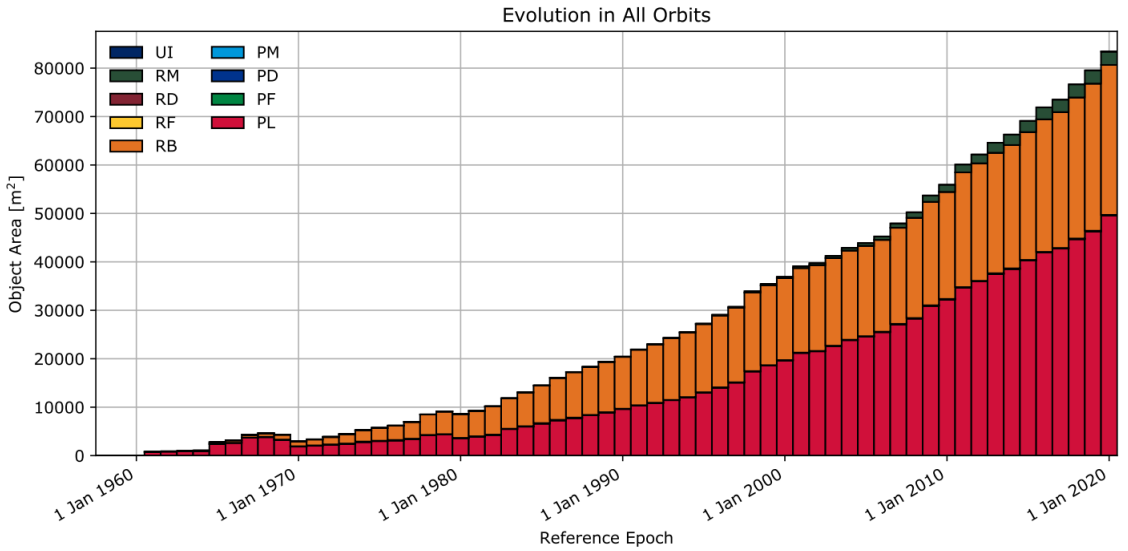

Figure 2.5: Object area in orbit around Earth over time [21].

In the figures an accelerating growth can be seen for both the object count and the object area. The relative faster growth of the count compared to the area can be explained by the fact that most of this growth is in relatively small satellites.

Besides the type of object it is beneficial to analyse where these objects are in space. This was done for these objects by classifying them according to their orbital properties using the semi-major axis a, the eccentricity e, inclination i, perigee height h_p, and apogee height h_a. The different orbital classes and their definitions used by ESA are given in Table 2.2.

Table 2.2: Orbital Classification with km and degrees as units. Adapted from ESA [21].

Orbit	**Orbit Description**	**Definition**		
GEO	Geostationary	$i \in [0, 25]$	$h_p \in [35586, 35986]$	$h_a \in [35586, 35986]$
IGO	Inclined Geosynchronous	$a \in [37948, 46380]$	$e \in [0.00, 0.25]$	$i \in [25, 180]$
EGO	Extended Geostationary	$a \in [37948, 46380]$	$e \in [0.00, 0.25]$	$i \in [0, 25]$
NSO	Navigation Satellites	$i \in [50, 70]$	$h_p \in [18100, 24300]$	$h_a \in [18100, 24300]$
GTO	Geo Transfer	$i \in [0, 90]$	$h_p \in [0, 2000]$	$h_a \in [31570, 40002]$
MEO	Medium Earth	$h_p \in [2000, 31570]$	$h_a \in [2000, 31570]$	
GHO	GEO Crossing	$h_p \in [31570, 40002]$	$h_a > 40002$	
LEO	Low Earth	$h_p \in [0, 2000]$	$h_a \in [0, 2000]$	
HAO	High Altitude Earth	$h_p > 40002$	$h_a > 40002$	
MGO	MEO-GEO Crossing	$h_p \in [2000, 31570]$	$h_a \in [31570, 40002]$	
HEO	Highly Eccentric Earth	$h_p \in [0, 31570]$	$h_a > 40002$	
LMO	LEO-MEO Crossing	$h_p \in [0, 2000]$	$h_a \in [2000, 31570]$	
ESO	Escape			
UFO	Undefined			

With these definitions the orbits of all objects were classified as well and are shown in Figure 2.6. Here it can be seen that the majority of objects are in LEO, followed by Extended geostationary orbit and LEO-MEO crossing orbits. Once again it can also be seen that the total number of objects is growing fast, especially in the most recent years.

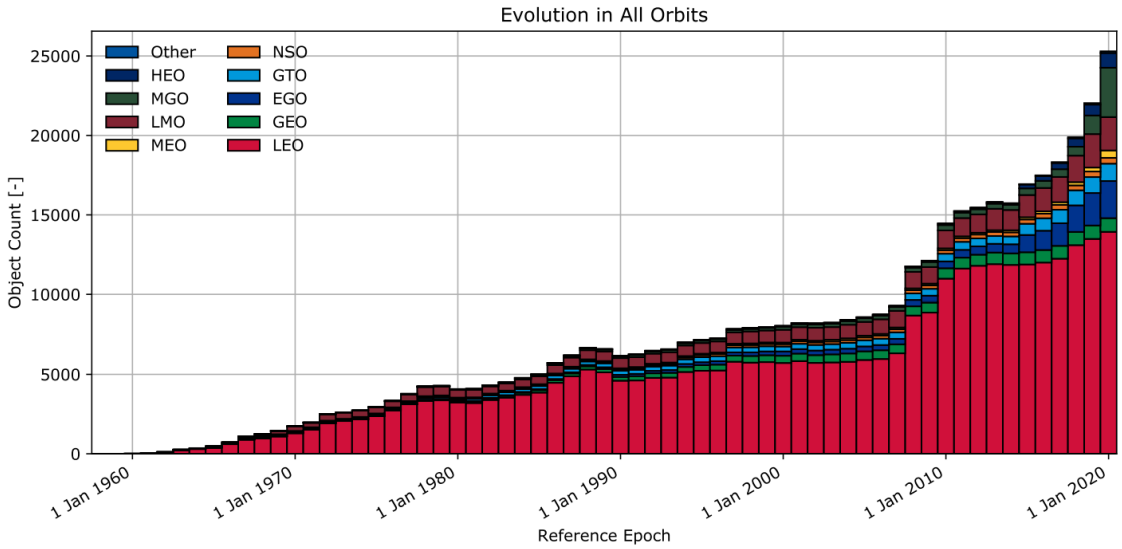

Figure 2.6: Number of objects in orbit around Earth over time [21].

This evolution is also observed for the area of those objects in Figure 2.7 where once again this had a similar distribution if mass were to be used instead of area.

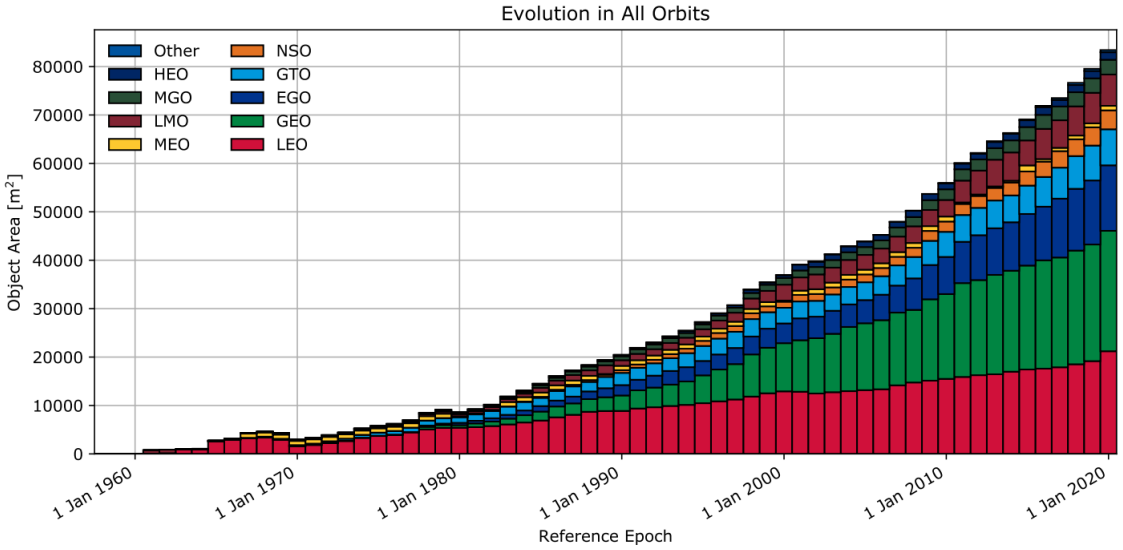

Figure 2.7: Object area in orbit around Earth over time [21].

First of all these figures show that a large number of relatively small objects are launched into LEO while a few large satellites are put in GEO. Secondly it can be observed that most of the satellites are in either LEO, GEO, Extended GEO or GTO and just a minority are in other orbits. This was the reason these two most popular regions, LEO and GEO, were protected by the regulations discussed earlier. For LEO a more in-depth analysis will be done next.

2.2.2. Low Earth Orbit

To see what type of objects can be found in this region they were classified according to their funding source in Figure 2.8 and their mission type in Figure 2.9 and shown according to their year of launch.

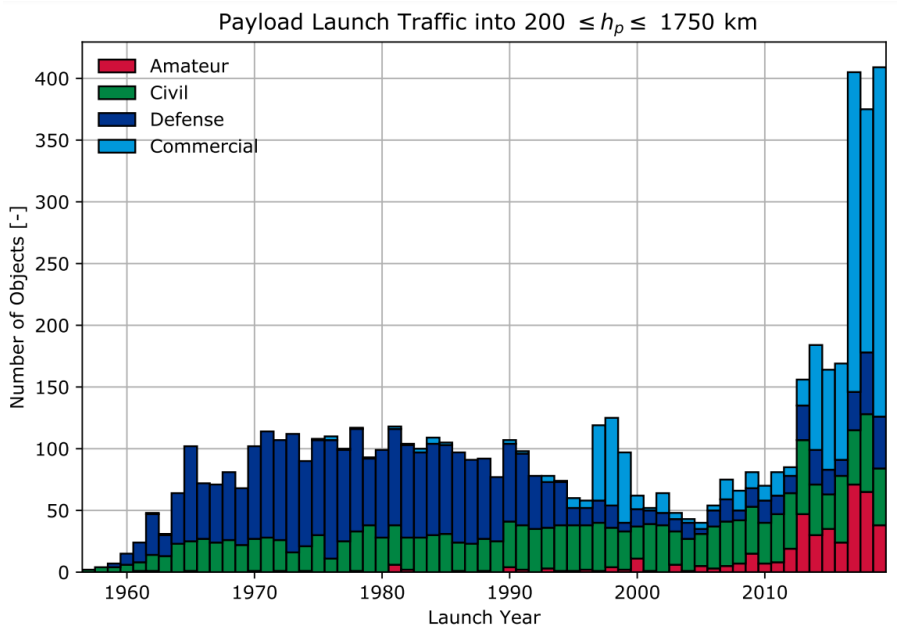

Figure 2.8: Number of objects in the LEO protected region [21].

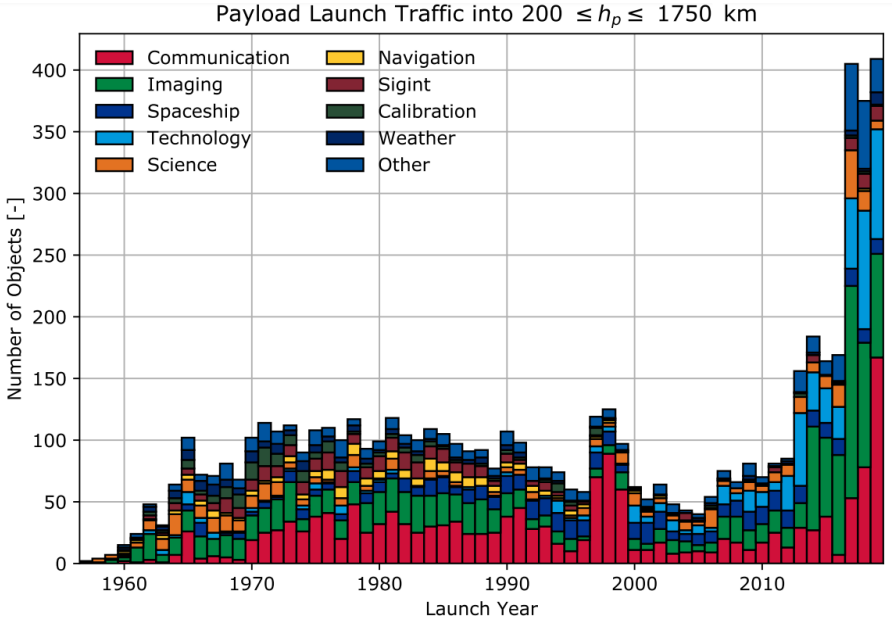

Figure 2.9: Number of objects in the LEO protected region [21].

It can be seen that due to the increasing accessibility to space, as the cost per kilogram for launch keeps decreasing and the miniaturisation technology is maturing, the recent years have seen a very large increase in commercial and to a lesser extent amateur launched satellites. Most of the satellites launched in this region are used either for communication or imaging purposes.

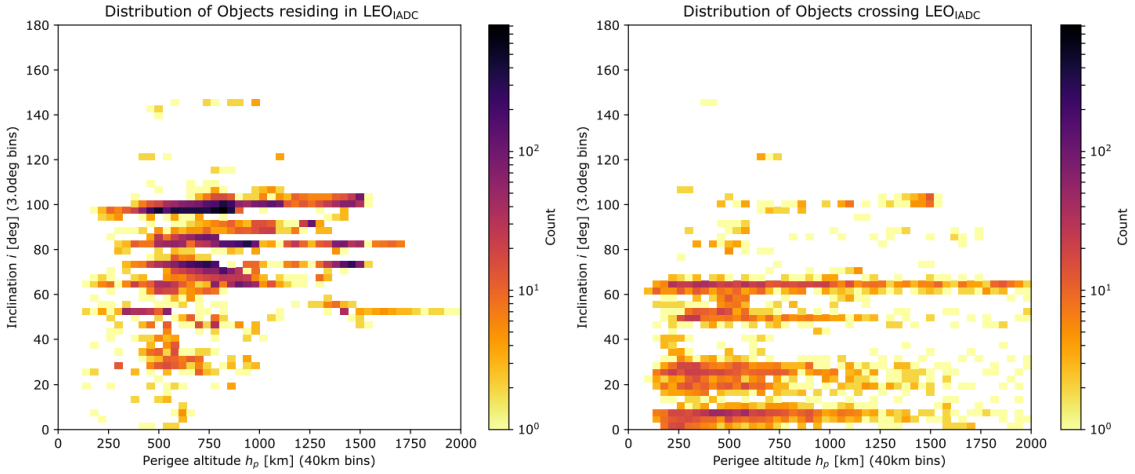

(a) Distribution of objects residing in LEO.

(b) Distribution of objects crossing LEO.

Figure 2.10: Orbital distribution of objects in LEO [21].

It was shown that the majority of objects are within LEO, but also within this region the objects are clearly clustered as shown in Figure 2.10. The figure on the left corresponds to orbits with both nodes in the LEO protected region and the figure on the right shows objects with orbits that pass through this region. A large part of the objects in LEO are in the Sun-synchronous orbit (SSO) with an inclination of $i \approx 98°$.

Other visible bands can mainly be attributed to the Cosmos-3M and Vostok stages and the Parus and Meteor satellites for $i \approx 82°$, and the International Space Station at $i \approx 52°$ [17]. Note the log scale in the figures and the therefore high popularity in these specific inclination bands. Other groups can be identified as well. Clearly visible are the bands corresponding to the Baikonur Cosmodrome at 45.6°, Guiana Space Centre at 5.2° and Kennedy Space Center at 28.6°, as well as the Molniya satellites at 63°.

2.2.3. Sun-synchronous Orbit

Previously it was seen that the Sun-synchronous Orbit regime is the most popular within LEO. This can be explained by the many advantages this orbit provides. First of all due to the nature of the orbit satellites pass over the same part of the Earth at the same time of day every day. These time-constant conditions are of benefit for many research and observation missions. This is combined with a relative low altitude providing excellent ground resolution and high inclination providing almost global coverage. A third advantage is that due to the relative constant orientation of the orbital plane with respect to the Sun, it has an almost constant ratio of time in sunlight to time in eclipse.

The most characteristic property of this special orbit is the precession of the Right Ascension of the Ascending Node (RAAN) induced by the J_2 effect due to the irreggular gravity field of the Earth. This will be discussed more in-depth in Chapter 3.

In this study the Sun-synchronous Orbit regime is defined as:

- 96.5° < Inclination < 102.5°
- Perigee altitude < 2000 km

This altitude is defined with respect to a spherical Earth with a radius of 6378 km. The payloads currently in this regime are shown in Figure 2.11. The dashed line represents the theoretical circular SSO orbits for different altitudes. It shows that the majority of payloads in SSO are located in the lower part of this region, with a perigee between 400 and 1000 km altitude.

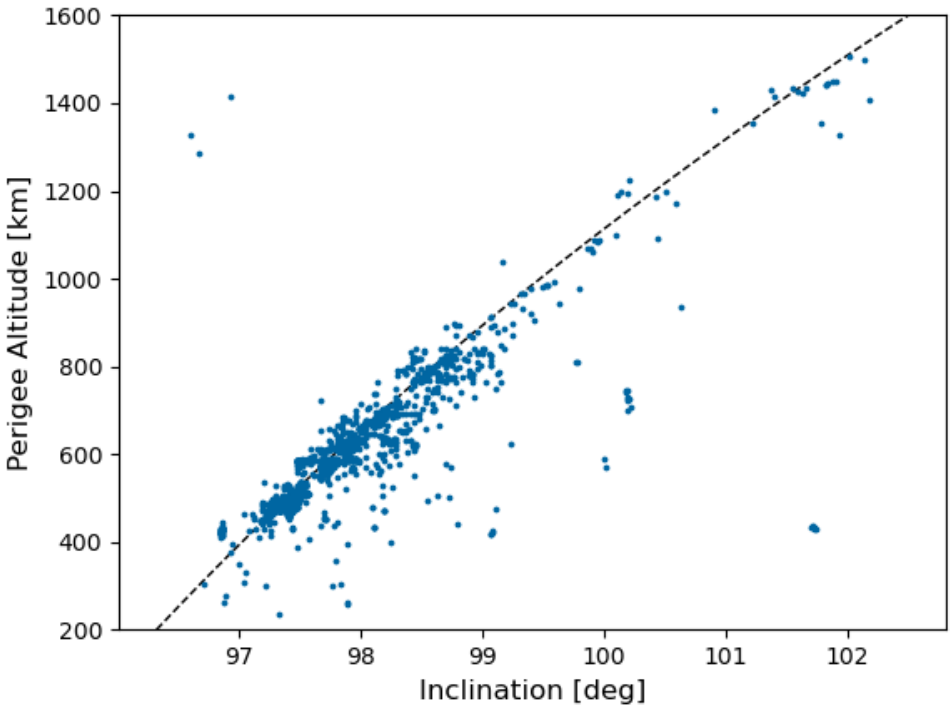

Figure 2.11: Distribution of objects in SSO on January 1, 2021.

It was already seen that the objects currently in SSO represent a large fraction of the total number of objects in LEO. This is shown even more clearly in Figure 2.12. Visible here is the enormous increase in launches from 2017 onwards. The past four years combined have seen as many objects launched as all earlier years together (812 versus 817).

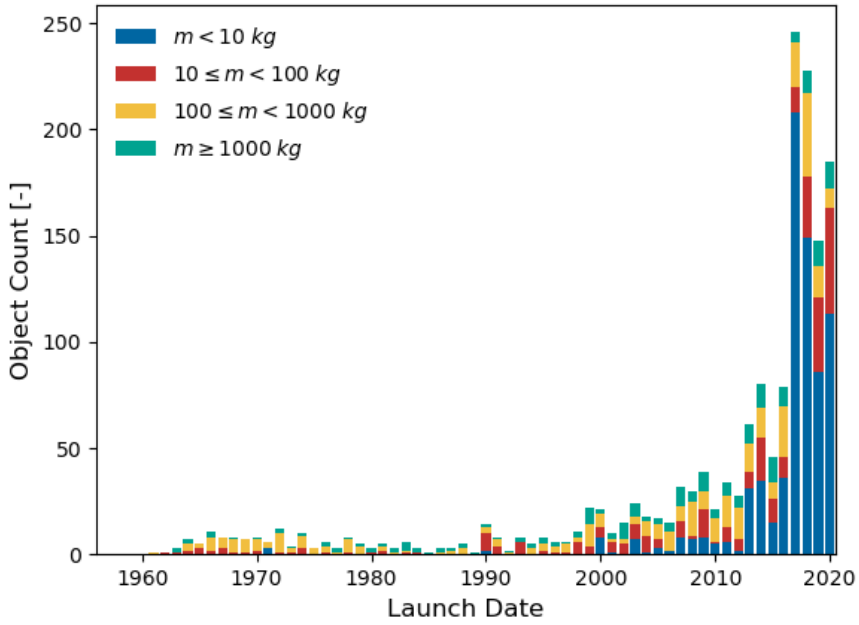

Figure 2.12: Payload launch traffic into SSO over time for different mass categories.

These increasing numbers are primarily driven by the very large increase of small satellites launched with a mass less than 10 kg, made possible by modern technological miniaturization advancements.

3

Orbital Mechanics

The analysis of space debris and its mitigation guideline compliance requires knowledge regarding how such objects in orbit behave over time. This chapter will discuss the concepts of orbital mechanics applicable to this problem, which is viewed as a perturbed Keplerian orbit. This is a widely researched topic but an attempt was made to keep this chapter concise and discuss only the most relevant subjects. For a more in-depth overview or information regarding fundamental astrodynamics the reader is referred to other publications such as the works of Wakker [60] or Curtis [15].

3.1. Reference Frames

In the discussion and analysis of space-related problems multiple different reference frames or state representations can be useful for different purposes. Depending on the application it might be beneficial to choose a frame co-rotating with the Earth, or one where the observer and not the Earth is at the origin. Although the actual behavior of an object is the same regardless of the reference system chosen, it is after all just a different way of formulating the same physics, choosing the most suitable can have serious advantages and simplify the mathematics and interpretation considerably. Furthermore, when cooperating or interacting with other researchers, systems and agencies it is convenient to express the data and found results in the same reference frames. This is why over the years certain standards of commonly used systems have been established. Many of such systems exist, with each of them having different advantages and disadvantages tailored to different research fields. The ones used in this study are given here and consist of inertial and non-inertial geocentric frames as well as topocentric reference frames.

3.1.1. Earth-centered Earth-fixed

The state representation most intuitive for a three-dimensional problem would be the Cartesian rectangular coordinates: $x, y, z, \dot{x}, \dot{y}, \dot{z}$. When one wants to describe the position or motion of an object relative to a position on Earth generally an earth-centered rotational frame is used. This has the origin in the center of mass of the Earth and is therefore often referred to as an Earth-centered Earth-fixed (ECEF) frame. In this frame, shown as x'y'z' in Figure 3.1, the origin is located in the center of the Earth, the positive z-axis is pointing along the rotational axis of the Earth, the x' and y'-axis are located in the equatorial plane where the positive x'-axis crosses the Greenwich meridian and the y'-axis is oriented in such a way to complete a right-handed reference system.

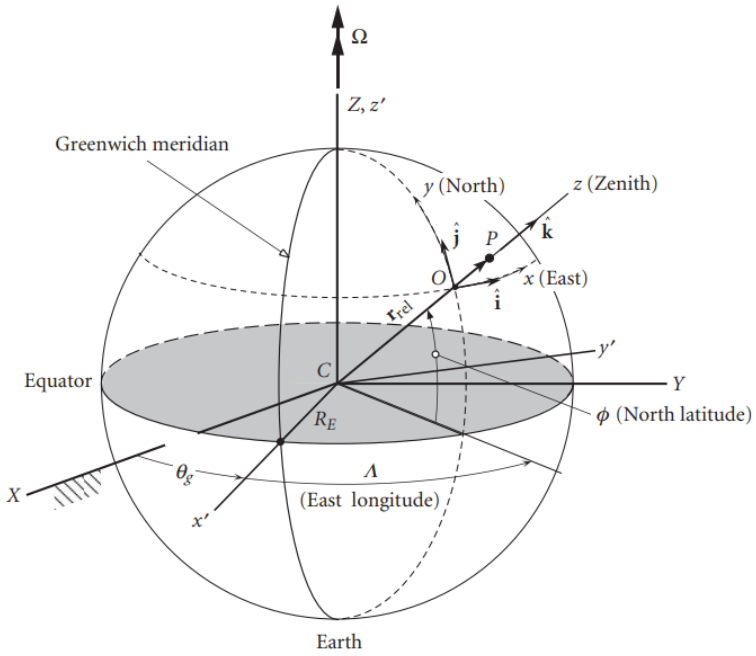

Figure 3.1: Earth-centered inertial frame (XYZ), Earth-centered non-inertial x'y'z' frame and the non-inertial topocentric-horizon frame xyz attached to a point O on the Earth's surface [15].

3.1.2. Earth-centered Inertial

To describe the motion of objects in Earth orbit it is more convenient to use an Earth-centered inertial (ECI), non-rotating, frame. This is shown in Figure 3.1 as the XYZ-frame. A commonly used implementation is the J2000 definition, where once again the origin is in the center of mass of the Earth, but this time the X-axis is in the direction of the Vernal equinox, which is the intersection of the equatorial and ecliptic planes. Since two of these points exist by convention the Sun's ascending node is used. The Z-axis is normal to the mean equator at epoch J2000 and the Y-axis completes the right-handed frame. The term J2000 is also used often to refer solely to this epoch which is at 12:00:00 on January 1st 2000 Barycentric Dynamical Time (TDB).

Radial Along-track Cross-track

In Figure 3.2 another local, object-based reference frame is shown. In this frame the $\hat{\mathbf{R}}$ vector is along the radial, the $\hat{\mathbf{S}}$ vector lies in the orbital frame along the local horizon and is positive in the direction of motion of the object. This is completed by the $\hat{\mathbf{W}}$ vector which is along the angular momentum vector. These three together form the **RSW** frame.

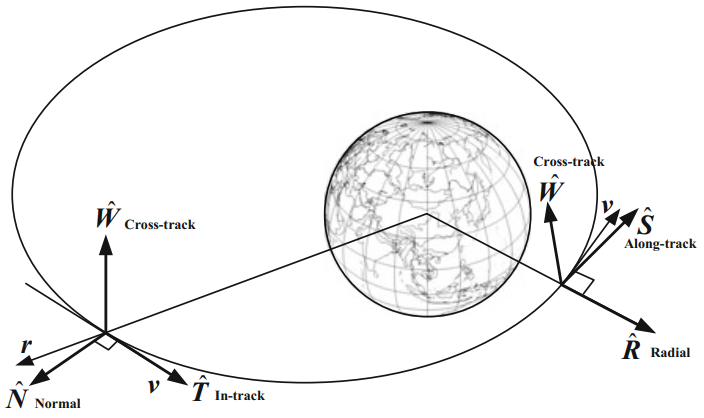

Figure 3.2: Object-based coordinates frames RSW and NTW [9].

3.1.3. Normal Tangent Cross-track

Another variant of the object based coordinate systems is also shown in Figure 3.2 as the **NTW** frame. This shares the same $\hat{\mathbf{W}}$ vector but uses the vector that is always tangent to the orbit $\hat{\mathbf{T}}$ and is positive in the direction of motion. Instead of using the radial direction the frame is completed by the $\hat{\mathbf{N}}$ vector that lies in the orbital plane and is normal to the $\hat{\mathbf{T}}$ axis. It can be seen that for perfectly circular orbits these two frames coincide.

3.2. Orbital Elements

To describe position and velocity, a set of orthogonal coordinates in line with the frame definitions previously is most logical. However, for ease of interpretation and analysis use is also made of orbital elements. Although different combinations exist since this is a six degree of freedom problem they all require at least six elements but can use more. Two of these sets will be discussed in this section, the first is the classical set of Keplerian elements and the other is the combination used in Two-Line Element (TLE) sets. More information regarding this TLE data format is given in Chapter 4.

3.2.1. Keplerian elements

The classical six Keplerian elements are given below:

- Semi-major axis, a, is defined as the sum of the apoapsis and periapsis distance divided by two and describes the size of the orbit.
- Eccentricity, e, determines the shape and elongation of the orbit, equal to zero for a circular orbit.
- Inclination, i, determines the tilt of the orbit and is defined as the angle between the angular momentum vector of the motion of the body and the positive Z-axis.
- Right Ascension of the Ascending Node (RAAN), Ω, describes the orientation of the orbit and is the angle from the reference direction to the ascending node in the equatorial plane. If instead of the equatorial the ecliptic plane is used this is called Longitude of the Ascending Node .
- Argument of periapsis, ω, determines the third aspect of orientation of the orbit and is the angle between the ascending node and the periapsis.
- True anomaly, θ, describes the position of the object in the orbit with respect to the pericenter.

The last four elements, the angles, are shown in Figure 3.3. Although for the two-body problem these elements are integration constants, in reality objects in Earth orbit are perturbed by other forces and these elements are therefore not constant. In all cases the true anomaly is the fastest changing parameter.

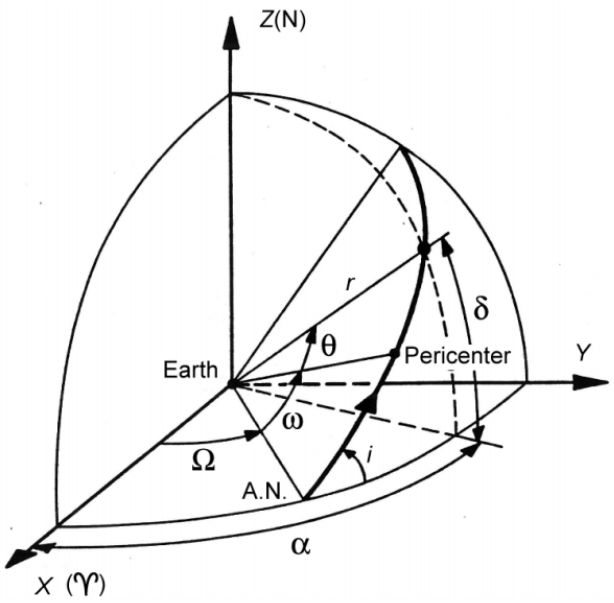

Figure 3.3: Orbital elements i, Ω, ω, θ and the position of the satellite in spherical coordinates [60].

3.2.2. Two-Line Elements

The TLE format shares four orbital parameters with the Keplerian set: the eccentricity, inclination, RAAN and the argument of periapsis. However, instead of the semi-major axis and the true anomaly it makes use of the following two parameters:

- Mean motion, n, the mean angular velocity.
- Mean anomaly at epoch, M_0, which is the position of a fictitious object moving around the orbit at a constant angular speed n. Therefore for a circular object this is equal to the true anomaly.

The mean angular motion can be expressed as:

$$n = \sqrt{\frac{\mu}{a^3}} \tag{3.1}$$

where a is the semi-major axis and μ the gravitational parameter.

3.2.3. Alternative Representations

Many more element sets exist with different advantages and disadvantages which can arise especially during numerical propagation. Such as the existence of singularities or the disadvantage of having multiple fast moving elements on the numerical accuracy. These can be mitigated by making use of more complex element sets, such as the use of quaternions, equinoctial orbital elements or modified unified state model [59].

3.3. Orbital Perturbations

The movement of an object in space around Earth is in general determined by the Earth's gravity field. If this field is radially symmetric the path of the object is a conic section also known as a Keplerian orbit. This has the consequence that the orbital elements are integration constants and simplifies the problem to an unperturbed two-body problem. However, in reality this gravity field is not symmetric but irregular and subject to both spatial and temporal changes. Furthermore, this gravity field does not provide the only force acting on the object and perturbing the object from its nominal Keplerian orbit. The most influential of these other forces are the aerodynamic drag, solar radiation pressure and third-body gravity effects. The magnitude of these perturbations is dependent on the properties of the object itself, (such as its area), and time but also depend heavily on the orbital parameters. Most significantly on the semi-major axis, this can be seen in Figure 3.4, where the magnitude of these perturbations is plotted.

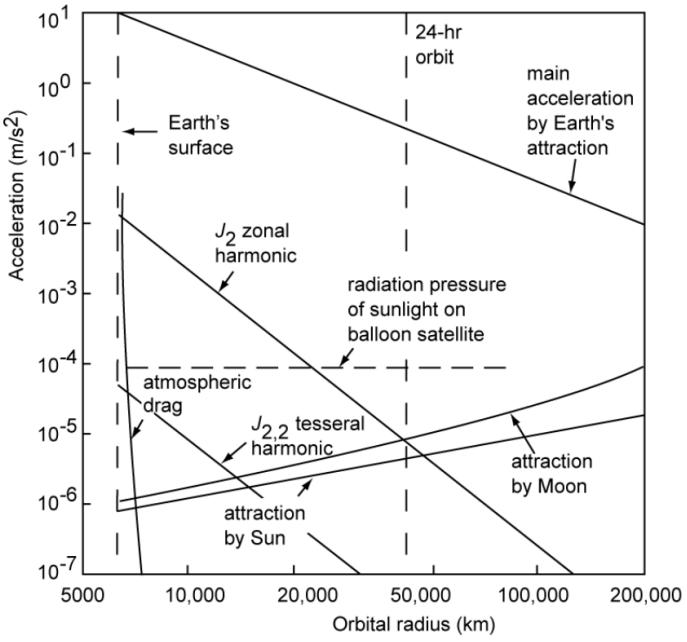

Figure 3.4: Magnitude of perturbing forces as a function of the orbital radius [60].

In this figure it can be seen that both the absolute and the relative magnitude of a perturbing acceleration can change several orders of magnitude depending on the orbital radius.

3.3.1. Aerodynamic Drag

This is most notably the case for atmospheric drag, where at very low orbits this is the main perturbing force but decreases rapidly with increasing altitude and being negligibly small for orbits with an altitude higher than ≈ 1600 km. Therefore this perturbing force is highly relevant for objects in LEO. The magnitude of the acceleration due to this force can be determined using:

$$a_{drag} = -\frac{1}{2}\rho C_D \frac{A}{m} |\bar{v}|\bar{v} \tag{3.2}$$

where ρ equals the atmospheric density, C_D is the drag coefficient, A is the reference area, m the mass and $\bar{v}$ is the relative velocity vector with respect to the atmosphere. Although the formulation of this force is very straightforward the actual determination of the value of these parameters is not. First of all the reference area is dependent on the orientation of the object and its components, such as the orientation of the solar panels. Furthermore, for larger satellites shading could occur where one part of the satellite is obscuring another. This is usually changing constantly throughout the orbit and is not always known exactly. Therefore usually a simplified approach is used where typically a spherical shape is assumed.

The composition of the atmosphere for altitudes below 90 km is well mixed and fairly consistent with about 78% N_2, 21% O_2 and 1% Ar, however above this altitude the composition starts to change with altitude [60]. Because of this both the density and the drag coefficient change as well. This is because at these low densities the drag coefficient is largely determined by the kind of particles that hit the satellite, their energy, their relative velocity and the characteristics of the surface material of the satellite. The typical value of this drag coefficient is around $C_D = 2$ for lower altitudes increasing to $C_D = 3$ for higher ones.

Finally the determination of the atmospheric density is not straightforward as well. Although as stated this is dependent on altitude it has also many cyclical changes and many factors influence this parameter making it difficult to model and predict. One of the major influences on this density is the solar activity, the relation can be seen in Figure 3.5 for a single location and altitude.

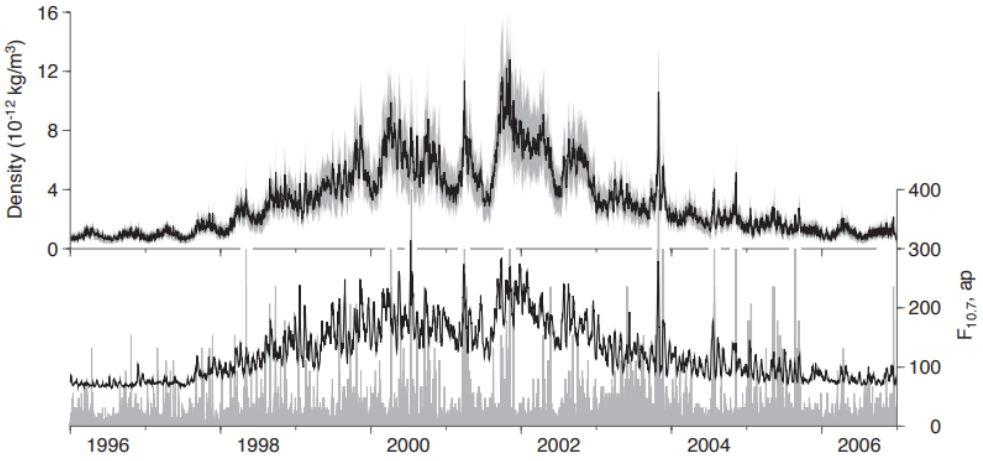

Figure 3.5: Change of density (top) and solar activity (bottom) 400 km above Delft, the Netherlands [20].

This solar activity is not just changing on long-term cycles but also has shorter cycles corresponding to day and night. Both the influence of altitude and solar activity and the day and night cycle on the temperature and density can be seen in Figure 3.6.

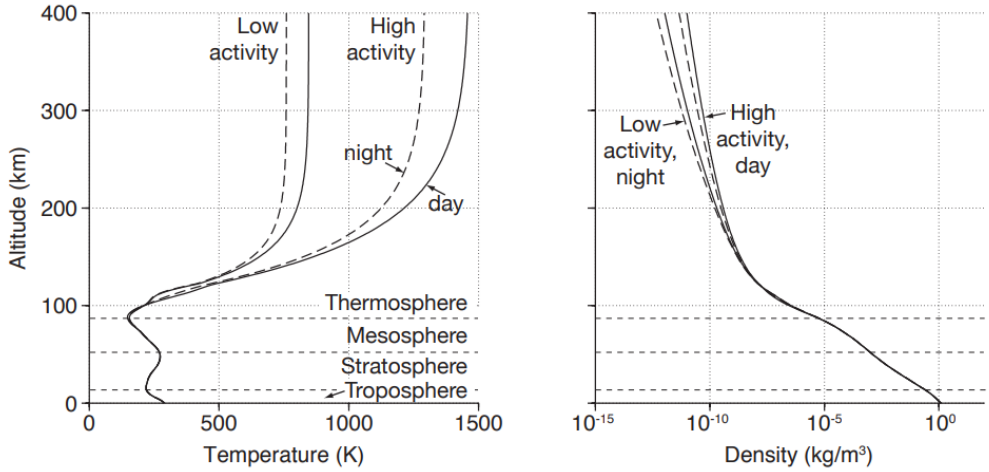

Figure 3.6: Change of density and temperature due to solar activity and altitude according to the NRLMSISE-00 model [20].

3.3.2. Gravity Field

The gravity field of Earth is, as was stated previously, neither uniform nor perfectly symmetric. Furthermore, due to the presence of tides and changes in the internal structure and composition of Earth it is also varying in time. In this report however Earth is considered static and those effects are considered negligible due to the relative short time span and required accuracy. However, for precise orbit determination purposes those effects do play a role.

These irregularities and non-uniformity can be modelled using spherical harmonics; for a point outside Earth the gravitational potential can be written as [60]:

$$U = -\frac{\mu}{r}\left[1 + \sum_{n=2}^{\infty}\sum_{m=0}^{n}\left(\frac{R}{r}\right)^n P_{n,m}(sin\phi)\left\{C_{n,m}\cos m\Lambda + S_{n,m}\sin m\Lambda\right\}\right] \tag{3.3}$$

where μ is the gravitational parameter, r is the distance from the point to the center of mass of Earth, ϕ is the geocentric latitude, Λ is the geographic longitude and R is the mean equatorial radius of Earth. Furthermore, $C_{n,m}$ and $S_{n,m}$ are constant model parameters and $P_{n,m}$ the associated Legendre functions of degree n and order m.

It can be seen from the $\left(\frac{R}{r}\right)^n$ term that the amplitude of this generally decreases with increasing degree and with an increasing distance r. In other words, the higher the orbital radius of an object, the more valid the approach of modelling the gravity field of Earth as a point mass. The magnitude of the constant model parameters varies from body to body. However, in general for larger rotating bodies the $J_{2,0}$ term is relatively dominant. This term corresponds to the flattening of the body and its bulge around its equator due to the balance of gravitational and centrifugal forces due to its rotation. The acceleration due this term can be expressed in spherical coordinates as [60]:

$$f_r = \frac{3}{2}\mu J_2 \frac{R^2}{r^4}(3\sin^2\phi - 1) \tag{3.4}$$

$$f_\phi = -\frac{3}{2}\mu J_2 \frac{R^2}{r^4}\sin 2\phi \tag{3.5}$$

$$f_\Lambda = 0 \tag{3.6}$$

It can be seen that it has components in the radial and latitudinal (North-South) direction. It is dependent on latitude, not on longitude and also has no direction component in longitudinal (East-West) direction. Because the J_2 term is about a thousand times larger than other coefficients it is often sufficient to use just this term to compute orbits of non-geostationary satellites. However, due to resonance in geostationary orbit, for very precise orbit determination or for satellites in very low orbits, other terms will have to be added for sufficient accuracy.

It is this oblateness effect that is the cause of angular precession of the nodes. If this precession rate is equal to 360° per sidereal year this means that the orbit plane is fixed relative to the Sun. Such an orbit is therefore called a Sun-synchronous Orbit.

3.3.3. Solar Radiation Pressure

An object in space around Earth experiences the pressure due to the radiation of the Sun, sunlight that is reflected by Earth and infrared radiation emitted by Earth. In Figure 3.4 it can be seen that this perturbing force is dominant at high altitude orbits. The acceleration due to this force can be described using Equation 3.7 [60]:

$$a_{rad} = C_R \frac{W \cdot A}{c \cdot m} \tag{3.7}$$

here C_R is the solar radiation coefficient, W is the energy flux, A is the effective cross-sectional area, m the mass and c is the speed of light. Although, as was seen in Figure 3.5, the changing solar activity in the 10.7 cm wavelength made it very difficult to make accurate predictions for atmospheric density, the total combined intensity of Solar radiation of all wavelengths remains almost constant. Making the overall total radiation pressure nearly constant throughout these cycles. The energy flux does vary slightly during the year from 1308 W/m^2 when Earth is at perihelion to 1408 W/m^2 at apohelion [60]. It can be seen that this perturbation, just like the one caused by atmospheric drag, has a higher impact on objects with a relatively low mass and high cross-sectional area. The solar radiation coefficient is heavily dependent on the type of materials used and the attitude of the spacecraft but is generally between $C_R = 1$ and $C_R = 2$. Of course the Sun causes a shadow behind Earth, in this cone there is no (umbra) or partial (penumbra) obscurence of the Sun. In this region there will therefore be no or a smaller solar radiation force.

3.3.4. Third-Body Gravity

Of course Earth is not the only body exerting a gravitational force on a satellite in orbit. However, due to the relative large distances to other bodies these other forces are several orders of magnitude weaker. Due to the distance (Moon) and mass (Sun) these two bodies are still significant enough to cause variations in the orbital parameters, especially in geosynchronous orbits. The variations caused by these bodies are similar to that caused by the J_2 effect.

The effects are most notable at high altitudes or at specific resonance altitudes and are less significant for satellites in LEO.

4

Methodology

Several steps are involved in order to determine the compliance rate with the 25 year lifetime guideline discussed in Chapter 2. What exact steps are taken in this study, and why they are needed will be discussed in this chapter. For each of the steps involved a more detailed description, and method of implementation will be given in later chapters.

First a brief overview of the methods used in previous studies is given in Section 4.1. With these studies the existing research gaps were identified and corresponding research questions are established in Section 4.2. From the heritage studies several lessons were learned, and the approach implemented to answer the established research questions in this study is shown in Section 4.3. Throughout the development, use was made of two test case satellites, Envisat and SARAL. Why this was done, and why these satellites were chosen will be discussed in Section 4.4. Finally, a brief description will be given of the different data sources that were used in Section 4.5.

4.1. Heritage

This section will give an overview of the heritage in this research field and will discuss the most recent and relevant studies done regarding the state of spacecraft compliance with national and international guidelines. It should be noted that to keep this section concise it does not cover all studies done by all institutions but just a subset and the focus will be on the method that was used. The results are given as well, as these will later be used for comparison in Chapter 8.

4.1.1. Compliance of Italian LEO satellites

In 2015 a study was published regarding the state of compliance of the Italian satellites in LEO [3]. In total 25 satellites were analysed.

Method

This analysis was started by categorising the satellites in four categories:

1. Those already decayed from orbit.
2. Those abandoned and still in orbit.
3. Those still operational but unable to carry out orbital maneuvers.
4. Those both operational and maneuverable.

Since the fourth category both is still operational and has on-board capabilities to still perform orbital maneuvers it was concluded that only the first three categories were to be considered. For the first category compliance is determined by the duration of the operational phase as the total orbital lifetime is known. While for the second category the remaining lifetimes have to be determined in order to determine compliancy. For the third category, since it has no means of maneuvering it can be concluded that the state of compliance is a direct consequence of the orbit chosen. However, because these satellites are also still operational an estimate will have to be made of the duration of the operational phase that has to be added to the allowed 25 years.

Although the article gives an overview of the to be analysed Italian satellites, it does not give an overview of the exact result of this categorisation. However, the satellites belonging to the first category can be identified by their reentry date. For the operational state of the satellites, the authors mention that for micro and nanosatellites which are not managed by institutional operators or universities this is often not published. However, it is not made clear how this problem was solved. To determine the remaining lifetime the published shapes and sizes of the satellites under consideration were used to compute the average tumbling cross-sections. These were then used in STELA, the semi-analytic orbit propagator developed by CNES.

Results
It was found that as of mid-2014 none of the satellites made a manoeuvre to reduce its remaining orbital lifetime but that 64% (16 out of 25) had decayed or were predicted to do so within the 25 year limit. When looking at satellites launched after the approval of the guidelines as published by the IADC in 2002 this percentage grew to 66.7% (6 out of 9) and 75% (6 out of 8) when taking the satellites launched after the signing of the European Code of Conduct in 2004. It can therefore be concluded that it appears that the guidelines have had a positive effect regarding space debris in LEO caused by Italian satellites. However, the number of data points is very low which makes it difficult to make definitive statements. It should furthermore be noted that within these guidelines a compliance success rate of 95% is given, which is still well above the current state of Italian compliance as given by this study.

4.1.2. CNES LEO Compliance Study
A study was done by CNES investigating mitigation guidelines compliance by space operators between 2000 and 2013 [42]. The study follows the same procedures of establishing operational status and predicting remaining lifetime as was seen earlier.

Method
The method to determine this compliance is given in the following steps [42]:

1. Identify objects with a perigee altitude below 6000 km.
2. Detect End of Mission date for these objects.
3. Estimate physical parameters of these objects.
4. Compute compliance rate of following guidelines:
    - Maximum orbital lifetime of 25 years.
    - No interference with the LEO region for 100 years, meaning a perigee altitude above 2000 km.

For their data source the authors made use of the TLE data as given by the United States Strategic Command. A filter was applied to remove objects corresponding to the following criteria [42]:

- Objects launched before 1st January 1980.
- Objects re-entered before 1st January 2000.
- Objects flagged as DEB in the database, except for specific objects identified as SYLDA, SPELDA, SPELTRA and BREEZE-M debris.
- Objects related to human spaceflight.
- Objects with a perigee altitude > 6000 km.

This resulted in a total of 2528 objects, of which 1504 are satellites and 1024 are rocket bodies. In this database, satellites that are not functioning are still designated as payload PAY and not as debris DEB. Similar to identified rocket bodies which are designated as R/B. Once again the end of mission date has to be identified which in this study was done differently for the different types:

- For spacecraft this was determined by analysing TLE data with a moving window approach.
- For rocket bodies it was assumed that the end of mission starts directly after launch.

Results
Using the aforementioned method the compliance rate of all these objects launched between 2000 and 2013 were analysed and the following results and conclusions were stated by the authors [42]:

- 59% of satellites and 60% of rocket bodies are compliant with the 25 year lifetime guideline.
- There was no clear trend of improvement in terms of global compliancy with the guidelines.
- Most objects rely on the natural orbit decay as only 10% of the spacecraft perform a disposal maneuver at the end of their operational lifetime.

4.1.3. ESA Studies
In the most recent Space Environment Report by ESA, published in September of 2020 [21], an overview is given of the current state of the space environment around Earth. Among studies regarding the distribution of satellites and their orbital parameters results are also published regarding space debris guideline compliance of LEO objects. Here the methods and results of this study will be shown.

Method
This study follows by now familiar procedures, starting with the identification of a spacecraft operational status. For objects where assessment of the end of mission is not possible, i.e. satellites without orbit control capabilities, a statistical approach is used. Afterwards the remaining time in the protected region is determined. This is done using an estimation of the Ballistic Coefficient and long-term space weather forecasts.

The exact method and parameters that were used to generate the result are not given but a reference is given to the TLE based maneuver detection method used [37].

In the results the satellites are classified in four distinct groups:

1. Naturally Compliant, where the mission orbit already complied with the 25 year rule and a maneuver was not required.
2. Successful attempt, when compliance was reached after an orbital maneuver.
3. Insufficient attempt, when compliance was not reached but an orbital maneuver was attempted.
4. No attempt, when compliance was not reached and no attempts were taken.

Results
In this study it was shown that the overall compliance is slowly trending upwards from 2008 onwards. Furthermore, it was seen that of those compliant objects most of them are naturally compliant and do not require an end-of-life maneuver. Such a naturally compliant orbit was chosen for 40 to 50% of the objects in LEO. Furthermore, it was concluded that over the years the number of objects attempting a disposal maneuver is slowly increasing to about 40% in 2017. However, this means that the majority of the non-naturally compliant objects still make no attempt whatsoever. Finally, although the majority of the objects performing such a maneuver successfully does so, the percentage of success is very irregular changing from around 90% in a good year such as 2006 to only about 50% in 2013.

In general the compliance with 25 year disposal guidelines has been poor in the past but is increasing in recent years. The majority of compliant satellites make no de-orbit maneuver and are naturally compliant.

4.2. Research Questions
From the studies done it can be seen that the focus is often on LEO as a whole. However, as was shown in Chapter 2, the objects within this region are not uniformly distributed but heavily clustered. The most popular of these are the Sun-synchronous orbits. Looking at LEO as one region can therefore be misleading as these local clusters might impact sustainable future use of these orbits. Therefore the following main research question was formed:

Do satellite operators adhere to the international guidelines regarding the 25-year time limit after end-of-life for satellites in Sun-synchronous Orbit?

Furthermore, the above-mentioned studies often use the date of the operational phase as reported by operators if available. Although easy, their is of course a possible conflict of interest when determining the

compliance of these operators with the guidelines. To prevent this in this study the operational status of a satellite will be determined by orbital data whenever possible.

Moreover, this study will provide more insight in what drives the compliance, and if differences exist between sub-classes of satellites by looking at different mass categories.

Does compliance with the 25-year time limit after end-of-life vary for satellites with different mass?

Besides mass it would be of interest to group the satellites by their orbital control capability. Are satellites operators performing end-of-life maneuvers or is there no real difference between satellites with this capability to do so and those that are purely ballistic from launch.

Does having orbital control capabilities impact compliance with the 25-year time limit after end-of-life?

Also of interest is the evolution of this compliance over time, are satellite operators increasingly adhering to the established guidelines or just ignoring them. When this research was initiated the compliance results of the study by ESA on the LEO region were not yet published. These recently published results, together with those obtained by other researchers for satellites in LEO and GEO will be used for comparison:

How does compliance with the 25-year time limit after end-of-life for Sun-synchronous satellites compare to satellites in LEO and GEO?

During this research several assumptions and modelling choices have to be made. In the previous studies these are not always clearly given, making the results harder to analyse. To improve on this these will be stated transparently to be able to study their impacts on the results later.

4.3. Method

The method used in order to determine the compliance rate of Sun-synchronous satellites with the 25 year lifetime guideline can be split up in two main segments. As this 25 year lifetime countdown only starts after the operational phase is ended, first the operational status of the satellite needs to be determined. Afterwards, the remaining orbital lifetime in the protected region needs to be predicted. These can then be combined together with the necessary input and output processing to determine the compliance of the satellite. This is done to the entire population of Sun-synchronous satellites to determine the overall compliance rate.

4.3.1. Operational Status

The determination of the operational status of a satellite is crucial to assess its compliance with the space debris mitigation guidelines. Unfortunately, most companies and institutions do publish extensively on their satellite launches but not when they stop functioning or are put out of service. There is also not a central registry to look up this information. In the heritage studies discussed previously, multiple different methods were used to detect this but they were all based on the same underlying principles.

For satellites with orbital control capabilities, first a long-term data set of the orbital parameters was obtained. This data then has to be filtered to determine non-natural behaviour which would correspond to active control and therefore an active and operational satellite. If after a few years such a satellite would stop showing this active behaviour it can be assumed that the satellite has stopped functioning. For satellites without orbital control capabilities, such as many of the smaller satellites, this will of course not work. These two groups will therefore be treated separately.

4.3.2. Orbital Lifetime

Using the methods described it can be determined if and when a satellite has become non-operational. From that point, as stated in the space debris guidelines, a satellite has a maximum of 25 years to leave the protected region. This can be done by a direct re-entry, but the most commonly chosen method is using natural orbital decay. Sometimes a small maneuver is also performed to lower the orbit to hasten this process.

It is therefore required to predict how long this decay will take. This can be done in multiple ways, such as reference figures, semi-analytic propagation and full numeric simulation. By doing so one can determine the remaining orbital lifetime.

4.3.3. Algorithm

By combining the information from the operational status determination using maneuver detection, with the decay date obtained from the orbital lifetime prediction the compliance of the satellite can finally be determined. The resulting algorithm of this study is shown in the flowchart in Figure 4.1.

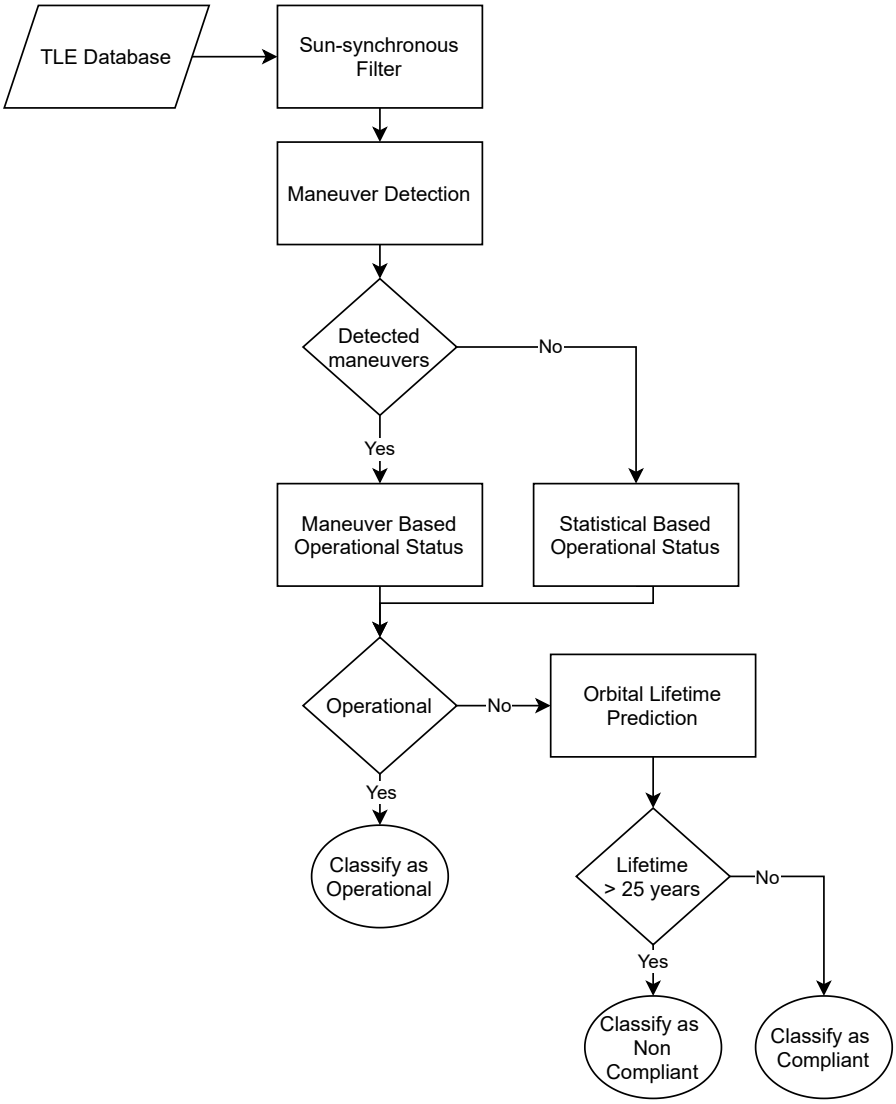

Figure 4.1: Flowchart of the compliance rate determination algorithm.

The entire TLE database is first filtered for all satellites in a Sun-synchronous orbit. This is defined as having an inclination between 96.5 and 102.5 degrees and an perigee altitude less than 2000 km. For each satellite it is determined when the last orbital maneuver was made in order to determine the operational status. A satellite is classified as active when it has made a maneuver within the past two years.

If it has done maneuvers in the past but it stopped doing so, it is classified as not operational and the date of the last maneuver is used for the end of the operational phase. If it never performed an orbital maneuver a statistical based model is used to determine operational status.

From this date, if the satellite has not already left the protected region, it is propagated in order to predict the remaining time in that region. The eventual compliance of satellite is a binary event, it either is or is not compliant, and can only truly be determined after the 25 years have passed. For an individual satellite before that time, the result can therefore only be interpreted as a current best estimation.

4.4. Development Cases

Two satellites were used during the development of the algorithm. This was done to immediately test and tune the settings and performance of the implemented methods. In this way the algorithm is also inherently validated, but to make sure it is not over-fitted to these two specific cases a separate validation is done as well on a larger group of satellites. The two satellites chosen were Envisat and SARAL; some of their relevant properties are shown in Table 4.1.

Name	SATCAT	Launch Mass [kg]	Launch Year	Semi-Major Axis [km]	Inclination [deg]
SARAL	39086	400	2013	7163	98.5
Envisat	27386	8200	2002	7143	98.1

Table 4.1: Properties of the two development cases SARAL and Envisat.

These two satellites were chosen as the development cases for a combination of reasons. First, the satellites are both in a Sun-synchronous orbit. Secondly, in order to develop the maneuver detection algorithm the date of the actual maneuvers has to be known. For both these satellites the International Laser Ranging Service (ILRS) publishes this data provided by the International DORIS Service (IDS). Finally, SARAL is much lighter than Envisat, allowing the algorithm to be developed for both these mass categories.

From the available TLE data for both these satellites the semi-major axis times series was constructed, these are shown in Figures 4.2 and 4.3 to give an overview of their orbital behaviour.

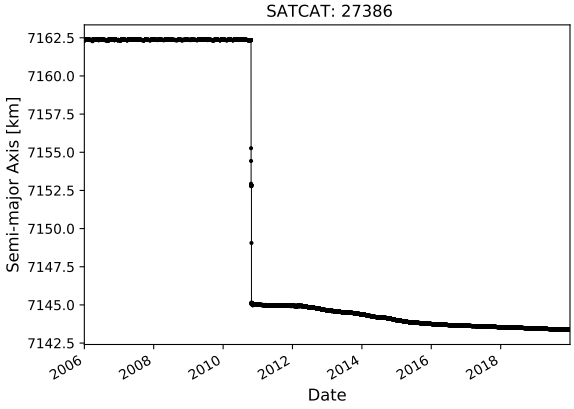

Figure 4.2: Semi-major axis series of Envisat.

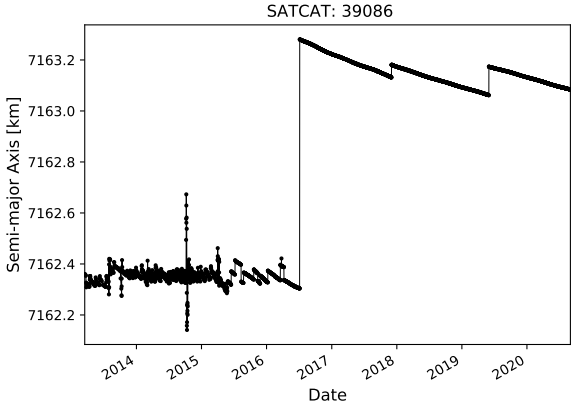

Figure 4.3: Semi-major axis series of SARAL.

When no maneuvers would be present in the data, one would expect the semi-major axis to slowly decrease over time due to the perturbations mainly due to drag. SARAL clearly shows many "jumps" in the semi-major axis especially early on, and two major jumps since 2017. All of these jumps are caused by orbital maneuvers and indicate that the satellite is still operational. For Envisat, on this scale, only one major maneuver is visible, decreasing the semi-major axis from 7162.5 km to 7145 km, note the scale difference between the two satellites. However, there are actually many more maneuvers performed but with a magnitude that is much smaller, as can clearly be seen when zooming in on a smaller timeframe in Figure 4.4.

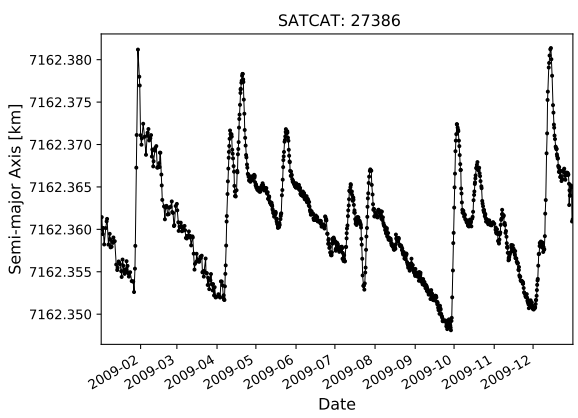

Figure 4.4: Semi-major axis series of Envisat in 2009.

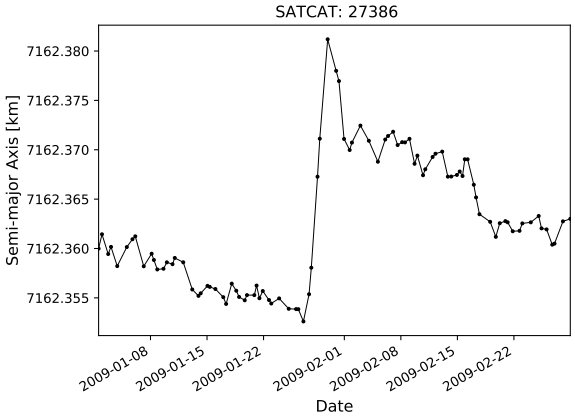

Figure 4.5: Overshooting behaviour in the TLE data.

In these figures multiple maneuvers can be observed, resulting in a semi-major axis that stays around 7162.36 km during these two years. Once again the small magnitude of these maneuvers can not be overstated, often only in the order of 10 meters. Furthermore, for semi-major axis increasing maneuvers, it can be seen that the semi-major axis is often initially overestimated before settling at a slightly lower value after a number of epochs. The same is observed when a reducing maneuver was performed, in that case the semi-major axis is often initially underestimated. This is likely due to the fact that the TLE data contains the mean orbital elements, and this is an artifact of this orbit fitting to multiple observations. This overshooting can be observed more clearly when zooming in again on the first three months of 2009 in Figure 4.5.

These small maneuvers continue to be present after the large orbital maneuver in 2010. The semi-major axis of Envisat in 2011 and 2012 is shown in Figure 4.6.

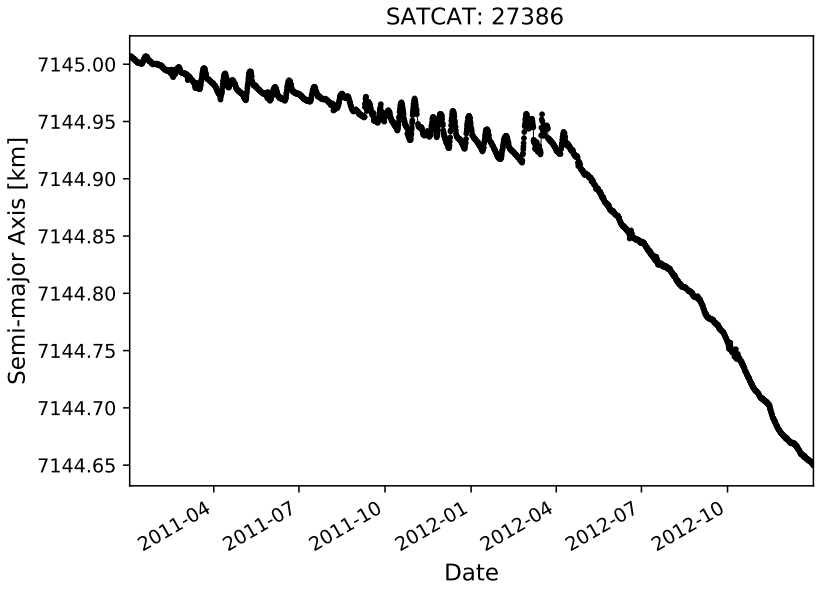

Figure 4.6: Semi-major axis series of Envisat in 2011 and 2012.

However, it can be seen that after April 2012 these maneuvers suddenly stop, they will also not reappear in the following years. This matches exactly with the reported communication by ESA: "Just weeks after celebrating its tenth year in orbit, communication with the Envisat satellite was suddenly lost on 8 April. Following rigorous attempts to re-establish contact and the investigation of failure scenarios, the end of the mission is being declared" [22]. It is exactly this moment, when the operational phase of the mission is over, that is of interest and it shows that for maneuvering satellites this can be determined by detecting these maneuvers.

4.5. Data sources

In this study use will be made of different datasets provided by different sources. For orbital information use will be made of Two Line Element data provided by United States Space Command (USSPACECOM).

4.5.1. Two Line Element Data

The TLE data sets are standardised sets used by the North American Aerospace Defense Command (NORAD) and in the space industry for a long time and the data is published by USSPACECOM. The elements in this data should be considered the mean elements corresponding to a fit using the SGP4 model to observations made. As the name suggests the data consists of two lines, the exact information given in these two lines is shown in Table 4.2.

Table 4.2: Two-line element data columns per line, adapted from https://www.space-track.org [52].

Line	Column	Description	Line	Column	Description
1	1	Line Number	2	1	Line Number
1	3-7	Satellite Catalog Number	2	3-7	Satellite Catalog Number
1	8	Security Classification	2	9-16	Orbit Inclination [deg]
1	10-17	International Designator	2	18-25	RAAN [deg]
1	19-32	Element Set Epoch (UTC)	2	27-33	Eccentricity
1	34-43	1st Derivative of Mean Motion	2	35-42	Argument of Perigee [deg]
1	45-52	2nd Derivative of Mean Motion	2	44-51	Mean Anomaly [deg]
1	54-61	B* Drag Term	2	53-63	Mean Motion [rev/day]
1	63	Element Set Type	2	64-68	Revolution Number at Epoch
1	65-68	Element Number	2	69	Checksum
1	69	Checksum			

As can be seen this data set contains information regarding the orbital state of the object as well as some physical parameters and launch information. The data can be obtained using the aforementioned website, this can be done for an individual object but also groups using filters such as launch date, object type or orbital parameters. Large pre-made sets of different groups exist as well, these allow the user to obtain the most recent TLE for the entire catalog or different subgroups such as LEO or GEO objects. The database can be accessed using software as well by making use of the application programming interface (API).

Simplified General Perturbations Models

The Simplified General Perturbations (SGP) model series are used to determine and propagate the state of objects in orbit around Earth. The first version of this was developed already in the 1960's and consists of the following five models: SGP, SGP4, SDP4, SGP8 and SDP8. The Simplified Deep Space Perturbations (SDP) models are used for deep space missions while the SGP models are suitable for objects in orbits with a period less than 225 minutes.

The SGP4 model has become the leading propagation model and is the one most widely used in research and applications all over the world. This is because this is the model used to generate the mean orbital elements as given in the TLE dataset by NORAD. It is important to note that the results of this is the result of an estimation and are therefore the mean set of orbital elements for a set of observations. It was developed by Ken Cranford, and a complete description and source code in Fortran can be found in the works of Hoots et al. [27] and Vallado et al. [58].

The SGP4 model has an uncertainty of about 1 km at epoch increasing by 1 to 3 km every day [58]. This makes it suitable to propagate between certain TLE time series and a few days ahead, but depending on the application it quickly becomes very inaccurate when attempting to propagate for longer time periods. The SGP4 model takes into account atmospheric drag, gravity effects of the Sun and the Moon, secular and periodic variations due to the oblateness of Earth as well as gravitational resonance effects.

4.5.2. Maneuver Data

For the validation of the maneuver detection algorithm use will be made of maneuver data provided by the International DORIS Service (IDS) and published by the ILRS. The information contained in this dataset is given in Table 4.3. If multiple burns were grouped in a single format they are appended as columns on the right of the file causing the column number to be dependent on the number of burns N. For the application here of interest are mainly the starting dates of the maneuvers.

Table 4.3: Maneuver files format

Column	Description	Column for each N with k = (N-1)*232	Description
1-5	Satellite identification	(47+k)-(50+k)	Median date of maneuver: year
7-10	Start of maneuver: year	(52+k)-(54+k)	Median date of maneuver: day of year
12-14	Start of maneuver: day of year	(56+k)-(57+k)	Median date of maneuver: hour
16-17	Start of maneuver: hour	(59+k)-(60+k)	Median date of maneuver: minute
19-20	Start of maneuver: minute	(62+k)-(67+k)	Median date of maneuver: second
22-25	End of maneuver: year	(69+k)-(88+k)	Boost duration [s]
27-29	End of maneuver: day of year	(90+k)-(109+k)	dV(1) [m/s]
31-32	End of maneuver: hour	(111+k)-(130+k)	dV(2) [m/s]
34-35	End of maneuver: minute	(132+k)-(151+k)	dV(3) [m/s]
37-39	Maneuver type	(153+k)-(172+k)	Acceleration, acc(1) [10-6m/s^2]
41-43	Maneuver parameter	(174+k)-(193+k)	Acceleration, acc(2) [10-6m/s^2]
45	Number of burns (N)	(195+k)-(214+k)	Acceleration, acc(3) [10-6m/s^2]
		(216+k)-(235+k)	Delta acc(1) w.r.t. prediction [10-6m/s2]
		(237+k)-(256+k)	Delta acc(2) w.r.t. prediction [10-6m/s2]
		(258+k)-(277+k)	Delta acc(3) w.r.t. prediction [10-6m/s2]

4.5.3. Satellite Property Data

For information regarding spacecraft information and description the Database and Information System Characterising Objects in Space (DISCOS) was used. This database is maintained by ESA's Space Debris Office and provides information for all trackable unclassified objects in space. Operational since 1990 it contains more than 39000 objects and contains information regarding [24]:

- Launch information
- Launch vehicle description
- Object size
- Object mass
- Object shape
- Mission objectives
- Owner
- Orbital Data History

Table 4.4: Data example using DISCOS for the Delfi satellites; not all available information is shown.

ID	Name	SATNO	COSPAR ID	Class	Mass [kg]	Area [m^2]	Operator	Country
32786	Delfi-C3	32789	2008-021G	Payload	3	0.035	TU Delft	Netherlands
39425	Delfi-n3xt	39428	2013-066N	Payload	3	0.035	TU Delft	Netherlands

The database can be accessed with a registered Space Debris User Account at `https://discosweb.esoc.esa.int/`. This can be accessed by software as well using the DISCOSweb API.

5

Maneuver Detection

The detection of maneuvers allows the determination of the operational status for spacecraft with orbital maneuver capabilities. The developed detection algorithm is based on the ideas and recommendations of previous studies that were discussed in Chapter 4. It is primarily based on the fundamental ideas of the TLE Time Series Analysis (TTSA) algorithm by Lemmens and Krag [37]. Together with some additions, such as a user set global threshold acting as a sensitivity setting and a "grace period" during event detection, modifications and omissions, the goal was to not only develop a robust and reliable algorithm but also one that is adaptable and transparent in its implementation.
This chapter will show and discuss the developed algorithm which takes a semi-major axis time series which was generated from TLE data and returns the dates of detected maneuvers. In general it can be summarised in the following steps:

1. Using a moving window, the semi-major axis series is corrected by a line fitted using repeated median regression with a Theil-Sen-Siegel estimator.
2. Based on the interquartile range of this corrected series, a global minimum lower and upper threshold is determined for the entire series.
3. A moving window is used to generate a local lower and upper threshold per epoch based on the interquartile range.
4. Using a Lomb-periodogram the possible presence of harmonics within the window is detected. The amplitude of this harmonic is then added to the local threshold. The final threshold used for each epoch is the largest of the global and local threshold and a fixed set minimum value.
5. Maneuvers are detected by checking the corrected series for events exceeding these thresholds.

During development, use was mainly made of the two test cases Envisat and SARAL. Other satellites were used as well, both during development and for illustrative purposes in this chapter. These other satellites were either discussed in reference literature or showed interesting behaviour. As stated above, the maneuver detection algorithm is made out of distinct steps. The first step determines the slope caused by the natural orbital decay and corrects for this, this is discussed in Section 5.1. The generation of the threshold time series for both the entire series and in a local window can be found in Section 5.2. Section 5.3 shows the method of finding the events where the thresholds are exceeded. Finally, the performance of the algorithm is reviewed in Section 5.5.

5.1. Linear Slope Correction

Due to the effect of perturbations, the semi-major axis of a satellite in Sun-synchronous orbit will decrease over time in absence of any maneuvers. Too more clearly distinct this natural decay from maneuvers, this is corrected for by fitting a line and subtracting this from the original data. Although the actual observed long-term effect of this natural decay is not linear, it was found that over short timeframes, such as one or two months, it was sufficient to model it as one.

5.1.1. Theil-Sen-Siegel Estimator

This line fitting could be done naively by just taking the difference between two consecutive points. However, this would be very susceptible to data outliers and noise and would work poorly when maneuvers take multiple TLE epochs to become fully visible.

Therefore, a more robust method was chosen by making use of repeated median regression using the Theil-Sen Siegel Estimator to determine the slope and intercept of the regression line $y = mx + b$. This is a variant of the Theil-Sen estimator for the slope m which is given in Equation 5.1 [53] [50]:

$$m = median\left\{\frac{y_j - y_i}{x_j - x_i}\right\} \quad \text{for all } i \neq j \tag{5.1}$$

and intercept b is determined by:

$$b = median\{y\} - m \cdot median\{x\} \tag{5.2}$$

The breakdown point of an estimator is the percentage of incorrect input data the estimator can process while still giving the desired result. This estimator is already robust against outliers with a breakdown point of 29.3 %. However, this can be improved to 50% when using the repeated median regression variation by Siegel [51], shown in Equation 5.3:

$$m = \underset{i}{median}\left(\underset{i \neq j}{median}\left\{\frac{y_j - y_i}{x_j - x_i}\right\}\right) \tag{5.3}$$

with intercept b determined by Equation 5.4 [51].

$$b = \underset{i}{median}\left(\underset{i \neq j}{median}\left\{\frac{x_j y_i - x_i y_j}{x_j - x_i}\right\}\right) \tag{5.4}$$

The effect of this variation can be seen in Figure 5.1, where these two methods are shown together with a linear fit using a least squares estimator. Here random points were generated with a standard normal distribution variation along $y = x$ and outliers were added near the start and end of the series.

It can be seen that the Theil-Sen-Siegel method manages to best ignore the outliers and produce the most accurate slope and intercept and was therefore chosen as the estimator.

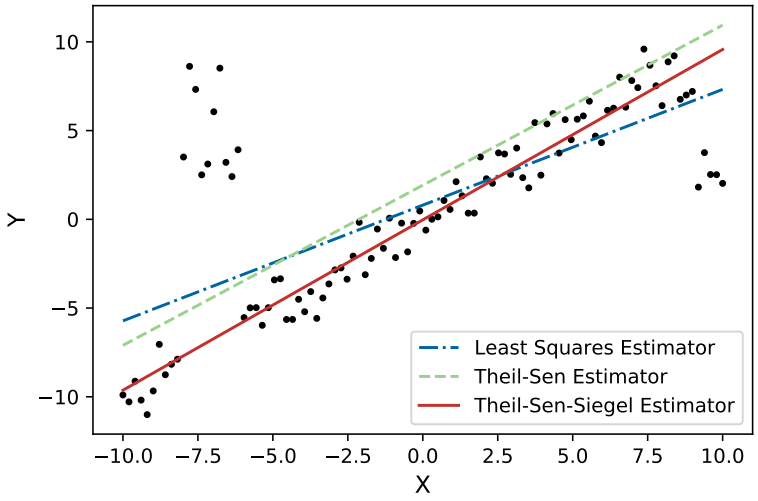

Figure 5.1: Comparison of a line fitted using three different regression methods.

5.1.2. Corrected Series

A moving window is run trough the original semi-major axis time series, and assigns a value corresponding to the original data minus the corresponding value of the fitted line. Done to the entire series it attempts to zero all data except for the maneuvers. The effect of this can be seen for SARAL in Figures 5.2 and 5.3.

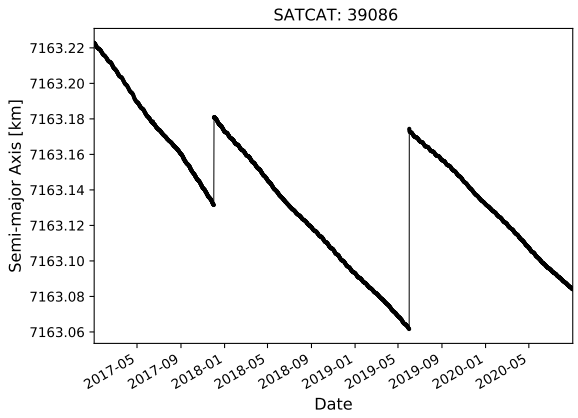

Figure 5.2: Semi-major axis series of SARAL since 2017.

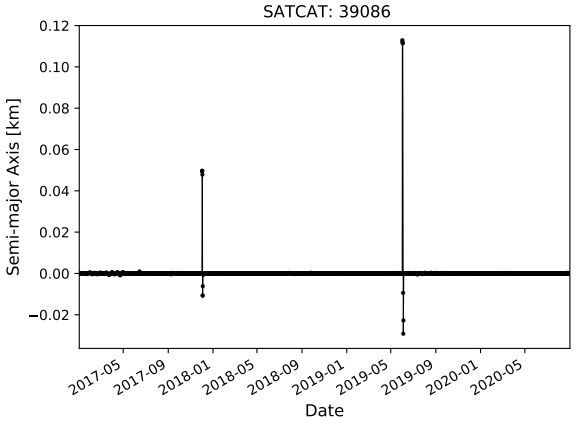

Figure 5.3: Corrected semi-major axis series of SARAL since 2017.

For the window size it was found that it should be at least an order of magnitude larger than the time between TLE's. However, if it is set too large it will not work properly when multiple maneuvers are performed quickly after another such as can be seen in Figures 5.4 and 5.5.

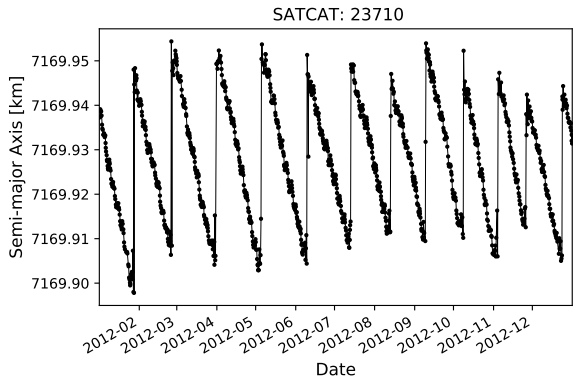

Figure 5.4: Semi-major axis series of SATCAT 23710 in 2012 before slope correction.

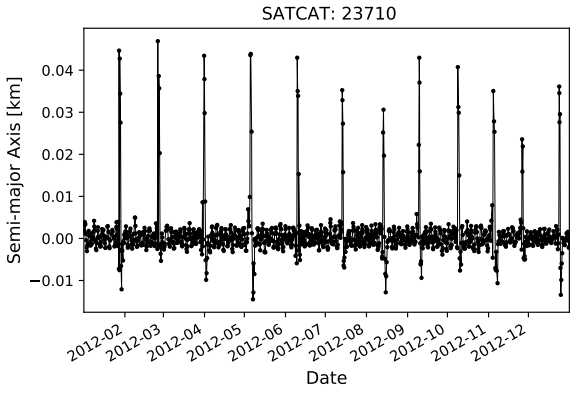

Figure 5.5: Slope corrected semi-major axis series of SATCAT 23710 in 2012.

So far the time series that were shown had clearly visible maneuvers, but this is not always the case. Especially when noisy data is combined with very small maneuvers it becomes very difficult to distinguish between the two. Envisat for example was found to perform many very small maneuvers with a change in semi-major axis of tens or even single meters magnitude. This is shown for 2008 in Figures 5.6 and 5.7.

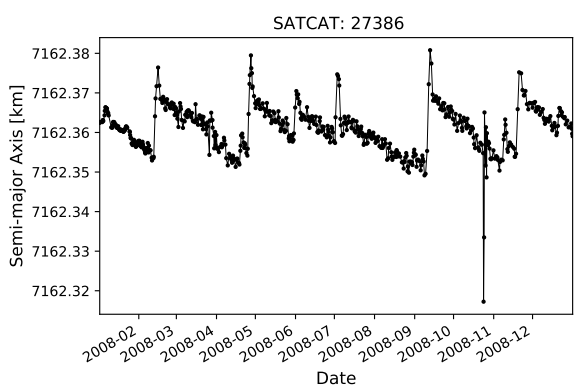

Figure 5.6: Semi-major axis series of Envisat in 2008 before slope correction.

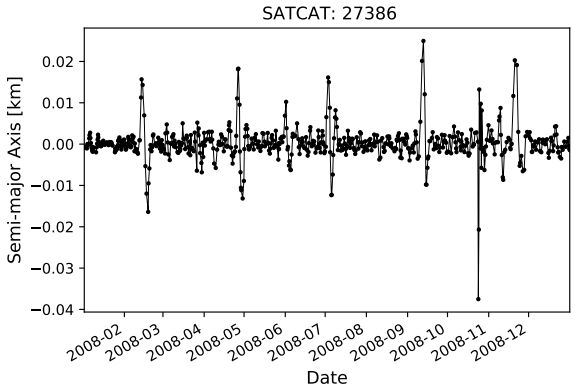

Figure 5.7: Slope corrected semi-major axis series of Envisat in 2008.

5.2. Threshold Generation

To be able to distinguish the maneuvers from the noise, lower and upper thresholds were constructed. Maneuver events would be indicated by violations of these thresholds. As was already seen, if one wants to detect these small maneuvers these threshold have to be quite tight. Furthermore, the distribution, or deviation of this noise differs greatly per satellite. Not only that, but as will be seen it will also vary over time for a single satellite. It was therefore decided to use a combination of global, where the entire available series is considered, and local, using a moving window, methods to construct these thresholds.

5.2.1. Interquartile Range

The first main component of the generated threshold is the use of the interquartile range (IQR). This was chosen instead of using the standard deviation as it is more robust against outliers [46].

The IQR of a dataset can be determined by:

$$IQR = Q_3 - Q_1 \tag{5.5}$$

where:

$$Q_1 = median\{\text{first half of the sorted data set}\} \tag{5.6}$$

and

$$Q_3 = median\{\text{second half of the sorted data set}\} \tag{5.7}$$

Therefore Q_3 is always bigger than Q_1 and the IQR is the distance between the two and therefore always positive. These were then used to construct the global upper and lower thresholds for the entire series per satellite:

$$T_{\text{upper}}^{\text{global}} = Q3 + IQR \tag{5.8}$$

$$T_{\text{lower}}^{\text{global}} = Q1 - IQR \tag{5.9}$$

To determine the local thresholds, $T_{\text{upper}}^{\text{local}}$ and $T_{\text{lower}}^{\text{local}}$, the exact same methods were used but now instead of the entire series just a subset was considered. This was once again done using a moving window approach but this window was set to be two orders of magnitude larger than the time between TLE's. By doing so it was found to provide a large enough window to construct the IQR even when maneuvering rapidly and still small enough to be affected by structural changes over time.

Besides these global and local thresholds a user-set minimum threshold was included as well. This can be considered as a sensitivity setting and was implemented as it was found that the filter would sometimes settle too tightly when the data was relatively calm and then when the noise suddenly spiked it would cause detection problems. For each epoch for both the lower and upper threshold the largest of the three values is chosen:

$$T_{\text{upper}} = max\left\{ T_{\text{upper}}^{\text{global}},\ T_{\text{upper}}^{\text{local}},\ T_{\text{upper}}^{\text{user}} \right\} \tag{5.10}$$

$$T_{\text{lower}} = min\left\{ T_{\text{lower}}^{\text{global}},\ T_{\text{lower}}^{\text{local}},\ T_{\text{lower}}^{\text{user}} \right\} \tag{5.11}$$

This threshold generation is therefore dynamic and dependent on the input data. Allowing the thresholds to remain constantly low when the data is consistent such as for Envisat in 2008 shown in Figure 5.8 and expand when the data is more noisy, as in the case of SATCAT 15427 in 2001 shown in Figure 5.9. It was seen that this increase in noise is related to the solar cycles, this will be discussed more in the next chapter.

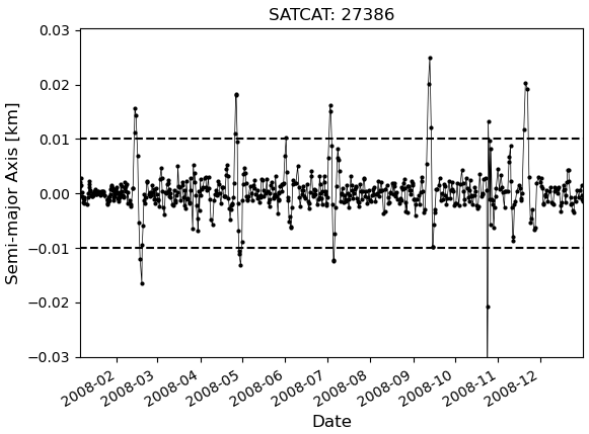

Figure 5.8: Threshold generated for Envisat in 2008, using a user set minimum of 10 m.

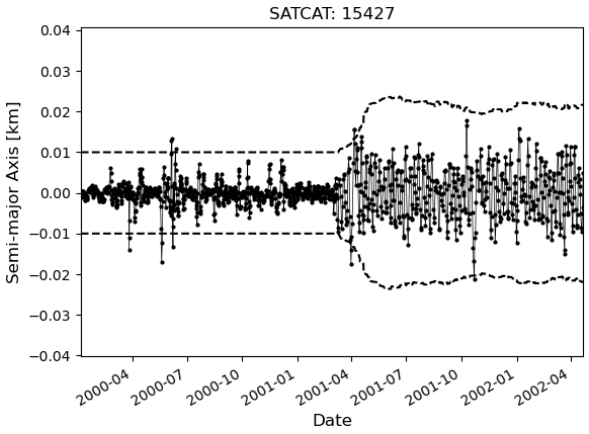

Figure 5.9: Threshold generated for SATCAT 15427, using a user set minimum of 10 m.

5.2.2. Harmonic Analysis

In the semi-major axis series of multiple spacecraft, oscillations of variable magnitudes were observed. For some spacecraft these oscillations had a large amplitude while for some they were only small or not visible at all. Although the exact cause of this harmonic behaviour is unclear, it is likely an artefact of the process by which these TLE's, from which the semi-major axis series was obtained, were constructed due to the J_2 induced long-period oscillation. This is namely a fitting process resulting in a mean element set based on multiple observations. An example of this behaviour is shown in Figure 5.10.

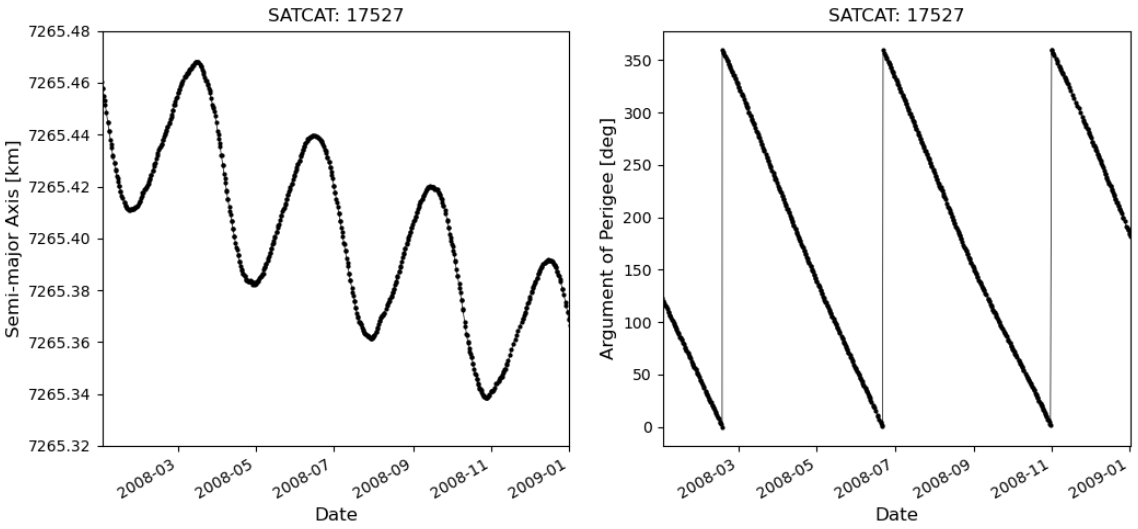

Figure 5.10: Oscillations in the semi-major axis series and argument of perigee of SATCAT 17527.

To confirm, what is seen are not multiple successive long-duration maneuvers with for example electric propulsion. The spacecraft identified as SATCAT 17527, known as Marine Observation Satellite-1, was decommissioned already in 1995. The amplitude of this oscillation is rather large, especially when compared to the small-magnitude maneuvers that were observed earlier. Therefore, the amplitude of this oscillation was determined using the Lomb–Scargle periodogram method as it can find harmonic signals in data with uneven temporal sampling [39] [49].

To improve calculation performance a variation introduced by Townsend [54] was used. For a series of N_t data points $X_j \equiv X(t_j)$, which is sampled at times $t_j (j = 1...N_t)$ the periodogram at frequency f can be determined by [54]:

$$P_n(f) = \frac{1}{2}\left[\frac{(c_\tau XC + s_\tau XS)^2}{c_\tau^2 CC + 2c_\tau s_\tau CS + s_\tau^2 SS} + \frac{(c_\tau XS - s_\tau XC)^2}{c_\tau^2 SS - 2c_\tau s_\tau CS + s_\tau^2 CC}\right] \tag{5.12}$$

$$\tan 2\omega\tau = \frac{2CS}{CC - SS} \tag{5.13}$$

where $\omega \equiv 2\pi f$ is the angular frequency and c_τ and s_τ are defined as:

$$c_\tau = \cos\omega\tau, \qquad s_\tau = \sin\omega\tau \tag{5.14}$$

while the sums, all running from $j = 1$ to $j = N_t$ are [54]:

$$XC = \sum_j X_j \cos\omega t_j \qquad CC = \sum_j \cos^2\omega t_j \tag{5.15}$$

$$XS = \sum_j X_j \sin\omega t_j \qquad SS = \sum_j \sin^2\omega t_j \tag{5.16}$$

$$CS = \sum_j \cos\omega t_j \sin\omega t_j \tag{5.17}$$

$$\tag{5.18}$$

This was applied on the slope-corrected semi-major axis series. The amplitude A can be found by:

$$A = \sqrt{\frac{4 * P_{\max}}{N_t}} \tag{5.19}$$

where $P_{\max}$ is the maximum power found in the Lomb-Scargle periodogram. The frequency can be obtained directly as the frequency of $P_{\max}$. Figure 5.11 shows the corrected semi-major axis series in the top and the corresponding periodogram in the bottom figure for the SATCAT 17527 example. A harmonic with an amplitude of 0.0325 km and a period of 92.8 days was found, which is in line with the observed period of the argument of perigee in Figure 5.10. To show how well this matches with the data the detected harmonic is shown in blue. This harmonic analysis is done in a moving-window approach with a window size of 200 days. If such an harmonic is found this amplitude is added to the generated threshold.

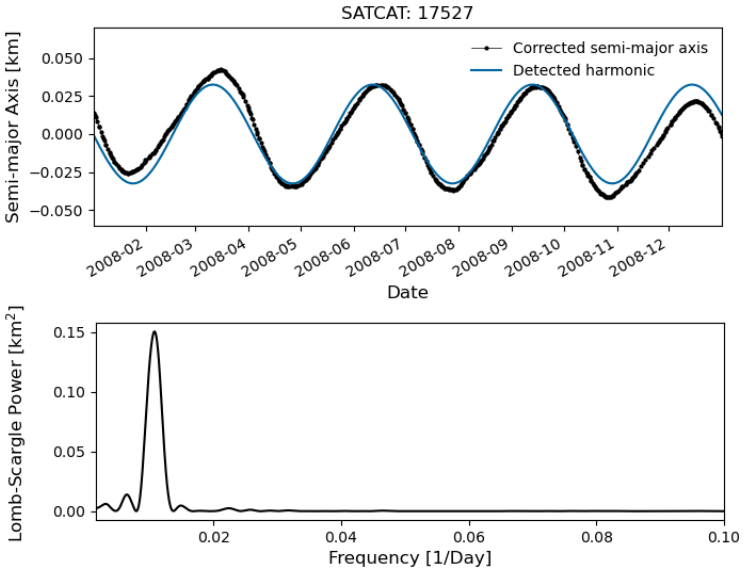

Figure 5.11: Top figure shows the corrected semi-major axis of SATCAT 17527 and the constructed detected harmonic, the bottom figure shows the corresponding Lomb-Scargle periodogram.

5.3. Event Detection

Finally for the actual event detection, each epoch is checked successively if its value exceeds either of its corresponding generated thresholds. If this is the case it is marked as a potential maneuver event. To be classified as an actual maneuver however, at least three consecutive epochs have to exceed their threshold values. This is to prevent large noisy outliers triggering a detection.

As an addition to the TTSA algorithm a "grace period" was added as well to reduce the chance of detecting the same maneuver as has happened in Figure 5.12. Here the blue lines mark the detected maneuvers, and as can be seen it has found three maneuvers while in reality it was only a single one. This can be explained when looking in the corresponding corrected series with threshold in Figure 5.14. It can be seen that after the lower threshold is exceeded for multiple epochs in a row a maneuver detection is triggered. This is stopped however when the values return to within the thresholds but immediately after exceed the upper threshold.

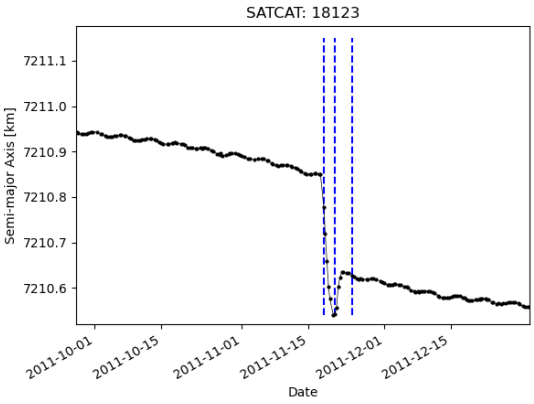

Figure 5.12: Example of false positives in SATCAT 18123 before the grace period was added: 3 apparent detected maneuvers.

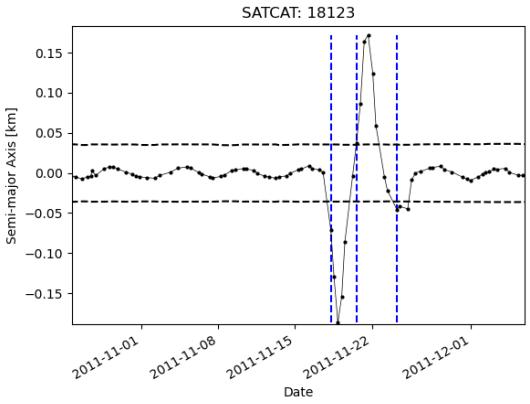

Figure 5.13: false positives in SATCAT 18123 before the grace period was added: 3 apparent detected maneuvers.

To prevent this, a grace period of two epochs was added. Meaning that after a maneuver is triggered it is allowed to return to within the thresholds for a maximum of two epochs. If after those two epochs it exceeds the thresholds again a new maneuver is not triggered but instead it is assumed to still correspond to the previous one. This resolves the previously mentioned false detections as seen in Figure 5.13.

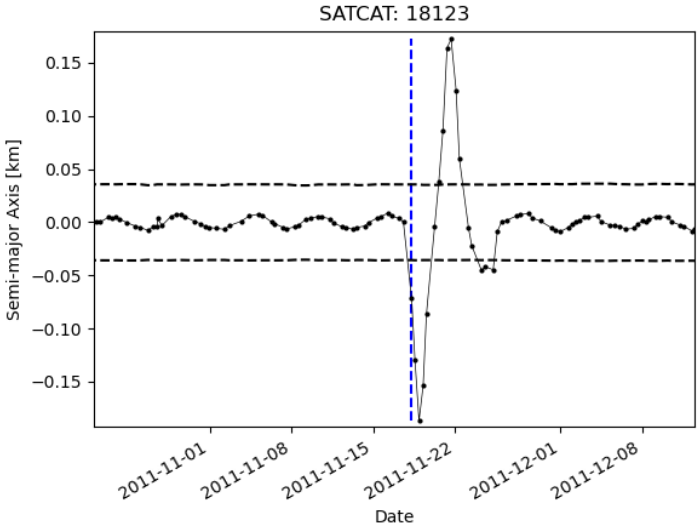

Figure 5.14: Resolved false positives SATCAT 18123 after the grace period was added: only 1 maneuver detected.

5.4. Performance with parameter tuning

To test the performance of the implemented algorithm it was compared with the TLE Time Series Analysis (TTSA) and the TLE Consistency Check (TCC) algorithms by Lemmens and Krag [37] and actual observed maneuvers. In their study 30 satellites operating in SSO were manually checked for existing maneuvers in 2011. These were then compared with the detections made by the two algorithms. These satellites are all meteorological satellites operating in Sun-synchronous orbit (SATCAT 15427, 16969, 17527, 18123, 18822, 19467, 19531, 20788, 20978, 21263, 21574, 22739, 22823, 23455, 23710, 23751, 25338, 25682, 25730, 25756, 25757, 25758, 25940, 25994, 26536, 26620, 27386, 27421, 27424, 27430).

The performance of the implemented algorithm was tested using three different sensitivity settings by changing the user-set global minimum threshold. The results for these three settings, the performance of the two reference algorithms and the actual number of maneuvers can be found in Table 5.1. Shown in the table are only the satellites that were found to have actual maneuvers, or where one of the algorithms detected one.

Table 5.1: Detected maneuvers for different minimum threshold limits compared to literature and the actual performed maneuvers as manually identified.

	Reference Literature [37]			**Algorithm Performance**		
SATCAT	**Human**	**TCC**	**TTSA**	**Limit = 5m**	**Limit = 7.5m**	**Limit = 10m**
15427	0	2	0	0	0	0
18123	1	1	1	3	3	3
19531	0	2	0	0	0	0
21263	1	1	1	1	1	1
21574	0	0	0	1	0	0
22739	0	4	0	2	1	0
23710	12	12	10	16	14	11
25682	16	15	11	26	28	25
25730	0	0	4	4	4	0
25994	8	8	7	17	18	17
26536	0	7	1	0	0	0
26620	3	3	3	6	3	5
27386	19	8	6	10	4	0
27421	6	7	7	9	10	9
27424	13	16	17	22	24	21

The results can be categorised in maneuvering and non-maneuvering satellites, coming with it are two types of errors. The first are called false positives, where a satellite is concluded to have performed a maneuver, while in reality it has not. False negatives are the opposite, here the algorithm has classified a satellite as not maneuvering while it actually has performed at least one. This classification is shown in Table 5.2.

Table 5.2: Performance and errors classified by type of the maneuver detection algorithm for different minimum threshold limits compared to literature.

	Reference Literature [37]			**Algorithm Performance**		
	Human	**TCC**	**TTSA**	**Limit = 5m**	**Limit = 7.5m**	**Limit = 10m**
Total Satellites	30	30	30	30	30	30
-Maneuvering	9	13	11	12	11	9
-Not Maneuvering	21	17	19	18	19	21
False Positives		4	2	3	2	0
-Percentage Total		13.3%	6.7%	10.0%	6.7%	0.0%
False Negatives		0	0	0	0	1
-Percentage Total		0.0%	0.0%	0.0%	0.0%	3.3%

It can be seen that the number of false positives decreases and false negatives increases as the limit is set to higher values. This is as expected, as this limit value can be interpreted as a sensitivity setting below which the data, and thus possible small maneuvers are ignored. Furthermore, it shows that the implemented algorithm performs better than the TCC and on-par with the TTSA algorithms. Finally, when going from 7.5 m to a limit of 10 m the first false negative was shown. This mean that using such a large limit would mean that a satellite that is actually maneuvering is not detected as such.

False positives versus false negatives

Naturally one wants to keep both false positives and false negatives to a minimum. However, often one is vastly preferred over the other. In this case it is more unclear, as one could favour either one depending on the exact purpose. If one wants to detect every maneuver a satellite makes it would make sense to make the algorithm very sensitive by making use of a low minimum threshold. This would come at the cost of detecting some maneuvers that have not actually happened.

For the purposes of this study this is not the goal. The goal is to detect if a spacecraft has ever maneuvered and when it stopped doing so. Because there is such a long timeframe to analyse and detect possible maneuvers, the chance is increased that maneuvers are being detected somewhere and a spacecraft is wrongly designated to be still maneuvering while in reality it has long ago stopped doing so. It is therefore beneficial to use a higher minimum threshold and miss some small maneuvers. This strengthened further by the fact that large maneuvers are easier to detect and small maneuvers are often done with a frequency, this is also visible in Envisat and SARAL. It does not, for the purpose of this study, matter if one maneuver that was performed in a month is missed if two others in the same month are detected. Therefore ultimately the 10 meter limit was chosen.

5.5. Validation

The first part of the validation was already included in the tuning as was shown in the previous section. The second test is a comparison of the detected maneuvers of the two development cases SARAL and Envisat with their actual maneuvers as reported by the ILRS.

5.5.1. Test Cases

Using these settings the test cases were evaluated and compared with their actual maneuver data as reported by the ILRS. In the following figures, the reported maneuver dates are indicated by a vertical red line while the detected maneuver dates are shown in blue. For Envisat this is shown on the corrected time series in Figure 5.15.

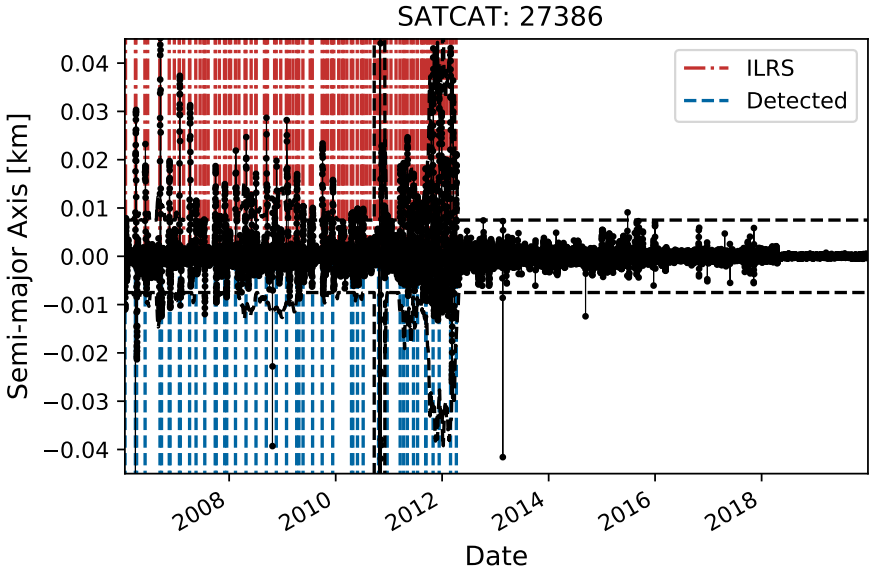

Figure 5.15: Detected and actual maneuvers of Envisat as reported by the ILRS.

Since the figures shows such a large timeframe details are hard to distinguish, but already it can be seen that the algorithm manages to detect the date of the last maneuver quite accurately. It also manages to detect many of the actual maneuvers done. The ultimate purpose of this algorithm should also be kept in mind as it affects the required accuracy. It does not matter if the last detected maneuver date is a day, a week or even a month off. To get a better view the detected and actual maneuvers are also shown on the semi-major axis time series. To get sufficient detail in the figure it is split in two, to not include the year with the very large orbital maneuver, resulting in Figures 5.16 and 5.17.

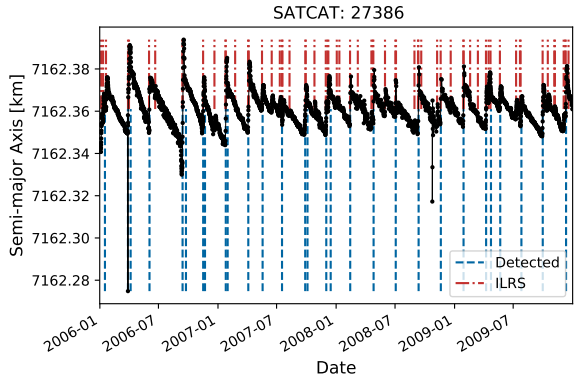

Figure 5.16: Detected and actual maneuvers of Envisat as reported by the ILRS.

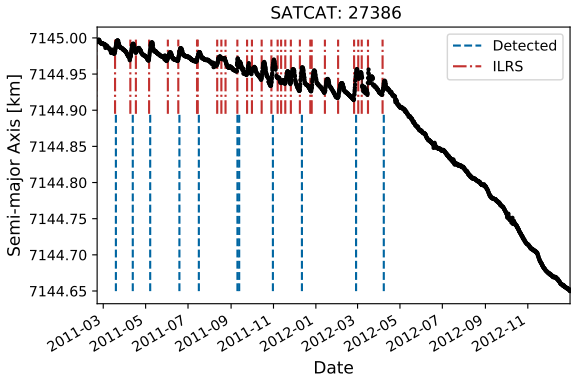

Figure 5.17: Detected and actual maneuvers of Envisat as reported by the ILRS.

The same can be done for SARAL, shown in Figure 5.18, once again the reported maneuvers are in red and the detected maneuvers are in blue.

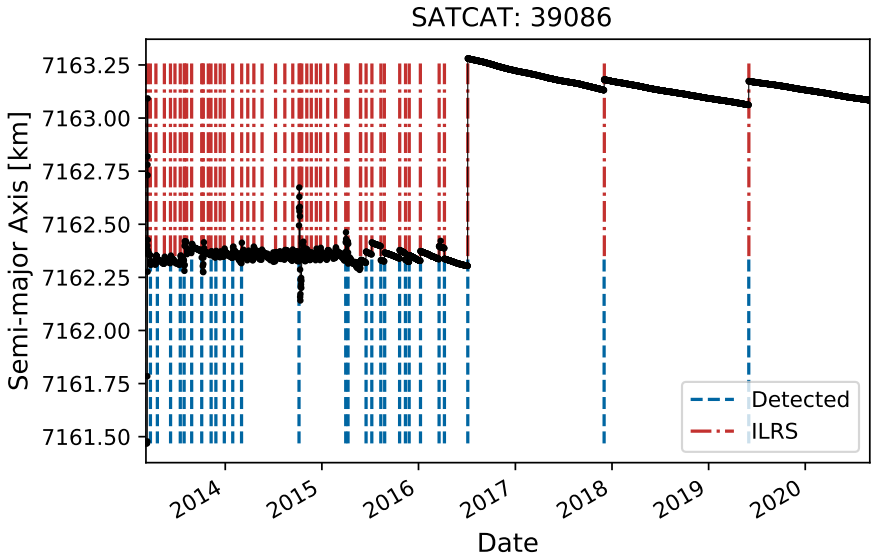

Figure 5.18: Detected and actual maneuvers of SARAL as reported by the ILRS before 2017.

From these figures several conclusions can be drawn. First of all, the algorithm manages to detect the date of the latest maneuver with sufficient accuracy. Secondly, when the orbital maneuvers are large, such as significant orbital lowering end-of-life maneuvers, the algorithm has no problem detecting them. However, when maneuvers are very small in magnitude, and especially when these are done rapidly, the algorithm struggles to detect them. This is because it is very difficult to distinguish this from being just noisy data.

6

Operational Status Determination

Determining the operational status of a spacecraft is the first half of being able to determine its compliance with the 25 year lifetime rule. This chapter describes how this determination was done. With the detection of maneuvers it is possible to determine the operational status of the spacecraft with orbital control capabilities, this can be found in Section 6.1. Afterwards, in Section 6.2, the spacecraft that did not have any detected maneuvers will be discussed. The results will then be combined to determine the overall operational status of the entire SSO satellite population in Section 6.3.

6.1. Maneuver Based

The maneuver detection algorithm was applied to all satellites in SSO including all published TLE data until January 1, 2021. For each satellite the detected maneuver dates were recorded. An overview of the result of this can be found in Figure 6.1. Shown here in the bottom part are the satellites that maneuvered in a given year, grouped by their launch year. Above that the solar flux density at 10.7 cm wavelength for the same period is given.

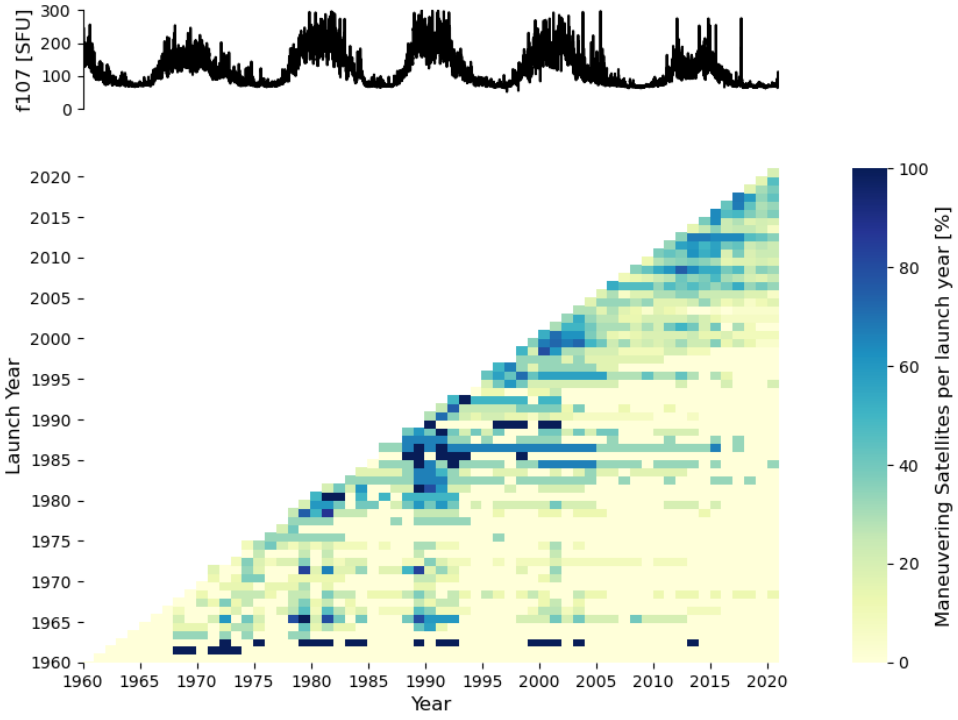

Figure 6.1: Top: Solar flux density at 10.7cm wavelength.
Bottom: Maneuver matrix grouped by launch year colored by percentage of satellites that maneuvered.

One would expect in this figure that the diagonal would show the highest percentage. As time goes by, this would be the horizontal direction in the figure, and satellites stop functioning and maneuvering one would expect to see a slow fade to the right, to zero maneuvering satellites.

In general, this is also what is observed. However, Figure 6.1 appears to have some vertical bands where an increase in detected maneuvers appears. These bands correlate with the 11-year solar cycle as shown above the heatmap. This can be explained by two possible causes. The first possible contribution is that the increase in drag prompts satellite operators to perform altitude increasing maneuvers. The second one is that the increase in strength of the solar radio emission causes an increase in density which causes a change in slope of the natural decay. Which is then incorrectly interpreted as the detection of an maneuver. As is the case with a satellite launched in 1963, which has no maneuvers for the first 10 years but which has detected maneuvers every cycle even in 2014. This indicates that these detected maneuvers during these cycles are falsely identified.

These bands are more visible in the earlier cycles than in the recent ones. This has two reasons; first it can be seen that the past solar cycle has a distinct smaller maximum magnitude than the previous three. Secondly, it was observed that over time the data from the TLE has become more consistent and less noisy. This is likely due to improved models, and more accurate measurement data.

To prevent these false positives during these cycles a filter was applied to the detected maneuver. If a satellite has maneuvered in the past two years this filter classifies the satellite as active. If at one time, the satellite has not performed a maneuver in the past two years it is classified as inactive. Once inactive the satellite is not reclassified, even if a maneuver is detected for instance 10 years later. This two-year limit was chosen as it provides a long enough timeframe for a satellite maneuver to be detected. Although due to the large dataset not all spacecraft were checked, an interval between two maneuvers of more than 1.5 years was never observed. The resultant activity matrix is shown shown in Figure 6.2.

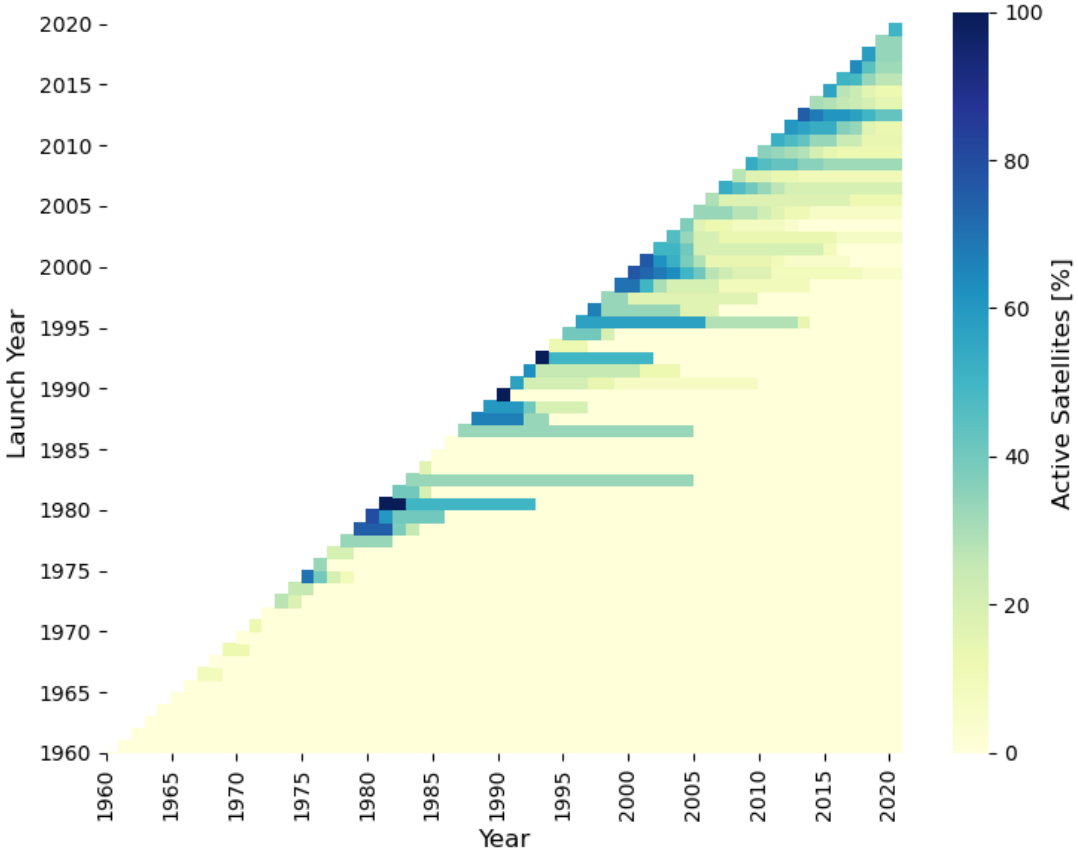

Figure 6.2: Active satellite matrix with the two-year maneuver filter.

With this classification the operational status situation as it was on January 1, 2021 can be shown. This can be interpreted as a vertical slice just to the right of Figure 6.2. This is displayed in Figure 6.3 and shows

in blue satellites for which no maneuvers were detected. In green and red it shows satellites that maneuvered and are classified to either be operational and still maneuvering, or not operational if they stopped doing so. The satellites that have not yet had any maneuvers detected, but no two years have passed since launch, are colored yellow and classified as unknown.

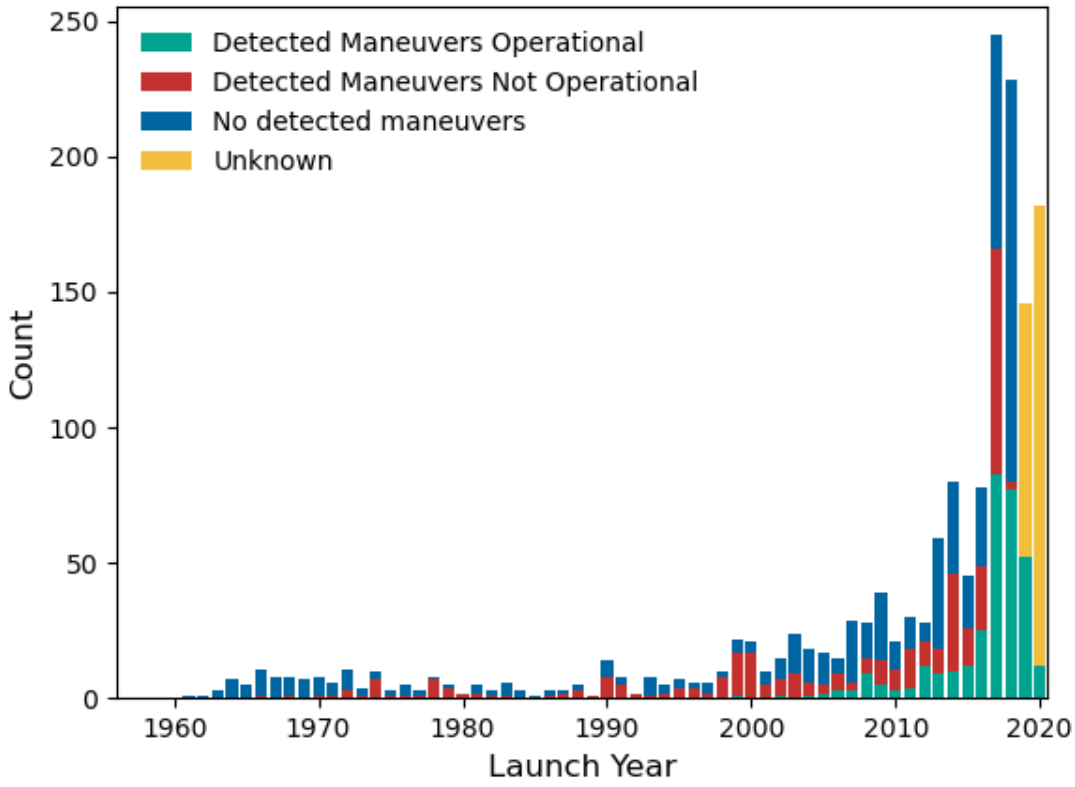

Figure 6.3: Detection of maneuvers and operational status of spacecraft with detected maneuvers on January 1, 2021.

The drop in spacecraft with detected maneuvers and still operational in the recent two years is expected. The maneuver detection requires at least three months of data, so operational spacecraft launched too recently are unable to be assessed as such.

This concludes the determination of the operational status for the maneuvering satellites, the classification of satellites that had no maneuvers detected will be discussed next.

6.2. Non Maneuver Based

It might be trivial to state but the methods using the TLE data to detect orbital maneuvers, and therefore an operational status of a satellite, of course only works if such an orbital control system is present. Therefore for satellites without such a system, as is the case for many of the small satellites in LEO, an alternative method must be used.

The most accurate would be making use of reports published by the operators regarding the operational state of their satellites. However, as was stated earlier, these reports do not always exist and if they were to be used for compliance registration might not be accurate as well. One major indicator of operational status would be the existence of a radio signal from that satellite. There could be a system, either on the ground or in space, that would pick up all these signals and identify them. With this it might be possible to create an overview of the operational status for all spacecraft orbiting Earth with a high temporal resolution.

However, currently such a system does not exist, and no system is in place to register the operational status. Without being able to detect it via orbital maneuvers there is at this moment no alternative way to do so. For this group of satellites alternative methods will have to be applied, based on statistical lifetime models. A method would be to use a statistical distribution for orbital lifetime, using reference spacecraft populations with similar characteristics. Although this might work fine when multiple spacecraft of the same

type are launched, as is the case for upcoming constellations, this might not work as accurately for individual satellites.

A variation of this method was used by Morand et al. [42]. In this study a published end-of-mission date was looked up for non-maneuverable satellites and if none was found the following durations were assumed [42]:

- Cubesats: 1 year.
- COSMOS Satellites: 4 years.
- Molniya and ORBCOMM FM Satellites: 10 years.
- UNISAT and MEGASAT Satellites: 3 years.

Thereby making a distinction based on the mass and mission type of the satellite. Creating an advanced statistical model based on satellite and mission properties would take a significant effort and is therefore considered to be outside the scope of this research. Instead a more simple approach is taken and a distinction is made solely on the mass of the spacecraft.

6.2.1. Mass based model

To determine the assigned operational lifetime based on mass two approaches were considered. The first approach would be to make use of the results of the maneuver-based operational status and look at the satellites that have turned into non-operational status. By taking the time between the last operational date and the launch date one could determine the operational lifetime. However, this has the major downside that it will give a significant underestimation of the expected lifetime as still-operating satellites are not taken into account.

Therefore the approach chosen was to make use of the design lifetime of the satellites. The information was obtained from literature [40] [25] and is displayed per mass category in Figure 6.4.

It can be seen that the distributions vary per mass category, with increasing lifetimes with increasing mass. One explanation is that smaller spacecraft tend to perform a simpler and shorter duration mission. Furthermore, the total cost of the mission of the spacecraft increases with increasing mass. It would therefore require an higher operational lifetime to make it commercially viable. Satellites with a mass between 100 and 1000 kg show the most varying design lifetime with 3, 5, 8 and 15 years as the most popular choices.

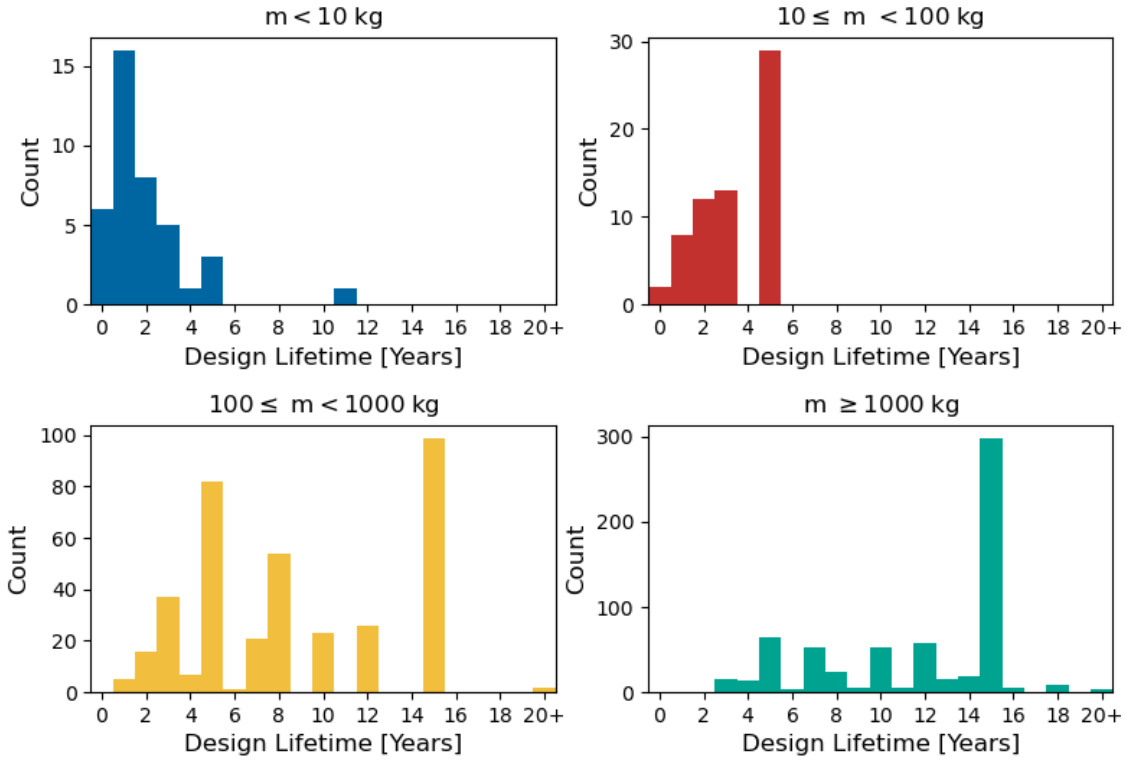

Figure 6.4: Design lifetime of a spacecraft for four different mass categories.

For the different mass categories the mean, median, mode and standard deviation of their design lifetime can be found in Table 6.1.

Table 6.1: Design lifetime in years per mass category.

		Design Lifetime [Years]			
Mass Category	**Database Count**	**Mean**	**Median**	**Mode**	**Standard Deviation**
m< 10 kg	40	2.0	1.3	1	1.9
10 ≤ m < 100 kg	64	3.4	3.0	5	1.6
100 ≤ m< 1000 kg	373	8.7	8.0	15	4.7
m ≥ 1000 kg	647	11.8	14.0	15	4.1

The number of satellites with a mass below 10 kg is relatively small in this design lifetime dataset, however cross-referencing the Nanosats Database [34] shows similar results. Based on the distribution above a single operational lifetime was chosen per mass category. This is shown in Table 6.2. This operational lifetime will be used for satellites without maneuver capabilities.

Table 6.2: Chosen operational lifetimes for satellites without maneuver capabilities for the different mass categories.

Mass Category	**Representative Operational Lifetime [Years]**
m< 10 kg	2
10 ≤ m < 100 kg	4
100 ≤ m< 1000 kg	9
m ≥ 1000 kg	12

As was seen, this can change significantly on individual basis, especially for the two heavier categories, but will give a good representation of the population as a whole. This method of assigning a fixed lifetime for each mass category was preferred over a fitted function depending on the mass, as it would allow for easier and more transparent analysis of the results. The impact of the choices made will be addressed in the discussion of the results in Chapter 8.

6.3. Combined Population

The results of the maneuver-based and non maneuver-based operational status determination can be combined to generate results for the entire population of satellites in SSO. The combined operational status can be classified in three different ways:

- *Operational*, if the satellite has maneuvered within the last two years or if it never maneuvered and is still within the design lifetime.
- *Not Operational*, if the satellite has stopped maneuvering for the last two years or if it never maneuvered and is outside the design lifetime.
- *Unknown*, if the satellite has not maneuvered and was launched in the past two years.

The resultant combined operational status determination can be found in Figure 6.5.

It can be seen that the majority of the satellites that are still operational were launched in the second half of the past decade. For the determination of compliance the ones that are classified as unknown will be considered to be still operational. This is because these satellites, by definition, have been launched within the past two years. This means that they would be within the design lifetime of all different mass categories shown in Table 6.2.

In the figure a large group of satellites with detected maneuvers, but not operational anymore, can be observed in 2017. Further investigations showed that almost all satellites in this group are from a single launch of Dove satellites by Planet Lab on the 14th July, 2017. Almost all these satellites with a prefix FLOCK 2K have detected maneuvers while reports by the company indicate no traditional orbital control capabilities are present. However, it does mention the use of differential drag to slowly space them out evenly along the orbital plane. With deployment, commissioning and orbital spacing taking a few months to complete. Although the exact cause of the maneuver detection is not pinpointed it is likely that it is due to either one or a combinations of these reasons.

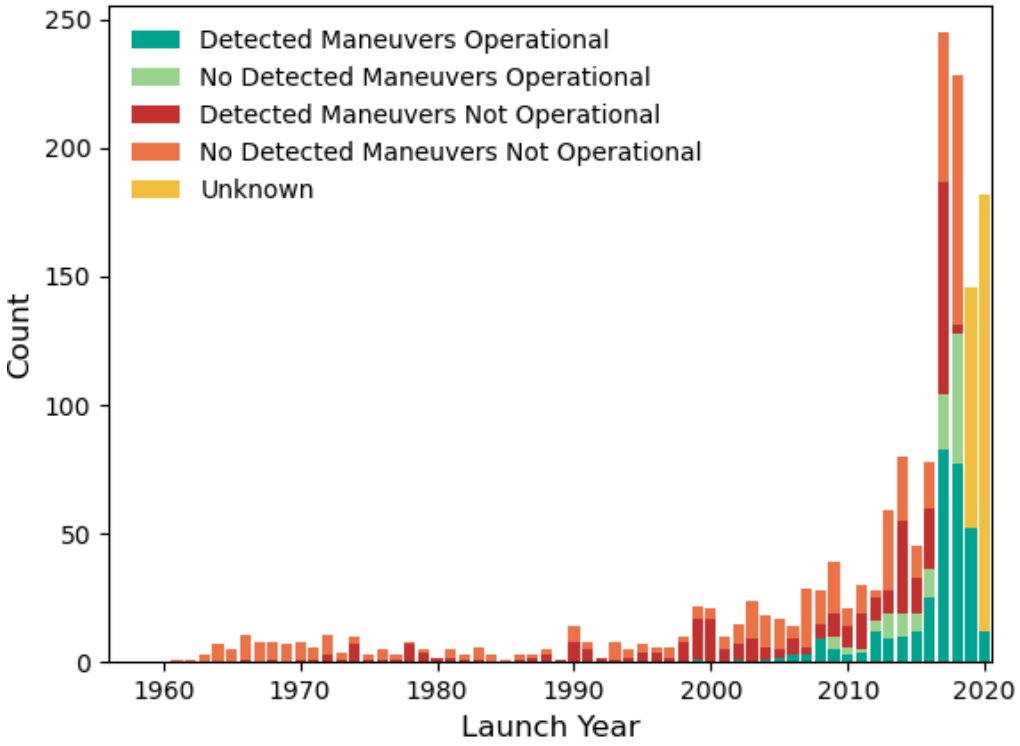

Figure 6.5: Operational status of all satellites in SSO on January 1, 2021.

Now for all satellites that are not operational, the date of the end of the operational phase is determined. This is the date after which, according to the space debris guidelines, a satellite has only 25 years to leave the protected region. Because these satellites at that point are not operational anymore this can only happen due to the natural decay. The time it takes to do so therefore has to be determined; how this was done is discussed in the next chapter.

7

Orbital Lifetime Estimation

Using the methods described in the previous chapter it was determined if and when a satellite has become non-operational. From that point, as stated in the space debris guidelines, a satellite has a maximum of 25 years to leave the protected region. This can be done by a direct re-entry, raising its orbit but the most commonly chosen method is using natural orbital decay [21]. Sometimes a small maneuver is also performed to lower the orbit to hasten this process. The eventual compliance of a satellite is a binary event, it either is or is not, and can only truly be determined after the 25 years have passed. However, if one wants to analyse the compliance rate before this period, predicting the remaining orbital lifetime is one of the crucial tasks. This is why multiple agencies,universities and research institutes have developed methods and software to do this.

This chapter will discuss how this remaining orbital lifetime was determined. This is done by first giving an overview of the available methods in Section 7.1. In this section these available methods will be compared and one will be selected as most suitable. The selected method, along with its implementation and parameters, will be shown more in-depth in Section 7.2. Finally, in Section 7.3 this method will be applied to the spacecraft population in Sun-synchronous orbit.

7.1. Estimation Methods

In general the methods available to estimate orbital lifetime can be split in three different groups: analytic, semi-analytic and full numerical integration [57]. Each of these methods has its own use cases, advantages and drawbacks.

7.1.1. Analytical

The analytic approach can generally be split in two different types. The first would be making use of a lookup-table or figure and the second making use of an equation with simplified perturbations determining the remaining lifetime based on orbital and spacecraft parameters.

These tables, figures and formulas are fitted to pre-computed estimations of orbital lifetimes done with accurate models or measurement data. An example of such a reference figure was already shown in Figures 2.1 and 2.2 in Chapter 2. Another example is given in Figures 7.1 and 7.2, here the orbital lifetime of a nano-satellite launched in SSO at an altitude of 550 km can be found.

A well-known example of the second type, a simple formula, is the one given by Wertz for circular orbits in Equation 7.1 [62]:

$$L = -\frac{H}{\Delta a_{rev}} \tag{7.1}$$

where H is the atmospheric density scale height and Δa_{rev} can be determined by Equation 7.2 [62]:

$$\Delta a_{rev} = -2\pi (C_D A/m) a^2 \rho \tag{7.2}$$

where C_D is the dimensionless drag coefficient, A and m the cross-sectional area and mass. Semi-major axis a is the initial value and Δa_{rev} the change in semi-major axis per revolution. As can be seen determining the orbital decay using this method is fairly straightforward. However, as with all orbital lifetime estimations the atmospheric density ρ is key here, and often hard to determine accurately.

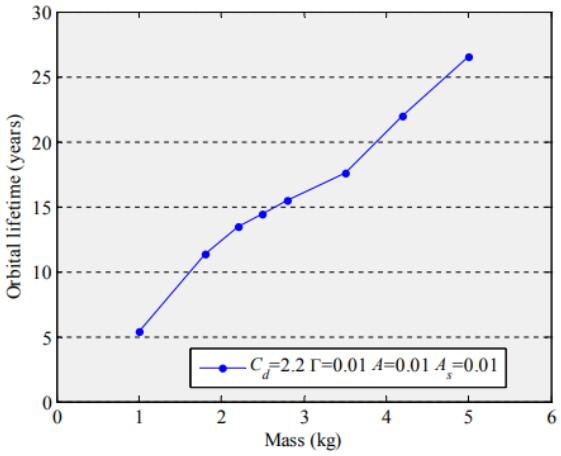

Figure 7.1: Orbital lifetime for a nano-satellite in quasi circular orbit in SSO with an altitude of 550 km based on the mass of the spacecraft [13].

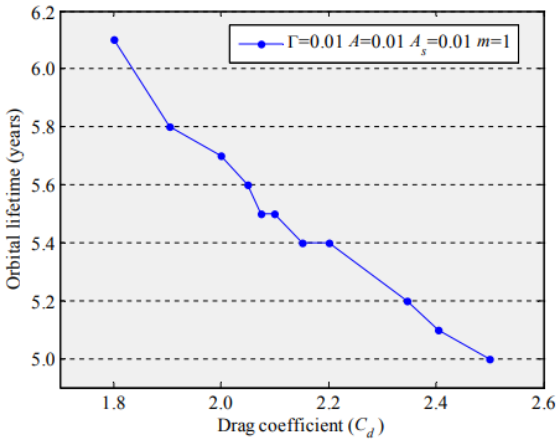

Figure 7.2: Orbital lifetime for a nano-satellite in quasi circular orbit in SSO with an altitude of 550 km based on drag coefficient [13].

Also well known and used is the SGP4 model, which is discussed more in-depth in Chapter 4. This can be used to propagate the TLE data really efficient [27]. However they are only useful to generate approximate solutions on a short timeframe. Already after just a week of propagation Sang and Bennett found the 7-day maximum prediction error to be in the order of several kilometers for a spacecraft in LEO [48]. Thereby making it unsuitable at the large timeframes of more than 25 years as is required for this study.

The main advantage of these approaches is that by simplifying the perturbation forces the equations of motion can be solved directly. This can be done very fast with a runtime in the order of a second or less. This comes at the cost of accuracy, especially when using it for satellites in varying orbits and with different physical spacecraft parameters for a long duration.

7.1.2. Numerical Integration

Numerical integration methods can be used to determine the remaining lifetime of an object. This is done by setting up and solving sets of differential equations. To obtain the required accuracy detailed models have to be setup. For perturbing forces, as discussed in Chapter 3, this would require including a highly detailed gravity field model, solar-radiation pressure, third-body effects and an atmospheric drag model. Furthermore, it would have to include a rotational model or pre-determined vehicle attitudes.

Since high-accuracy orbits require this numerical approach, programs to do this have been widely developed and tested all over the world. One of such programs was developed by Delft University of Technology and is called the TU Delft Astrodynamics Toolbox (TUDAT). This a toolbox of C++ libraries developed by Delft University of Technology to support astrodynamic research. Everyone can use and contribute to these libraries and they can be found on `https://github.com/Tudat`. It can be used to numerically propagate trajectories and includes a wide range of acceleration and environment models including:

- Spherical Harmonics
- Atmospheric Models
- 3rd-Body Gravity
- Cannonball Solar Radiation Pressure
- Relativistic Effects

It also has an established record of being used in peer-reviewed research for more than five years such as the works of Dirkx et al.[18] and Hoogendoorn et al. [26] making it a well-verified toolbox. It is also well documented including descriptions of built-in functions and examples on `https://tudat.tudelft.nl/`.

Although widely used and understood and, when using detailed models, numerical integration can provide accurate results, the major drawback is its computation time. This can become extremely large especially when having to do a large number of simulation runs and propagating for a long time. For a 50-year orbital lifetime propagation this can take about 2500 s of processing time per object. Finally, for predictions

over these large durations even very precise numerical integration will have inaccuracies in its results due to smaller errors accumulating over time, and might give false confidence in the accuracy of the results.

7.1.3. Semi-Analytic

Semi-analytic methods aim to achieve high accuracy while keeping computation time to a minimum. This is achieved by not doing a full numerical integration but instead split the osculating elements in two parts: one for the mean elements that are slowly changing over time and an expression for the short-periodic variation. This allows the slowly changing elements to be solved with a much higher timestep of usually one day [38], while the short-periodic coefficients are recovered using an analytical solution at the integration intervals. This allows the full osculating elements to be recovered by combining the two. By including the most influential zonal terms such as J_2 and J_3, solar radiation pressure and atmosphere models, one can quickly analyse many long-duration propagations.

Due to this short computation time while remaining accurate over longer duration of time, many methods based on this semi-analytic satellite theory (SST) exist with slightly different approaches aiming to improve accuracy and reduce computation time [57]. Examples are methods such as the Draper Semi-analytic Satellite Theory (DSST) [16], the Semi-analytic Tool for End of Life Analysis (STELA) implementation by CNES [36] and the implementation by Bezděk and Vokrouhlický [5] based on the work of King-Hele [33]. They found that for a 10 year propagation the estimated lifetime only differs by a few percent. Becoming and order of magnitude larger when extrapolating to the future due to the uncertainties in the prediction of solar activity. All required just ≈ 5 s of computation time [5].

For a 50-year orbital lifetime propagation the processing time per object can be brought back to 25 s, a significant improvement over the full-numerical models.

7.1.4. Selection

Standard ISO 27852 shows how to determine what methods to use based on the orbit type and spacecraft area-to-mass ratio [29]. This is shown in Table 7.1, here 3Bdy are third-body perturbations and SRP is solar radiation pressure. All methods have to include gravity zonals J_2 and J_3 at a minimum.

Table 7.1: Applicable methods with required margins of error and perturbation modelling for orbital lifetime estimation according to ISO 27852 [29].

	Special Orbit		**Conservative margin applied to each method**			
Orbit apogee altitude [km]	**In SSO**	**High Area to Mass**	**1. Numerical Integration**	**2. Semi-analytic**	**3. Analytic Table look-up**	**3. Analytic Graph/Formula**
<2000 km	No	No	No margin	5 % margin	10 % margin	25 % margin
<2000 km	No	Yes	No margin use SRP	5 % margin use SRP	10 % margin	N/A
<2000 km	Yes	No	No margin	5 % margin	N/A	N/A
<2000 km	Yes	Yes	No margin use SRP	5 % margin use SRP	N/A	N/A
>2000 km	Either	Either	No margin use 3Bdy+SRP	5 % margin use 3Bdy+SRP	N/A	N/A

For our case, row 3 and row 4 are relevant as the satellites have an apogee below 2000 km altitude and are in SSO. The distinction between using one of these two is whether the satellite has a high area-to-mass ratio. If it has, one should include the solar radiation pressure in the model. A spacecraft is considered to have a high area-to-mass ratio if it exceeds 0.1 m^2/kg. It also shows that depending on the method a conservative margin may have to be applied to the determined lifetime.

From the table it can be seen that according to the ISO standard the analytic method is not applicable for this research use case. Therefore a decision has to be made between the full-numerical integration and the semi-analytic method. To do this a first-order estimation was made of the total computation time required, the result of this is shown in Table 7.2.

Table 7.2: First-order total computation time estimation for the two methods based on one nominal run and four with different settings for the sensitivity study.

Parameter	**1. Numerical Integration**	**2. Semi-analytic**
Average propagation time per object	50 years	50 years
Computation time per object	2500 s	25 s
Objects	1500	1500
Number of Runs	5	5
Total Time	5200 hrs	52 hrs

In this computation it is assumed that the average propagation length is 50 years and the number of objects to be propagated is 1500. Furthermore, besides the one run with nominal settings four other runs will be done with slight changes for the sensitivity study. As can be seen the total computation time for the semi-analytic method is already quite high at more than two full days. Looking at the full numerical integration taking it can be seen that this is completely infeasible even when reducing the propagation time to only 25 year. It was therefore decided to go with the semi-analytic method. The STELA implementation by CNES was chosen as it was freely available, was developed for this purpose, has good documentation and is developed by a reputable organization. It has been well used and tested for different published research such as the work by Le Fèvre et al.[35] and Choi et al. [10]. This reduces the validation burden and provides good confidence in the accuracy of the results.

7.2. STELA Implementation

STELA was written in JAVA and is available as a library, as a manual executable but is also available for batch processing. This last feature was used to process the objects for the multiple required runs. A brief overview of STELA and its implementation will be given here, but for the full documentation the reader is referred to the user manual [12].

7.2.1. Semi-analytic extrapolation method

As was explained STELA is based on a semi-analytic extrapolation method where long-term mean evolution of the elements is solved numerically and short-period effects have been removed. If the mean orbital parameters state at date t_n is represented by E_n^{mean}, then the state E_{n+1}^{mean} at t_{n+1} is derived using the derivative $\frac{dE^{mean}}{dt}(t_n)$ which is calculated by [12]:

$$\frac{dE^{mean}}{dt} = \frac{dE^{mean}_{Kepler}}{dt} + \frac{dE^{mean}_{Earthpot}}{dt} + \frac{dE^{mean}_{lunisolarpot}}{dt} + \frac{dE^{mean}_{drag}}{dt} + \frac{dE^{mean}_{SRP}}{dt} \tag{7.3}$$

where $\frac{dE^{mean}_{Kepler}}{dt}$ represents the movement due to the non-perturbed two-point gravitational force and $\frac{dE^{mean}_{Earthpot}}{dt}$ the perturbations due to the Earth irregular gravitational field. The $\frac{dE^{mean}_{lunisolarpot}}{dt}$ represents third-body perturbations due to the gravitational forces of the Moon and the Sun. Finally, $\frac{dE^{mean}_{drag}}{dt}$ and $\frac{dE^{mean}_{SRP}}{dt}$ represent perturbations due to atmospheric drag and solar radiation pressure respectively. This is solved by a numerical integrator based on a fixed timestep sixth-order Runga-Kutta method.

The osculating parameters are then computed in the integration intervals according to:

$$E_n^{osc} = E_n^{mean} + E_n^{shortperiod} \tag{7.4}$$

where $E_n^{shortperiod}$ is solved analytically and includes short-period effects from irregularities of the gravity field, Solar and Lunar gravity, atmospheric drag and Solar radiation pressure.

7.2.2. Model Settings

For the different perturbations different model settings can be chosen, but for this study the default recommended settings were used. A quick description of these settings will be given, for more information regarding these perturbations the reader is referred to Chapter 3.

Earth and Luni-solar Potential

The derivatives of mean parameters due to the Earths potential zonal perturbations are analytically expressed using a recurrence formula with J_2 up to J_7 contributions at first order and J_2 contribution at second order.

To complete the Earth potential model tesseral terms are also taken into account. The luni-solar potential is based on the Sun and Moon positions that are computed using a simplified Meeus and Brown model with six terms development in longitude, four terms development in latitude and four terms development in distance [41]. The luni-solar perturbation is then developed in Poisson series to the order 8.

Atmospheric Drag
The atmosphere is assumed to be rotating with the exact same velocity as the Earth. No wind is considered and the oblate shape of the Earth is taken into account. For the atmospheric density model the empirical NRLMSISE-00 model was used which requires knowledge of date, satellite and position of the Sun as well as data on solar and geomagnetic activities. This model was chosen for STELA as it provided results that were "centered" when it was compared to reentry duration results obtained with different atmospheric models [36] and is also included in the list of suitable models in the ISO standard [29].

Besides the cross-sectional area the drag coefficient is also required. Although often a fixed value of C_D = 2.2 or 2.4 is used, Le Fevre et al. [36] recommend using an altitude-dependent value as shown in Figure 7.3.

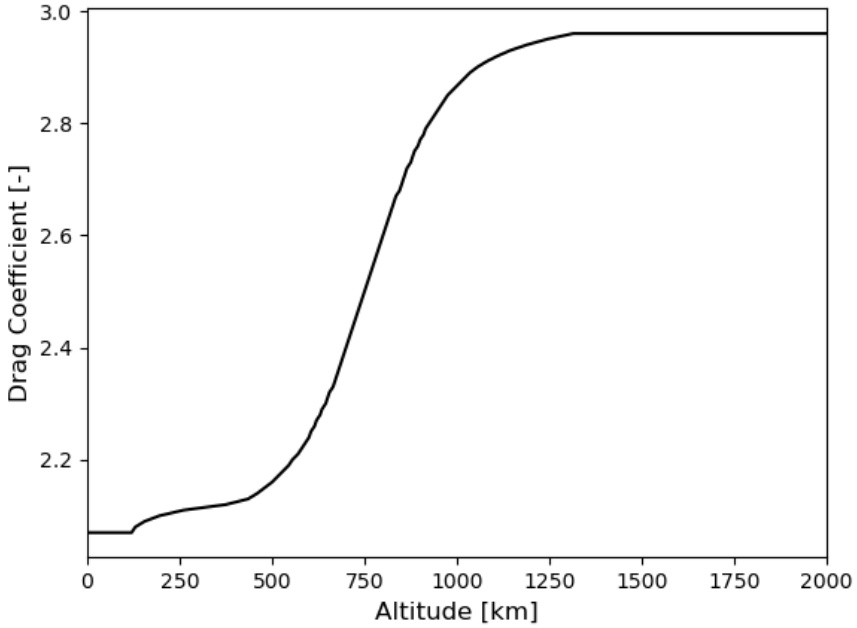

Figure 7.3: Drag coefficient as function of altitude. [12]

Solar Radiation Pressure
The calculation of the SRP force takes eclipses into account and models the shadow of the Earth as a cylinder. It neglects the albedo of the Earth and is calculated by Equation 7.5:

$$\vec{F}_{SRP} = C_R P_0 S \left(\frac{d_0}{d}\right)^2 \vec{u} \tag{7.5}$$

where C_R is the reflectivity coefficient taken to be 1.5, P_0 is the Solar radiation pressure at 1 AU and S the reflecting area of the spacecraft. Furthermore, d_0 = 1 AU, d the distance between the Sun and the spacecraft and $\vec{u}$ the Sun/spacecraft vector.

Solar Activity

The model for drag requires inputs for the solar activity defined by the geomagnetic activity Ap and the $F10.7$ cm Solar flux. As was seen in Chapter 3 this activity has a very significant effect on the atmospheric density. It is well understood that thereby assumptions on future solar activity have significant impact on the resultant orbital lifetime prediction. However, long-term predictions on duration and intensity of the next solar cycles are very uncertain.

Because the models are so uncertain, and often during the design and operation the exact date of end of mission is not known, Le Fevre et al. [35] and the ISO standard [29] argue that a mean constant equivalent solar activity approach allows for a more robust and reliable lifetime computation.

This constant equivalent solar activity is computed for LEO at the start of the extrapolation using for the geomagnetic activity:

$$A_p = 15 \tag{7.6}$$

and for the solar flux:

$$F10.7 = 201 + 3.25\log\left(\frac{C_D S}{m}\right) - 7\log(Z_a) \tag{7.7}$$

where C_D is taken to be 2.2, S the reflecting area, m the mass and Z_a the apogee altitude in km.

7.2.3. Inputs

For each satellite the mass, cross-sectional area, reflecting area and starting state has to be provided. For simplification the cross-sectional area and reflecting area were considered to be the same. For this use was made of the DISCOS database providing an average cross-sectional area and an estimation of the mass of the spacecraft. For the starting state a TLE can be provided which is converted internally by STELA to the proper elements. For this the latest TLE for each satellite was retrieved. This turned out to be either on January 1st, 2021 or, for a minority for which this was not available, the TLE of December 31st, 2020. This is, considering the long propagation timeframe, a non-significant difference.

7.2.4. Validation

As was already mentioned, one of the main advantages of STELA is that it is a well-used and tested application. In their validation study CNES compared the runs of STELA with their reference numerical propagators (PSIMU and ZOOM) which include complete dynamical force models. It was found that for LEO extrapolation the precision is around 1 % for a estimated lifetime of 25 years and better than 2 km for the minimum and maximum altitudes for 100 years [36][35].

Moreover, the results from STELA were compared to results obtained from numerical propagation using the aforementioned TUDAT and to the actual results obtained from the TLE data. To do this a satellite was needed that has already decayed and was in its ballistic phase for a considerable time. For that purpose one of the Chinese Ziyuan satellites with SATCAT 26481 was selected. The numerical implementation included the spherical harmonic gravitational field with degree 4 and order 4, cannonball-modelled radiation pressure with Earth's shadow being accounted for, the NRLMSISE-00 atmosphere model and third-body perturbations due to the Sun and the Moon. For both STELA and the numerical propagation a C_d of 2.2 and a C_r of 1.5 was used.

It uses the Cowell propagator with a Runge-Kutta-Fehlberg 8(7) Dormand-Prince integrator with an equal minimum and maximum timestep of 200 s. In this way this is transformed to a fixed timestep integrator. The timestep was found by starting with a very large timestep and decreasing it until the solution converged. Results of the comparison can be found in Figure 7.4. The propagation starts in 2005, when the satellite has performed its last maneuver; after that it has gone purely ballistic.

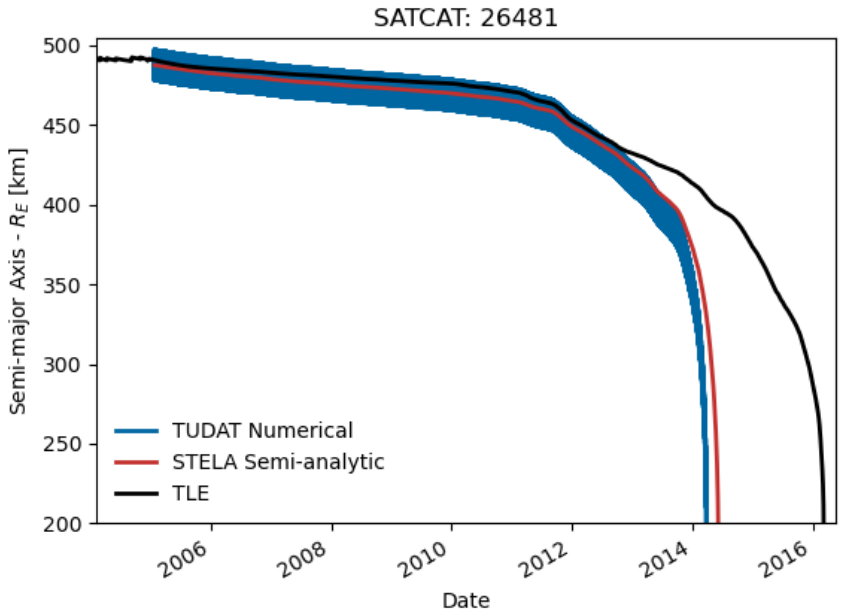

Figure 7.4: Lifetime comparison of the STELA and the TUDAT numerical integration method with the actual mean semi-major axis retrieved from TLE data. The propagation starts at the end of the operational phase on January 15, 2005.

As can be seen the numerical solution and the semi-analytic solution match closely, even on this 10-year timeframe. These matching results obtained using software developed by two independent reputable organisations further improve the validity of the models. However, it can be seen that they both underestimate the remaining lifetime by about 20%. Due to the 5% lifetime margin that is required to be added according to the ISO standard, part of this is conservatively dealt with. This divergence mainly occurs at the lower altitudes, where the orbital decay is highest. Because this is happening in both models the most likely explanation is that it is due to an error in the ballistic coefficient (BC), it should be noted that in some literature the inverse of this is used:

$$BC = \frac{m}{C_D A} \tag{7.8}$$

where uncertainties exist in all three parameters. This process was repeated for five more satellites that have already decayed and were ballistic during their entire orbital lifetime. Propagation using STELA was started from the first available TLE and compared to the actual results in Table 7.3.

Table 7.3: Orbital decay results compared to results obtained from STELA.

SATCAT	**Launch Date**	**Decay Date**	**Actual Lifetime [days]**	**Semi-analytic Lifetime [days]**	**Difference**
533	19-02-63	27-12-79	6155	4824	-27.5 %
1273	18-03-65	31-12-89	9054	7762	-16.6 %
4957	17-02-71	17-10-89	6817	6163	-10.6 %
4958	17-02-71	20-09-89	6790	6251	-8.6 %
19045	20-04-88	29-10-14	9688	12368	+21.6 %

In general it was found that the lifetime would be slightly underestimated by the semi-analytic propagation method but as can be seen it can also be overestimated as well. It was therefore decided to include uncertainties in the ballistic coefficient in the sensitivity study, by doing a run with a 20% increased and decreased BC.

7.3. Orbital lifetime

For the entire satellite population in SSO that was classified as not operational, and was not already decayed, the remaining orbital lifetime was determined using this method with a maximum propagation length of 100 years. The time between the end of operation date, as determined in the previous chapter, and the start of the propagation, either January 1, 2021 or December 31, 2020, was added to this. Added to these non-operational satellites were the satellites for which an actual decay date was recorded. Resulting for each in a total lifetime after operational phase in years, this was truncated to a maximum of 100 years. A histogram of the resulting lifetime after the end of their operational phase is shown in Figure 7.5.

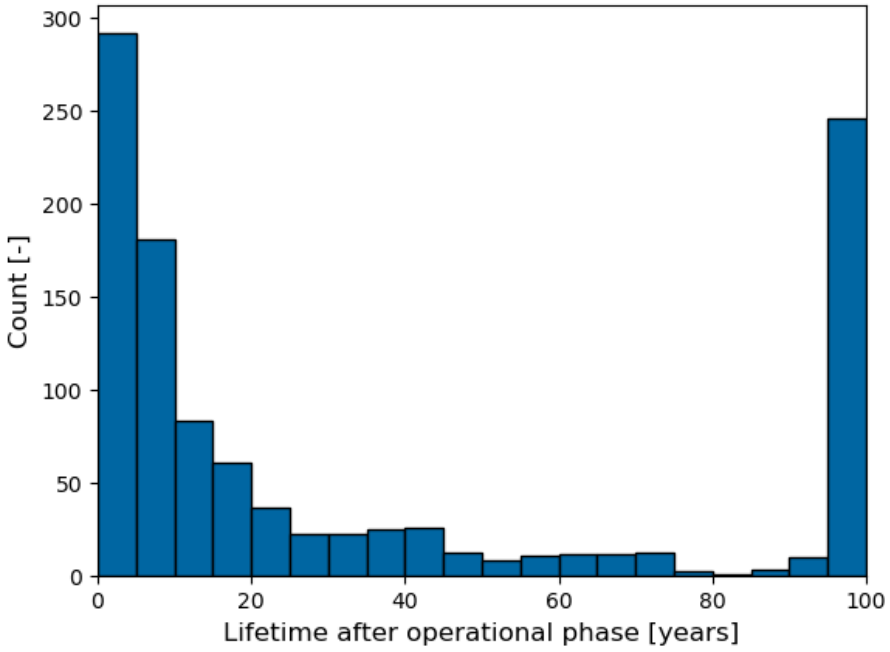

Figure 7.5: Orbital lifetime of non-operational satellites in Sun-synchronous orbit.

It can be seen that the population can be roughly split in three separate groups. The first group is the satellites that are expected to decay very quickly, within the first 10 years. This is a rather large group for which one can be highly confident that this will happen regardless of model errors in solar activity and/or ballistic coefficient. Another large group are the satellites that are expected to take more than a multiple of the required 25 years to decay. In the third group are the satellites that fall between these two, for which the result might not be as confident; this will be elaborated upon in the discussion and sensitivity study of the results in the next chapter. To see the evolution of this orbital lifetime over time a boxplot was created based on the end of operational phase year. This is shown in Figure 7.6.

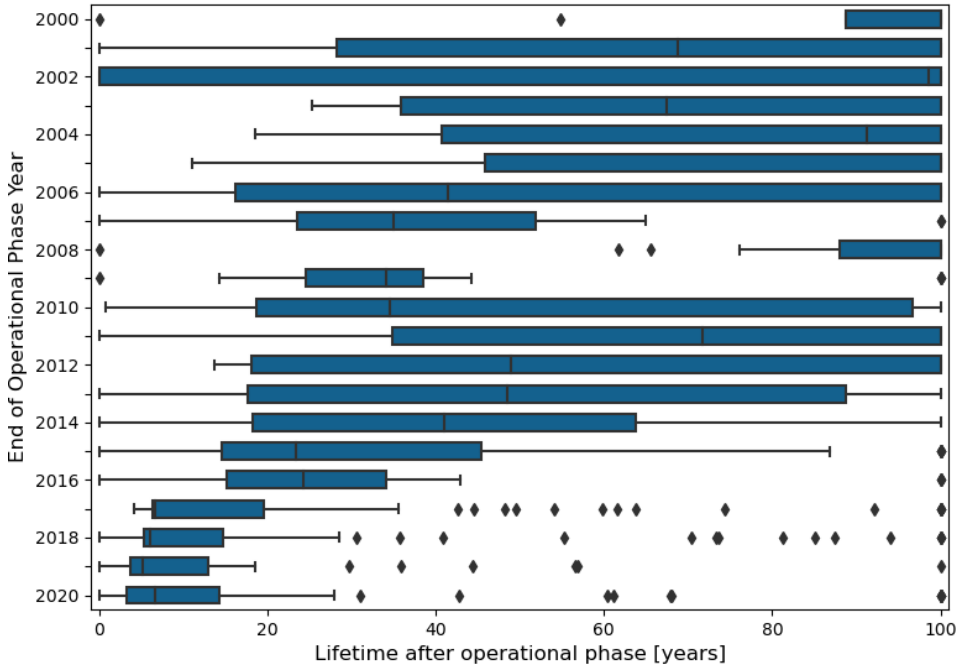

Figure 7.6: Remaining orbital lifetime of satellites in Sun-synchronous after their operational phase has ended.

In the figure the whiskers are extended to the lowest datapoint within:

$$Q_n(0.25) - 1.5 \cdot \text{IQR} \tag{7.9}$$

and the largest datapoint within:

$$Q_n(0.75) + 1.5 \cdot \text{IQR} \tag{7.10}$$

with the outliers marked as diamonds. Where IQR, the interquartile range, is determined by:

$$\text{IQR} = Q_n(0.75) - Q_n(0.25) \tag{7.11}$$

This grouping by end of operational phase year naturally has some lag in showing changes, as satellites that have their operational phase ended have been designed and launched multiple years before that. It can be seen that in the recent years the distribution of lifetimes has been significantly shifted lower than in earlier years. This would mean a positive trend in compliance. Even though this positive trend is observed, it can also be seen from the outliers that still some satellites have very long remaining orbital lifetimes indicating that even in the most recent years not all satellites will be compliant, this will be discussed more in-depth in the next chapter.

8

Compliance

This chapter will combine the determination of operational status and the remaining orbital lifetime of the satellites to determine compliance with the 25-year lifetime guideline. The resulting compliance and its evolution over time will be analysed in Section 8.1. The reader is reminded that ultimately compliance is a binary event and can only be determined if the true end of operational phase date is known and after the decay date or 25 years have passed. It was already seen that underlying assumptions regarding the atmospheric density modelling and ballistic coefficient can have an impact on these result. For the purpose of investigating these impacts a sensitivity study was performed and is discussed in Section 8.2. After this the results will be compared to other studies done both for LEO and GEO satellites in Section 8.3. Finally, the methods used, the underlying assumptions and confidence in the results will be reflected upon in Section 8.4.

8.1. Results

At the end of the previous chapter a decreasing trend in orbital lifetime after the operational phase was already observed. This will also be visible as an increase in the compliance rate as this compliance is determined by:

- *Compliant*, if the remaining orbital lifetime after the operational phase is less than 25 years.
- *Not Compliant*, if the remaining orbital lifetime after the operational phase is more than 25 years.

This was determined for all satellites for which no maneuvers were detected and are therefore assumed to be in their ballistic phase. This also includes the satellites that have already decayed. An overview of the total satellites analysed, their operational status and orbital control capabilities is given in Tables 8.1 and 8.2; the determination of this status was discussed in Chapter 6. Therefore, the following results will not include the satellites that have maneuvered within the past two years, as they would have the potential to lower or raise their orbits. Also not included are the satellites that were launched within the past two years as the operational status could not be determined for those. Remaining are the 870 not operational, the 126 operational satellites without orbital control capabilities and the 110 already decayed satellites.

Table 8.1: Overview of the number of satellites in SSO by their orbital control capability.

Status	**Number of Satellites**
Orbital Control Capability	564
No Orbital Control Capability	774
Unknown	278
Total	1616

Table 8.2: Overview of the number of satellites in SSO and their operational status.

Status	Number of Satellites
Not Operational	870
with orbital control capability	332
without orbital control capability	648
Operational	358
with orbital control capability	232
without orbital control capability	126
Decayed	110
Unknown	278
Total	1616

The compliance was determined for these 1106 satellites and is shown in aggregate in Table 8.3. Here it was determined that slightly over half of the satellites comply.

Table 8.3: Total compliance of satellites in Sun-synchronous orbit with the 25-year lifetime rule.

	Compliant	Not Compliant
Number of Satellites	654	452
Compliance Rate	59.2 %	40.8 %

Interesting however is its evolution over time. For that purpose the results were grouped by launch year. The resulting compliance is shown in Figure 8.1. Here it can be seen that satellites launched in recent years have been more compliant than in the past both in absolute and relative numbers.

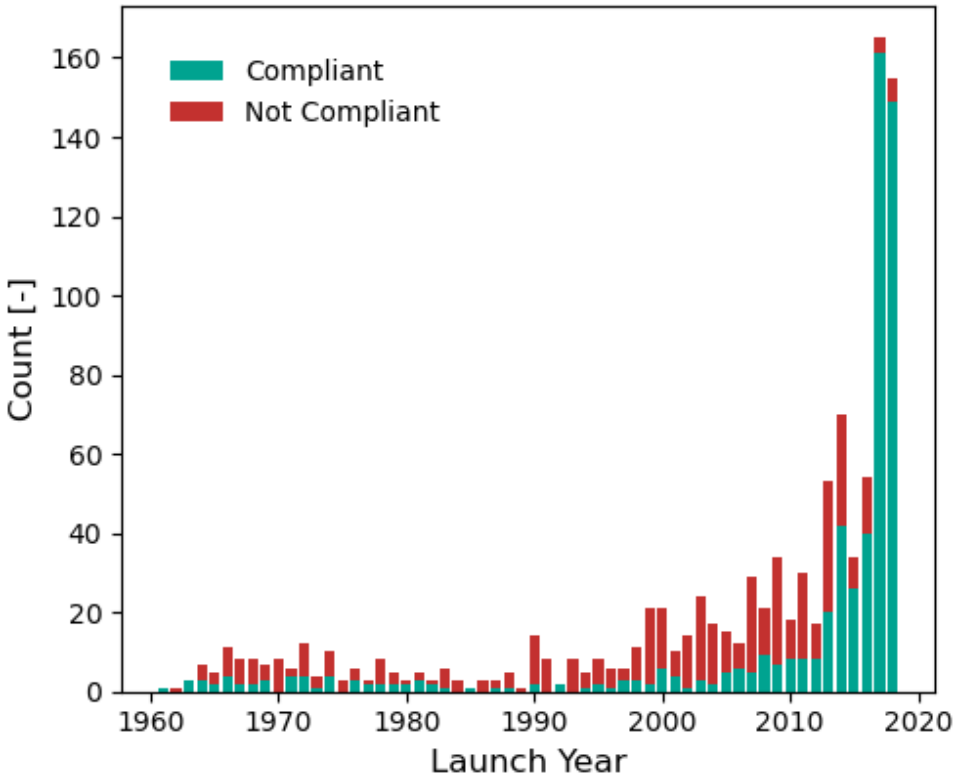

Figure 8.1: Compliance of satellites in Sun-synchronous orbit with the 25-year lifetime rule per launch year. Green is compliant, red is non-compliant.

The compliance rate, or percentage of satellites that are compliant with respect to the total satellites launched that year, is given in Figure 8.2. In this figure an increasing compliance trend can be observed starting around 2010 when compliance was 20 to 40 % to around 95% compliance in 2017 and 2018.

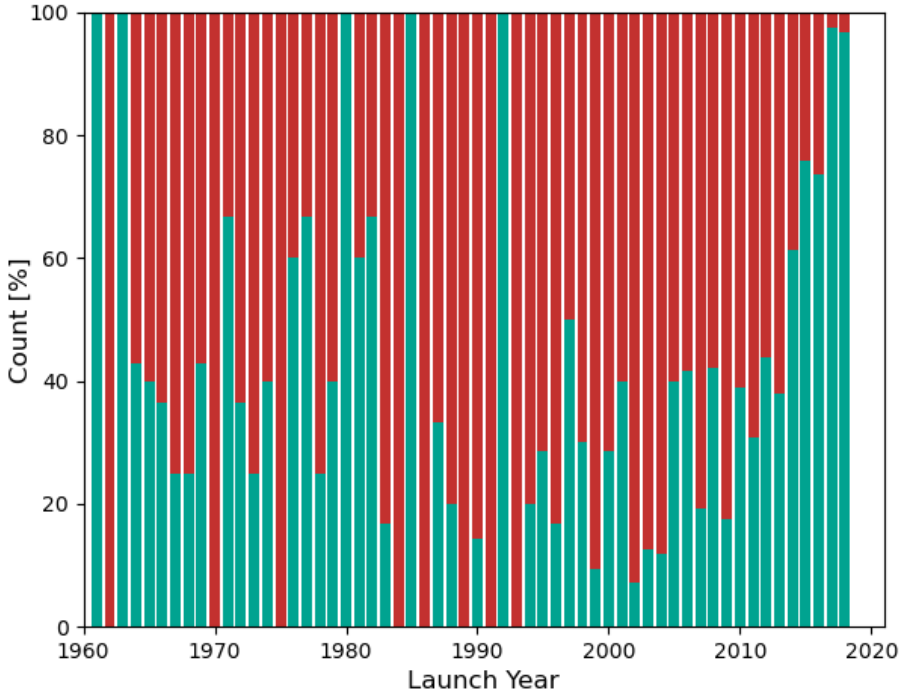

Figure 8.2: Compliance rate of satellites in Sun-synchronous orbit with the 25-year lifetime rule. Green is compliant, red is non-compliant.

To determine what is driving this increase in compliance it is useful to group the satellites in different mass categories. The overall compliance per mass category is displayed in Figure 8.3. Here the large difference between the smallest group of satellites and the rest of the mass categories can be seen.

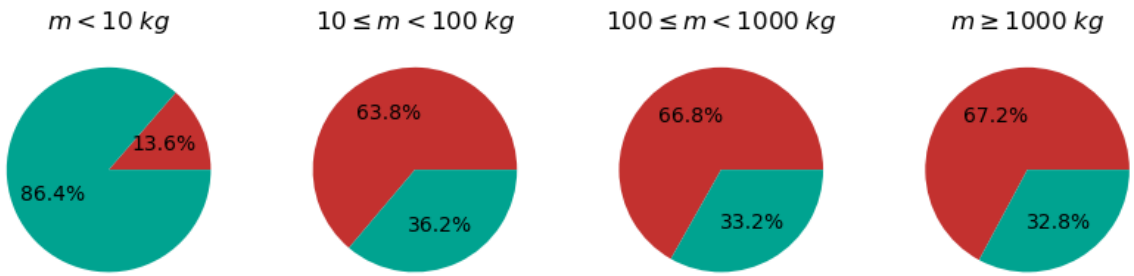

Figure 8.3: Compliance of satellites in Sun-synchronous orbit with the 25-year lifetime rule for different mass categories. Green is compliant, red is non-compliant.

As was discussed in the inventory of satellites in Chapter 2, it is also precisely this group which has seen a huge increase in launches to SSO. The large number of satellites combined with the high relative compliance is why the overall compliance is increasing in recent years.

This might at first be counterintuitive, after all, as was discussed in Chapter 6, the operational phase of a smaller spacecraft is often significantly lower than that of a spacecraft with a higher mass, allowing more time for a satellite to decay. However, when looking further it is actually exactly what one should expect for a few reasons.

The first would be due to the way the atmospheric density has an effect on a spacecraft. This is proportional to the ballistic coefficient (note that the definition of the BC of Equation 7.8 is used, with mass in the numerator). Assuming an identical shape and mass density, due to the fact that mass scales with volume the BC of an heavier satellite will be larger than one of lower mass. However, the most dominant reason the smaller satellites are more often compliant is due to the orbits they are initially launched in. This is shown in Figure 8.4, where a distribution of the altitude of the initial orbit is shown for each of the four mass categories.

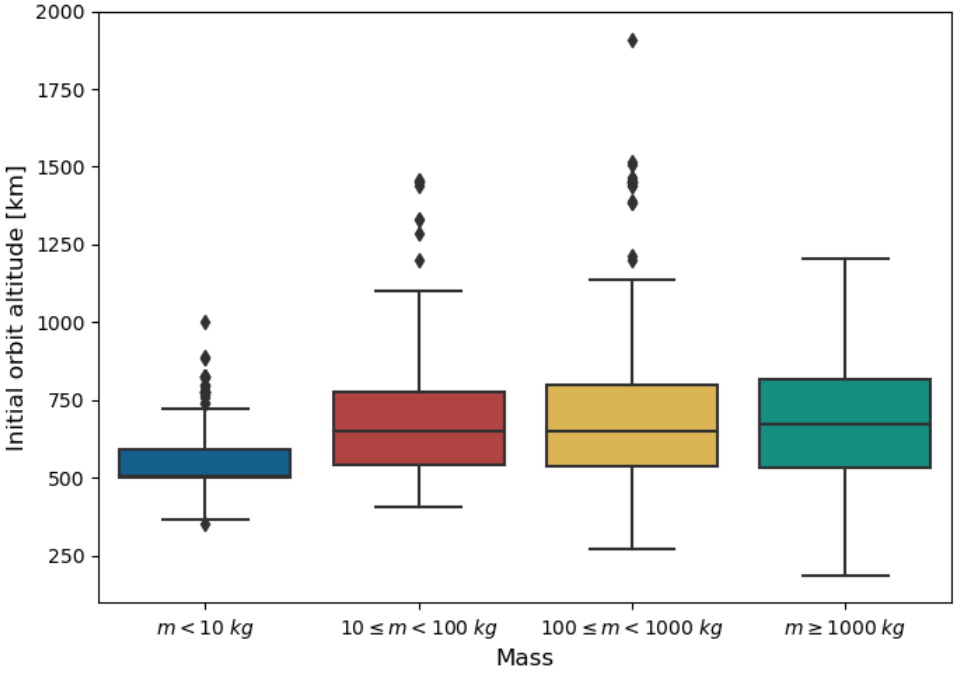

Figure 8.4: Initial orbit altitude distribution per mass category.

This relationship, between initial orbit and eventual compliance, is even more visible when dividing the mass categories in their respective compliance groups as done in Figure 8.5.

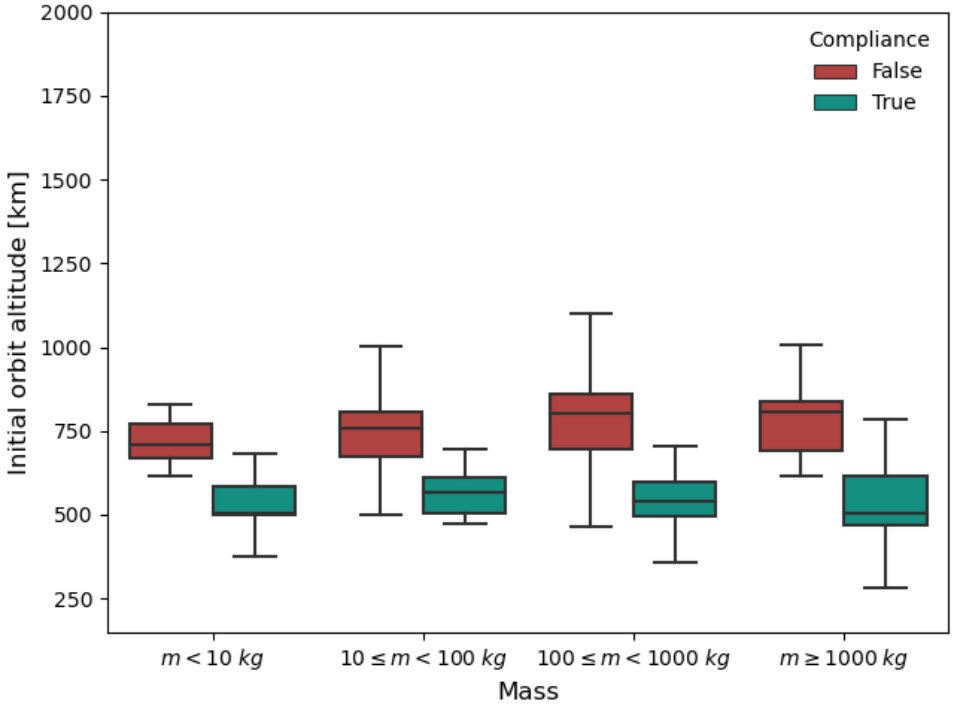

Figure 8.5: Initial orbit altitude distribution per mass category and compliance. Altitude here is determined by the semi-major axis minus the mean equatorial radius of the Earth.

This is as expected, after all a lower initial altitude will expedite the natural orbital decay. To investigate the behaviour of satellite operators further, the compliance rate is grouped by their orbital control capability (OCC). This capability was determined by the presence of detected maneuvers. In Figure 8.6 it can be seen that there is a slightly higher compliance rate for satellites without this capability. Which can once again be

explained by the fact that these smaller satellites often do not have OCC, and as was seen, these satellites are launched in lower orbits and therefore more often naturally compliant.

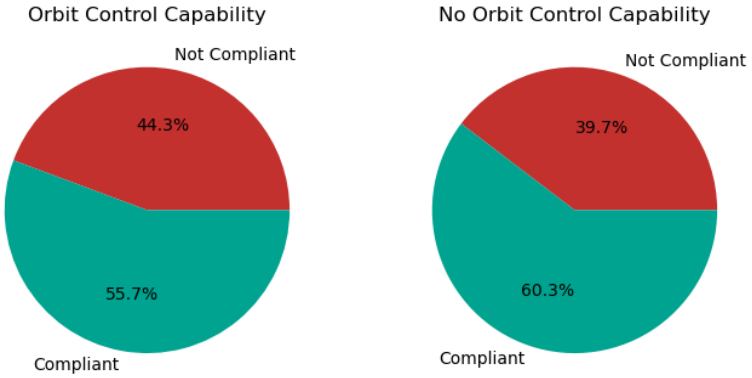

Figure 8.6: Compliance rate for satellites with orbital control capabilities and those without. Green is compliant, red is non-compliant.

In Figure 8.7 it can be seen that this small difference between satellites with or without OCC has been consistent over time.

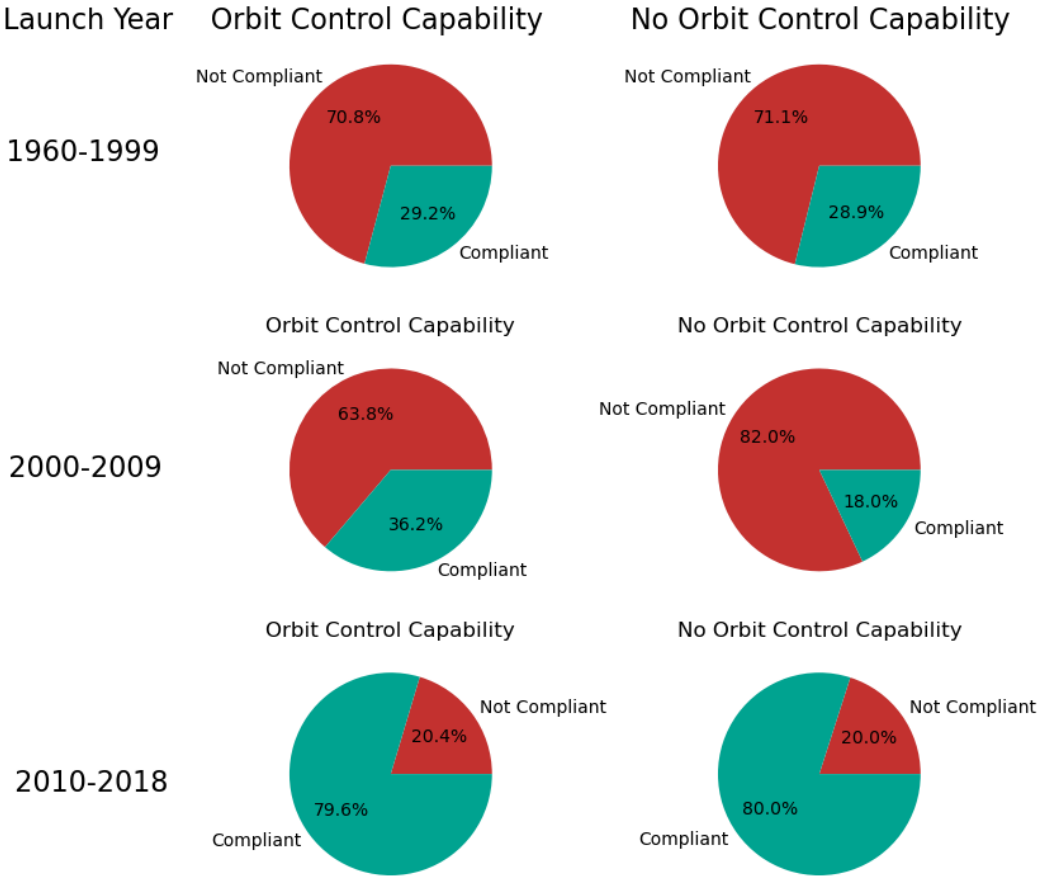

Figure 8.7: Compliance rate for satellites with orbital control capabilities and those without for different timeframes. Green is compliant, red is non-compliant.

Summarising, overall the compliance with the guidelines has been quite poor in the past. Looking at the dates of the release of the modern regulations, all happening in the early 2000's, it took a few years before satellite operators and mission designers actually started implementing it. As it was seen that compliance has been significantly increasing in recent years starting from 2014. It was also seen that this is mostly a result of choosing an orbit with a sufficiently low altitude to have a sufficient natural decay and less of operators choosing to perform altitude lowering maneuvers at the end of operational phase to achieve compliance.

8.2. Sensitivity Study

The results, as given in the previous section, are relying on a number of underlying assumptions. It is well known that uncertainties in the atmospheric density and ballistic coefficient can have significant impacts on the orbital lifetime of a spacecraft. In order to determine how sensitive these results are to those uncertainties, a sensitivity study was performed. This was done by comparing the nominal results to results obtained using slightly different parameters and model settings, resulting in a total of four different scenarios:

- *Nominal*, the settings as were described in earlier chapters and resulting in the compliance given in the previous section.
- *Variable Solar Activity*, while for the nominal case the constant equivalent solar activity was used, this run will use a variable solar activity as given by long-term space weather forecasts by NASA and NOAA [12] [35].
- *Low Ballistic Coefficient*, to investigate the effects of overestimating the ballistic coefficient the nominal value is decreased by 20%.
- *High Ballistic Coefficient*, to investigate the effects of underestimating the ballistic coefficient the nominal value is increased by 20%.

For the variable solar activity use can be made of measured solar activity when propagating from an historical date. For our purposes however, the propagation starts on January 1st, 2021 and use is made of long-term space weather forecast, this forecast is shown in Figure 8.8. As this equivalent Solar activity calculated by Equation 7.7 is dependent on mass, area, C_D and the apogee altitude, it is slightly different for each spacecraft. Although, both the two variable terms are in similar orders of magnitude and the logarithm is taken, so they will only differ slightly.

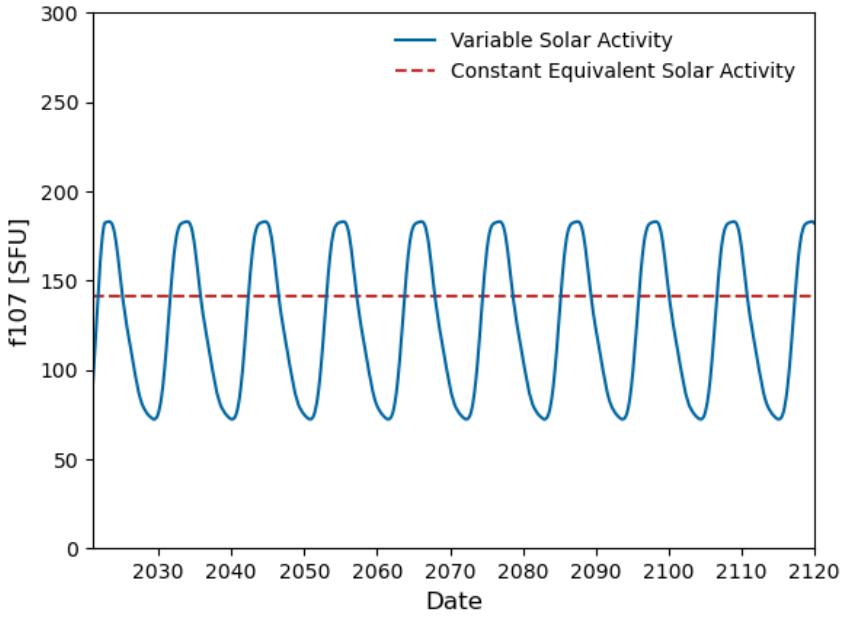

Figure 8.8: Variable and the constant equivalent Solar activity of SARAL as used by STELA [12].

For the two runs with a change in the ballistic coefficient the mass of the object used as input for the propagation was increased or decreased by 20%. For these three changed settings the semi-analytic lifetime propagation using STELA was repeated.

The resulting lifetime after operational phase (AOP) distributions of the three runs are shown in Figure 8.9, where for each run the nominal results are plotted as well. Also visible in each figure is the 25-year lifetime boundary marked as a dashed vertical line. The compliance statistics can be found in Figure 8.10.

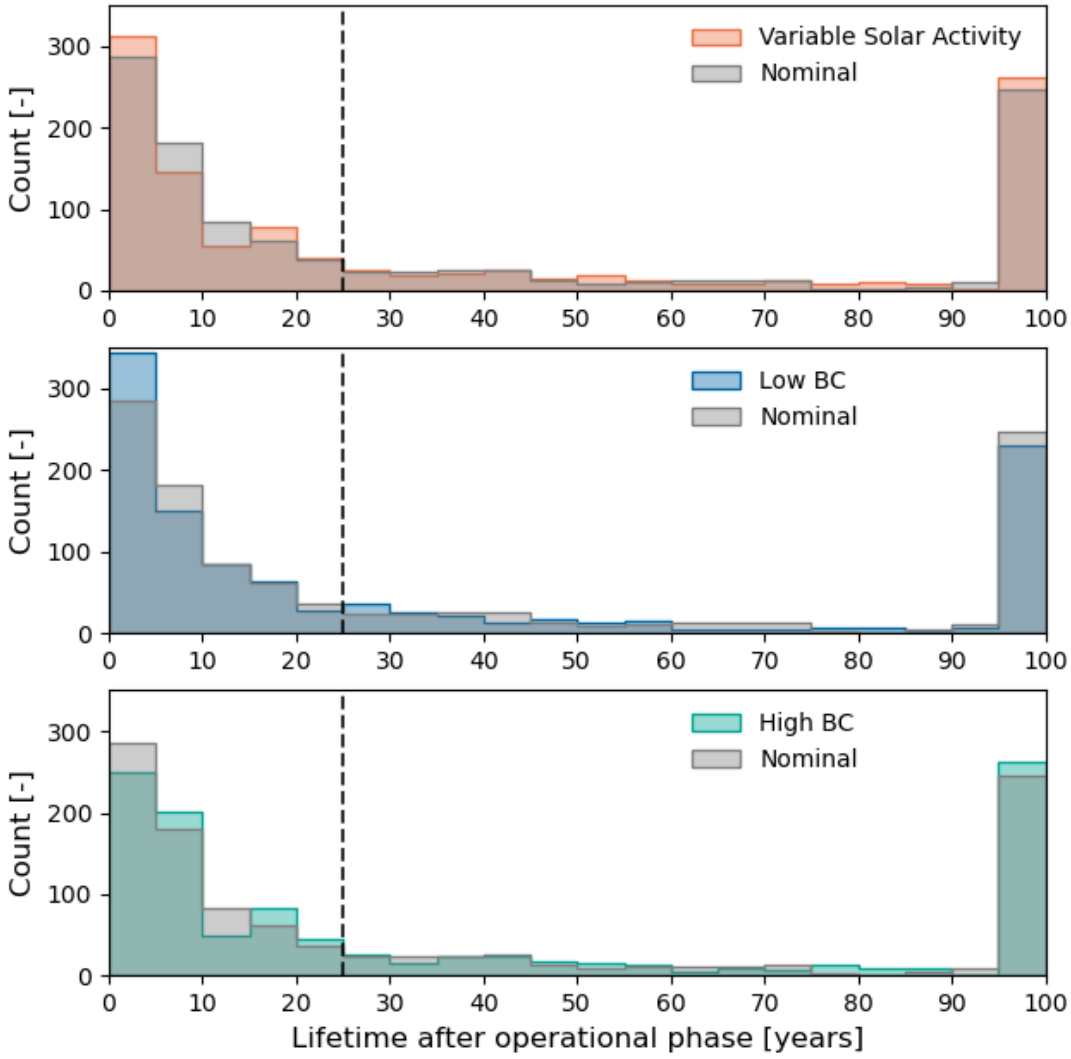

Figure 8.9: Remaining lifetime of satellites in Sun-synchronous orbit for the different sensitivity runs. The dashed line marks the 25-year lifetime boundary.

From these results several observations can be made. First of all the effects on the atmospheric density, and therefore orbital lifetime, can clearly be seen in the top-most graph corresponding to a variable Solar activity. In Figure 8.8 it was seen that currently the Solar activity is quite low, and predicted to increase in the coming years. This increase in activity will cause an increase in aerodynamic drag and therefore shorten the orbital lifetimes. This is seen as an increase in the number of satellites with a lifetime AOP of less than five years. However, after these years the Solar activity is predicted to decrease again, causing the opposite effect with lengthening the orbital lifetimes. Combined with the fact that some satellites have already decayed earlier, this causes a decrease in the number of satellites with a lifetime AOP of 5 to 15 years. Then again the Solar activity increases and this cycle continues, causing a wave-like effect on the distribution of remaining orbital lifetimes.

When looking at the low ballistic coefficient run, the effects are visible as well. Lowering the ballistic coefficient will primarily increase the acceleration due to aerodynamic drag, and therefore shorten the lifetime of the satellite. This results in a shift of the remaining lifetimes AOP to lower values, or to the left in the figure. Of course the opposite happens when using the increased ballistic coefficient, with a lower acceleration due to the aerodynamic drag and therefore a higher orbital lifetime. Resulting in a shift to higher values, or to the right in the figure.

However, this research is less concerned about the exact decay date of individual satellites and more about looking whether or not it exceeds the 25-year boundary, also indicated in Figure 8.9. After all, for this 25-year lifetime rule it does not matter if a spacecraft decays in 5 or 10 years or if another spacecraft does in 40 or 50. In both cases the compliance results are the same, compliant for the first and not compliant for the second.

When comparing the nominal case against the individual sensitivity runs, it can be seen that the total number of satellites to the left and to the right of the 25-year line remain highly similar indicating similar compliance rates. This total compliance for each different run is shown in Figure 8.10.

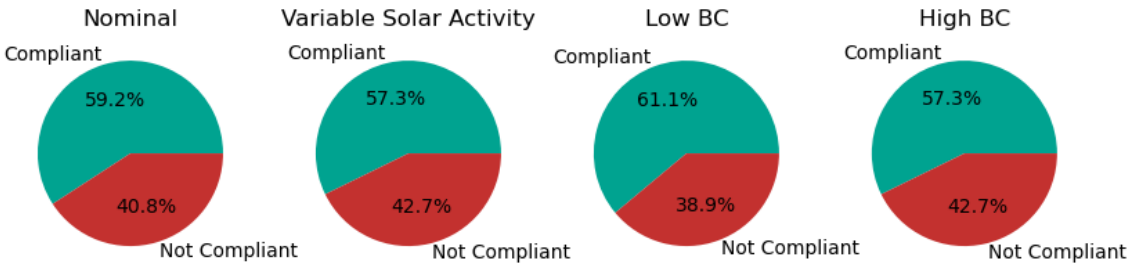

Figure 8.10: Compliance rate of satellites in Sun-synchronous orbit for the different sensitivity runs.

What was already suggested in the lifetime histograms is confirmed here, with all runs having very similar results, with as expected slightly higher compliance in the Low BC run and lower in the High BC run. Interestingly the Variable Solar Activity run produced the same results as increasing the ballistic coefficient run. Although the overall difference between this run and the nominal case is quite small, this might indicate that the constant equivalent solar activity approach, as described in Section 7.2, is a bit conservative and tends to underestimate the resulting atmospheric density.

The compliance results are also given grouped by launch year in Figure 8.11. Visible here is that although local compliance rates per year might be slightly different, the overall trend is the same.

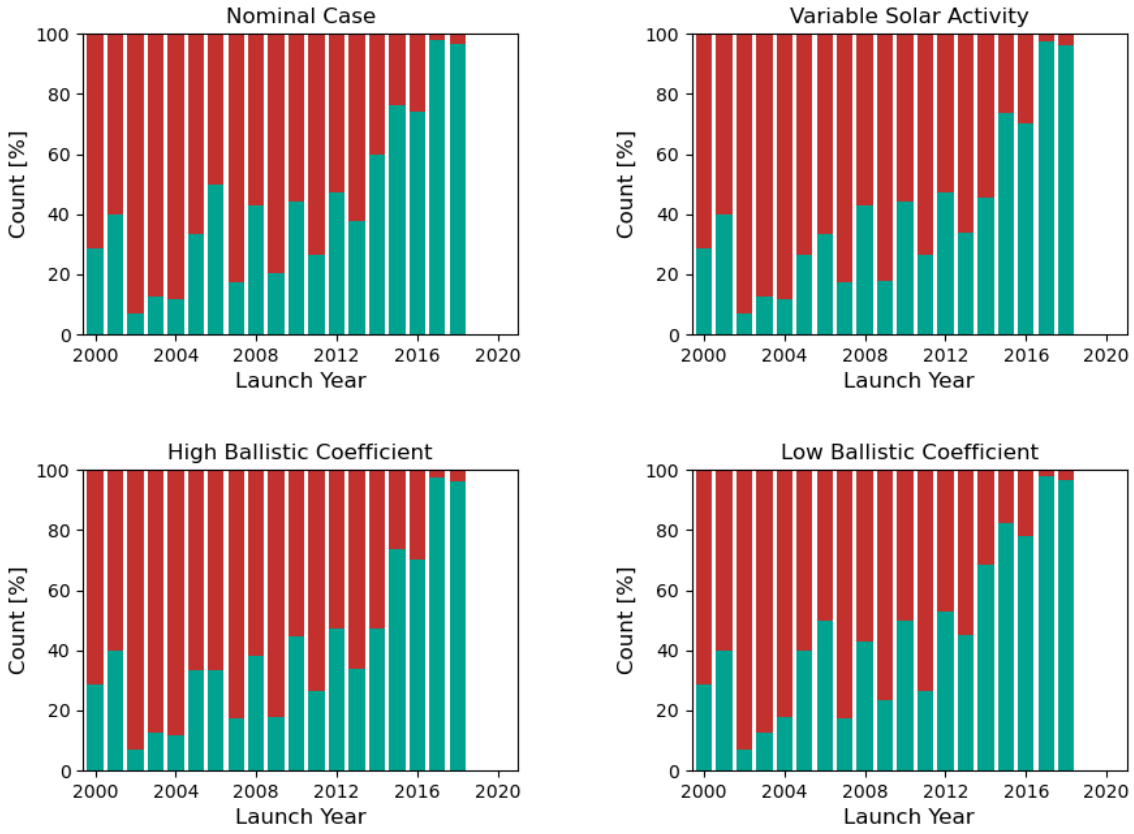

Figure 8.11: Compliance of satellites in Sun-synchronous orbit with the 25-year lifetime rule for different settings.

In general, the sensitivity runs show a low overall impact on the compliance. Giving confidence that although slight model and assumption errors might change the outcome for individual satellites, on a population basis the differences are very small. It was seen that this is mainly a result of the low number of satellites that are close to the 25-year lifetime boundary.

8.3. Comparison

To determine how the compliance results relate to those found in other research, a brief comparison will be done. Use will be made of the studies that were mentioned in Chapter 4. The first was the compliance study of Italian satellites by Anselmo and Pardini [3] where 25 LEO satellites were investigated. It was found that overall 64% of the satellites were compliant rising to 75% for the satellites launched after 2004. Although their study size is quite small, it observes similar compliance rates and the increasing trend.

The study done by CNES found for LEO satellites launched between 2000 and 2013 a compliance rate of 59% but observed no meaningful trend in global compliancy with the 25-year lifetime rule [42]. It also concluded that most satellites rely on their natural decay to meet this rule. Comparing this to the results found in this study for this period, here a lower compliance was observed, between 15 and 50% as was shown in Figure 8.2. However, just like Morand et al. [42] no trends were visible in this timeframe, starting only from 2014 onwards.

Similar results were also obtained in the ESA study [21] reiterating the importance naturally compliant orbits play in overall satellite compliance. Another study, regarding the protected region, was done by Minguijon Pallas and Noomen [45] to analyse the compliance of geostationary satellites, the result of this is shown in Figure 8.12. It should be noted that in the figure the y-scale goes up to 70 percent and that the compliance ratio here is defined as a percentage of the total satellites launched that year, including those who are still operational giving a distorted view of recent years as most satellites will still be operational. This operational status per launch year is given in Figure 8.13.

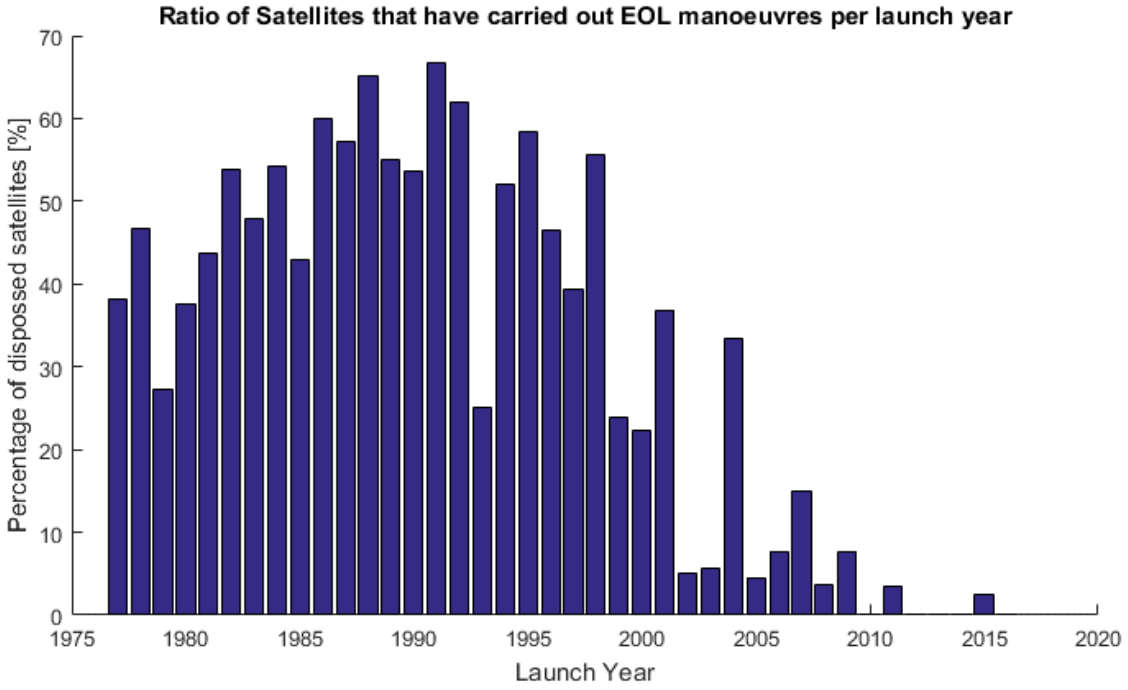

Figure 8.12: Compliance of GEO satellites [45].

As can be seen, since the GEO study was performed in 2018, and with an average lifetime of about 15 years, many satellites launched after 2000 were still operational and no real conclusions can be drawn regarding the compliance rate for launch years after that.

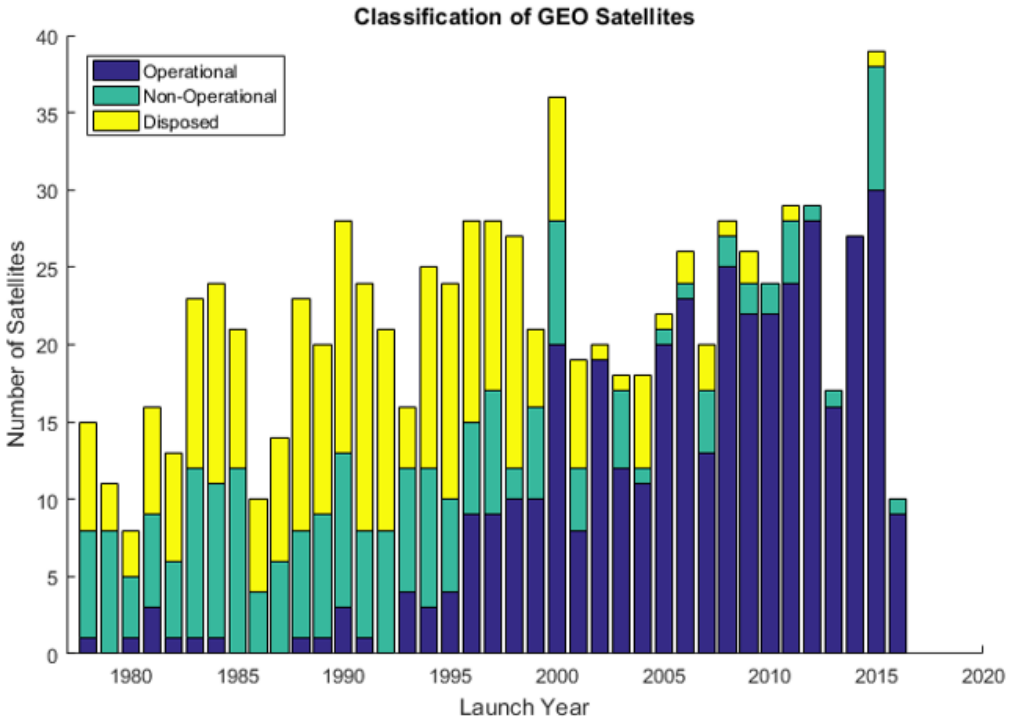

Figure 8.13: Classification of GEO satellites [45].

From this it was concluded that an increasing compliance trend was observed. Starting with spacecraft launched in the late 1970s, with a compliance less than 40% to almost 70% for satellites launched in the early 1990s [45]. Concluding that if this trend continues satellites launched after 2010 will have a near 100% compliance.

In general, it can be seen in these studies of different satellite subsets and regimes that, with slight variations on the exact numbers, they agree with the core findings with the results given in the previous sections. Namely an overall poor compliance in the past, but a significant increasing trend in compliance in the recent years. Furthermore, in LEO most compliant satellites are so due to natural decay and not due to orbit lowering maneuvers. In GEO however, the positive compliance rate trend already started much earlier, starting in the late 1970s compared to mid 2010s for LEO. Furthermore, since the natural decay for a satellite in GEO is so small, they have to rely exclusively on end-of-life maneuvers to remove themselves from the protected region. This capability of maneuvering of every satellite, combined with the used slotting system in GSO, may be the reason of this multi-decade lead in compliance. Weeden and Shortt [61] concluded that such a slotting system system could also provide benefits in long-term operating safety and sustainability for SSO, but due to the inherit mechanics in this regime this is much more complicated than the GSO slots.

8.4. Discussion

Uncertainties and assumptions are inherent to the task of compliance determination. It exists in all aspects of it, from operational status determination to lifetime propagation. During the maneuver detection for example, it was found that sometimes the maneuvers are of such a low magnitude that they almost become indistinguishable from the noise in the data. The effects of the Solar activity was seen as an increase in noise in the TLE data and with that some false positive detected maneuvers when determining the operational status of a spacecraft. Furthermore, with no detected maneuvers, and absence of a reliable public registry one has to rely on statistical models to determine the duration of the operational phase of the mission. Finally, the lifetime propagation models are based on assumptions of the ballistic coefficient and atmospheric density experienced by the spacecraft.

In each of their respective chapters these and more assumptions and uncertainties have been discussed. Where possible they were investigated and mitigated as best as possible. For others, such as during the parameter tuning of the maneuver detection, or the sensitivity study done their effects on the outcome have been researched.

All of this with the purpose to increase the validity and confidence in the results and conclusions of this research. However, it should be re-iterated that this is a current best-effort estimate. Complete certainty in compliance could otherwise only be achieved if the exact end of mission date is known and after that 25 years have passed or the satellite has decayed. This is best exemplified by the result that currently between ≈ 230 and ≈ 510 satellites in SSO are still operational with orbital control capabilities, 230 of those have confirmed maneuvers in the past two years and 280 were launched in the recent two years. These satellites are added back to the results in Figure 8.14 as *Not Determined*.

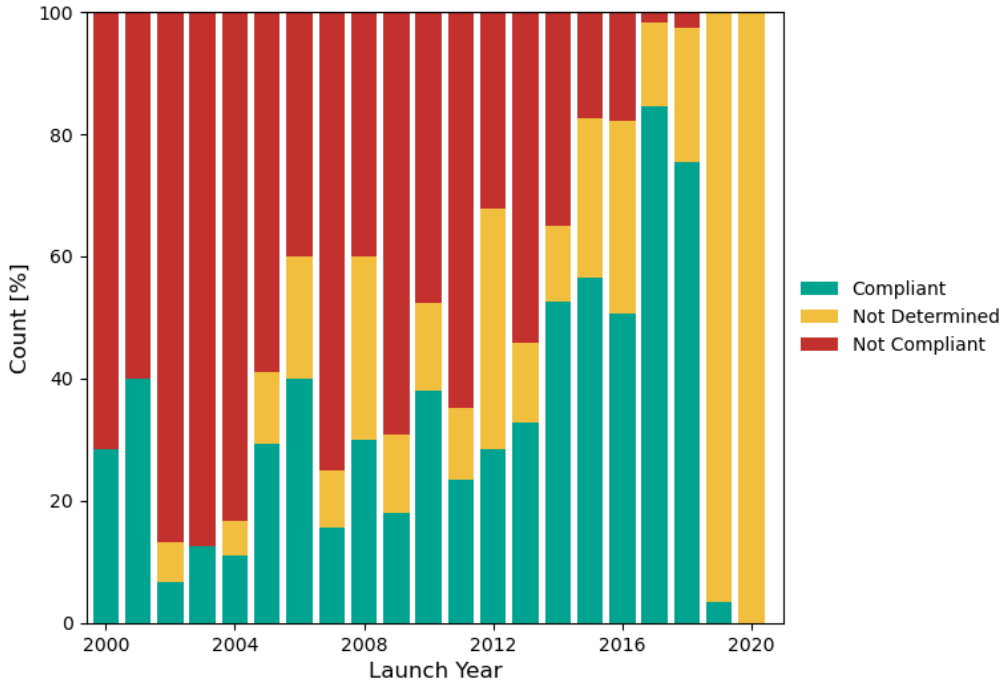

Figure 8.14: Compliance rate of satellites in Sun-synchronous orbit with the 25-year lifetime rule including those with orbital control capabilities and still operational as *Not Determined*.

These results can be interpreted as the still possible variation for the compliance rate of satellites launched in that year. As time goes on and more satellites become non-operational, their compliance can be determined. Thereby shrinking this margin until every satellite in a launch year has its compliance determined. It also shows why 2019 and 2020 are left out of the result, as for these years either the operational status could not yet be fully determined or the satellites are operational and maneuvering. Note the small number of satellites in 2019 that have been determined as compliant because these satellites have already decayed. As they in no way represent the entire population of spacecraft launched that year, they were left out of the results.

Although the satellites that have yet to be classified still represent a significant margin of about 20% of the satellites for the recent years, the overall trend will remain the same regardless of their outcome. Moreover, when looking back at the result obtained when grouping compliance of satellites with and without orbital control capabilities, Figure 8.6, it can be seen that for satellites with this capability the compliance is slightly lower than for satellites without it. Although the difference is small, this might indicate that the overall compliance might become slightly lower when everything is classified. However, it was also observed that the compliance of satellites is drastically increasing over the past years. This changing mindset may indicate that more satellite operators will implement an altitude-lowering maneuver to ensure compliance.

9

Conclusions and Recommendations

This study was done to get an overview of the current state of compliance of Sun-synchronous satellites with international space debris guidelines. The methods used and results obtained during this will briefly be reiterated and conclusions will be drawn regarding the key insights they provided in Section 9.1. Based on these insights, and overall obtained experience during this research work, recommendations will be given in Section 9.2. This will include both possible improvements on the implemented methods and general recommendations regarding the determination of compliance with the space debris guidelines.

9.1. Conclusions

This section will discuss the conclusions from the completed research by topic. For a complete implementation or further information the reader is referred back to the respective individual chapters.

Space Debris

In Chapter 2 a strong overall international consensus on the importance and urgency of space debris regulations was seen. With the most direct and concrete guideline the 25-year lifetime rule. This rule is endorsed by multiple international space agencies and national guidelines, as well as becoming an industry standard as introduced by the International Organization for Standardization. These guidelines protect two regions of space near Earth, the first one is low Earth orbit (LEO) and the second is the Geostationary region (GEO).

The need for these regulations was fortified by the results from the inventory of satellite analysis. This showed that the number of objects launched to LEO has seen a huge increase in the past years, mainly due to commercial launches. The growing launches by smaller companies or agencies, made possible due to the increasing accessibility to space, together with the upcoming satellite constellations, will lead to the number of satellites in the near future to increase tremendously. Very noticeable were the different clusters of satellites in LEO, when grouped by altitude and inclination. Here especially the Sun-synchronous orbit was seen to be a very popular choice, with the large increase in launched satellites to SSO primarily driven by satellites with a mass below 10 kg.

Investigating the orbital mechanics involved in this orbit it was concluded that the aerodynamic drag would be the major perturbing force although, partly due to resonance effects, the irregular gravitational field of the Earth, Solar radiation pressure and third-body gravity from the Sun and the Moon should also be taken into account. This aerodynamic drag would also be one of the main sources of uncertainty during the lifetime propagation as it is heavily influenced by Solar activity which in turn is difficult to predict.

Operational Status Determination

The determination of compliance consists of two key components. The first being the determination of the operational status of the satellite and the second being the remaining lifetime propagation. Since there is no public registry of operational status, the determination of this was done according to a maneuver detection algorithm implemented in TUDAT.

Using long-term TLE data the implemented algorithm was able to detect maneuvers after a linear slope correction, threshold generation and taking harmonics in the data into account. Using two satellite development cases, Envisat and SARAL, it was found that for individual satellites even very small maneuvers, in the

order of 10 m, could be detected. However, for a larger group of satellites it proved to be more difficult and required some parameter tuning. This was done by comparing its performance to human verified maneuver occurrences and other algorithms. For this detection algorithm, it was chosen to favour false negatives, where occurred maneuvers are not detected, over false positives, where maneuvers are falsely identified that in reality did not actually occur. This was done as for each satellite a long timeframe would have to be analysed. Thereby increasing the chance that a maneuver is being falsely detected somewhere, and a spacecraft is wrongly designated to be still maneuvering while in reality it has long ago stopped doing so. This choice was strengthened further by the fact that large maneuvers proved to be very easy to detect and smaller maneuvers were seen to be done with a high frequency.

Even though this approach was taken, some false positives were still observed during the determination of the operational status. This was correlated with the Solar activity, causing both an increase in noise and sometimes, by a sudden change in slope due to the increased density, a false maneuver detection. However, using a maximum allowed interval between maneuvers of two years these false positives were filtered.

Analysis of the design lifetimes of satellites for different mass categories was used to determine the operational status of satellites without orbital control capabilities. From this it was seen that large differences between these categories exist. The spread within a specific category was quite small for the smaller satellites but was increasing with increasing mass. Eventually the following lifetimes were selected as being representative for their category: 2 years for satellites with a mass below 10 kg, 4 years for $10 \leq m < 100$ kg, 9 years for $100 \leq m < 1000$ kg and finally 15 years for all heavier satellites.

Lifetime Propagation

Due to the large number of objects, about 1500, combined with the long required propagation time, it was determined that semi-analytic propagation would be the most suitable method. It is able to perform a 100 year propagation within one minute of computation time while retaining good accuracy.

From the resulting remaining orbital lifetimes the satellites could be split in three groups. The first were the satellites that were estimated to decay within 10 years. For these satellites the confidence is very high that even including worse-case modelling assumptions they will have decayed within the required 25 years. The other group is on the other end of the spectrum with a remaining orbital lifetime larger than 75 years. It is very unlikely that this group, even with substantial solar activity prediction errors, will in reality decay within 25 years. A third, smaller group exists with satellites that are close to the 25-year boundary. For this group of course the resulting compliance may change if for example the underlying assumptions regarding their ballistic coefficient are wrong or predictions in Solar activity fail to materialize. This group was found to be sufficiently small to have confidence in the found results.

Compliance

Combining the operational status with the lifetime propagation resulted in an overall compliance of 59.2%. By looking at the evolution of this compliance over time, it was seen that in recent years this has increased from 30-40% in the 2000s and early 2010s to around 95% in 2017 and 2018.

Furthermore, there is a large difference between the different mass categories. Where 86% of the satellites with a mass less than 10 kg are compliant, the other mass categories only reach a compliance of around 35%. It was also observed that satellites with orbital control capability had a compliance rate of 55.7% against 60.2% for those without. This can be explained by the previous observation: satellites below 10 kg in generally do not have orbital control capabilities. Looking at the semi-major axis it was seen that in general these smaller satellites are launched in a lower initial orbit. From this these observations it can be concluded that the overall increase in compliance is primarily a result of choosing an orbit with a low enough altitude to have sufficient natural decay, and less due to operators choosing to perform a de-orbit or orbit lowering maneuver.

9.2. Recommendations

During the development and implementation of the maneuver detection algorithm it was found that due to the difference in spacecraft and orbital parameters the same algorithm settings would perform with different accuracy for different spacecraft. To further develop this algorithm it would be advised to make these settings more dynamic, by for instance investigating the effect of mass, size and semi-major axis on the maneuver detection accuracy. To further reduce the generation of false positives one could incorporate the Solar activity in the threshold generation, tolerating more noisy data while this activity is high. Further research is also needed to improve the operational determination of spacecraft without orbital control capabilities. The data used here was based on design lifetimes but made no categorical distinctions apart from spacecraft mass. It is likely however, that this could be improved by looking at the differences in operational lifetimes of satellites according to their purpose, launch date or possibility of orbital control.

The lifetime propagation results could be improved by making use of a more accurate method of determining the ballistic coefficient as the method chosen was due to the limitation in scope of the research. A more sophisticated model could for instance use a large period free of maneuvers in the TLE data to fit a coefficient value. The semi-analytic propagation technique proved to be a very useful tool in the research. An implementation would make a very valuable addition to the TU Delft Astrodynamics Toolbox and could together with the maneuver detection be the start of a space debris focused library.

To better understand the behaviour of satellite operators, future studies could also investigate the use of de-orbit or orbital lowering maneuvers and its evolution over time. It was also found that compliance in GEO satellites has been higher for a significant longer duration than in LEO. Although some suggestions were given as to why, such as the slotting system and the orbital control capabilities, further research would be insightful to determine the cause. Finally, this study was focused on the actual satellites themselves, the launch payloads. However, with these launches also come other objects such as spent rocket bodies. To complete the picture of space debris in SSO these objects have to be analysed as well.

Looking at the bigger picture, the above-mentioned recommendations are all mainly to improve the approach that was taken in this study. However, the ultimate goal in the study was to obtain more insight in satellite operator compliance with the guidelines. It was found that to determine this quite some hurdles have to be taken, this could be made simpler and more transparent by introducing something of a public registry of operational status. Where a satellite would be asked, to register its operational status or done automatically by using received radio signals not unlike the satNOGS database. Finally, the foundation of the space debris guidelines were established already quite a while ago, before concrete launches of large constellations were well on their way. It was seen that in recent years the number of launched satellites is growing very fast. Future studies could address if the guidelines as they are currently are sufficient to protect the long-term sustainable use of space.

Bibliography

[1] F. Alby, D. Alwes, L. Anselmo, H. Baccini, C. Bonnal, R. Crowther, W. Flury, R. Jehn, H. Klinkrad, C. Portelli, et al. The European space debris safety and mitigation standard. *Advances in Space Research*, 34(5): 1260–1263, 2004.

[2] L. Anselmo, C. Portelli, R. Tremayne-Smith, F. Alby, H. Baccini, C. Bonnal, D. Alwes, W. Flury, R. Jehn, and H. Klinkrad. European code of conduct for space debris mitigation, 2004.

[3] Luciano Anselmo and Carmen Pardini. Compliance of the Italian satellites in low Earth orbit with the end-of-life disposal guidelines for space debris mitigation and ranking of their long-term criticality for the environment. *Acta Astronautica*, 114:93–100, 2015.

[4] Thomas Dale Bess. Mass distribution of orbiting man-made space debris. Technical Report NASA TN D-8108, Langley Research Center, 1975.

[5] Ales Bezděk and David Vokrouhlickỳ. Semianalytic theory of motion for close-earth spherical satellites including drag and gravitational perturbations. *Planetary and Space Science*, 52(14):1233–1249, 2004.

[6] Christophe Bonnal. A brief historical overview of space debris mitigation rules. *Clean Space Industrial Days. ESTEC, The Netherlands*, 2016.

[7] Christophe Bonnal. Space debris mitigation & remediation: a general update. volume JAXA-SP-18-011, pages 157–171. Japan Aerospace Exploration Agency, 2019.

[8] D.R. Brooks, T.D. Bess, and G.G. Gibson. Predicting the probability that Earth-orbiting spacecraft will collide with man-made objects in space. In *International Astronautical Congress*, number A74-34, 1974.

[9] Lei Chen, Xian-Zong Bai, Yan-Gang Liang, and Ke-Bo Li. Orbital prediction error propagation of space objects. In *Orbital Data Applications for Space Objects*, pages 23–75. Springer, 2017.

[10] Eun-Jung Choi, Sungki Cho, Deok-Jin Lee, Siwoo Kim, and Jung Hyun Jo. A study on re-entry predictions of uncontrolled space objects for space situational awareness. *Journal of Astronomy and Space Sciences*, 34(4):289–302, 2017.

[11] CNES. Standards collection, method and procedure space debris – safety requirements, RNC-CNES-Q-40-512, 1999.

[12] CNES. Stela user manual version 3.3. Technical report, CNES, 2019.

[13] A.A.L.C. Cojuangco. *Orbital Lifetime Analyses of Pico-and Nano-Satellites*. PhD thesis, University of Florida, 2007.

[14] COPUOS. *Compendium of space debris mitigation standards adopted by states and international organizations*. Number A/AC.105/C.2/2019/CRP. UNOOSA, 2018.

[15] Howard D. Curtis. *Orbital mechanics for engineering students*. Butterworth-Heinemann, 2013.

[16] Donald A. Danielson, Christopher Patrick Sagovac, Beny Neta, and Leo W. Early. Semianalytic satellite theory. Technical report, Naval Postgraduate School, 1995.

[17] Luigi de Luca, Franco Bernelli Zazzera, Filippo Maggi, Pietro Tadini, C. Pardini, L. Anselmo, M. Grassi, D. Pavarin, A. Francesconi, F. Branz, et al. Active space debris removal by hybrid engine module. In *63rd International Astronautical Congress (IAC)*, pages 2660–2673. Curran Associates, 2012.

[18] D. Dirkx, L.L.A. Vermeersen, R. Noomen, and P.N.A.M. Visser. Phobos laser ranging: Numerical geodesy experiments for Martian system science. *Planetary and Space Science*, 99:84–102, 2014.

[19] DLR. Product assurance and safety requirements for DLR space projects, RF-0S-001 Issue 7, 2012.

[20] Eelco Doornbos, Matthias Förster, Bent Fritsche, Tom van Helleputte, Jose van den IJssel, Georg Koppenwallner, Hermann Lühr, David Rees, and Pieter Visser. Air density models derived from multi-satellite drag observations. Technical report, Delft Institute of Earth Observation and Space Systems, 2009.

[21] ESA Space Debris Office. ESA's Annual Space Environment Report. GEN-DB-LOG-00288-OPS-SD, 2020.

[22] European Space Agency. ESA declares end of mission for Envisat. URL `http://www.esa.int/Applications/Observing_the_Earth/Envisat/ESA_declares_end_of_mission_for_Envisat`. Accessed on: 2020-10-12.

[23] European Space Agency. System safety requirements for ESA space systems. *Inter-Agency Space Debris Coordination Committee*, 2002.

[24] T. Flohrer, S. Lemmens, B. Bastida Virgili, H. Krag, H. Klinkrad, E. Parrilla, N. Sanchez, J. Oliveira, and F. Pina. Discos-current status and future developments. In *Proceedings of the 6th European Conference on Space Debris*, pages 22–25, 2013.

[25] T. Grimwood. The union of concerned scientists satellite database, 2020. URL `http://https://www.ucsusa.org/resources/satellite-database`. Accessed on: 2021-01-01.

[26] R. Hoogendoorn, E. Mooij, and J. Geul. Uncertainty propagation for statistical impact prediction of space debris. *Advances in Space Research*, 61(1):167–181, 2018.

[27] Felix R. Hoots, Ronald L. Roehrich, and T.S. Kelso. Spacetrack report no. 3. *Colorado Springs CO: Air Force Aerospace Defence Command*, pages 1–3, 1980.

[28] IADC Steering Group and Working Group 4. Space debris mitigation guidelines. *Inter-Agency Space Debris Coordination Committee*, 2002.

[29] ISO 27852:2016(E). Space systems - Estimation of orbit lifetime. Standard, International Organization for Standardization, Geneva, CH, 2016.

[30] N.L. Johnson. Developments in space debris mitigation policy and practices. *Proceedings of the Institution of Mechanical Engineers, Part G: Journal of Aerospace Engineering*, 221(6):907–909, 2007.

[31] A. Kato, B. Lazare, D. Oltrogge, and P.H. Stokes. Standardization by ISO to ensure the sustainability of space activities. In *Proceedings of the Sixth European Conference on Space Debris, ESOC, Darmstadt, Germany*, pages 22–25, 2013.

[32] Donald J. Kessler and Burton G. Cour-Palais. Collision frequency of artificial satellites: The creation of a debris belt. *Journal of Geophysical Research: Space Physics*, 83(A6):2637–2646, 1978.

[33] Desmond King-Hele. *Theory of satellite orbits in an atmosphere*. Butterworths, 1964.

[34] Erik Kulu. Nanosats database, 2021. URL `http://https://https://www.nanosats.eu/`. Accessed on: 2021-01-01.

[35] C. Le Fèvre, H. Fraysse, V. Morand, A. Lamy, C. Cazaux, P. Mercier, C. Dental, F. Deleflie, and D.A. Handschuh. Compliance of disposal orbits with the French space operations act: the good practices and the STELA tool. *Acta Astronautica*, 94(1):234–245, 2014.

[36] Clémence Le Fèvre, Hubert Fraysse, Vincent Morand, Florent Deleflie, Sébastien Wailliez, Alain Lamy, Thierry Martin, and Etienne Perot. Long term orbit propagation techniques developed in the frame of the French Space Act. In *22nd International Symposium on Space Flight Dynamics*, volume 28, 2011.

[37] Stijn Lemmens and Holger Krag. Two-line-elements-based maneuver detection methods for satellites in low Earth orbit. *Journal of Guidance, Control, and Dynamics*, 37(3):860–868, 2014.

[38] Bin Li, Jizhang Sang, and Jinsheng Ning. A multiscaling-based semi-analytic orbit propagation method for the catalogue maintenance of space debris. *Journal of Spatial Science*, 65(1):123–145, 2020.

[39] Nicholas R. Lomb. Least-squares frequency analysis of unequally spaced data. *Astrophysics and space science*, 39(2):447–462, 1976.

[40] Anil K. Maini and Varsha Agrawal. *Satellite technology: principles and applications*. John Wiley & Sons, 2011.

[41] JEAN Meeus. Tables of sun and moon. *Kesselberg Sterrenwacht, Kessel-Lo*, 1962.

[42] Vincent Morand, Juan-Carlos Dolado-Perez, Thomas Philippe, and David-Alexis Handschuh. Mitigation rules compliance in low Earth orbit. *Journal of Space Safety Engineering*, 1(2):84–92, 2014.

[43] NASA. NASA safety standard: Guidelines and assessment procedures for limiting orbital debris. Technical Report 1740.14, NASA, 1995.

[44] NASDA. NASDA space debris mitigation standards, NASDA-STD-18, 1996.

[45] P. Pallas and R. Noomen. GEO satellites end-of-life disposal - compliance status. In *Proceedings of the International Astronautical Congress, IAC*. International Astronautical Federation (IAF), 2018.

[46] Peter J. Rousseeuw and Christophe Croux. Explicit scale estimators with high breakdown point. *L1-Statistical analysis and related methods*, 1:77–92, 1992.

[47] Russian Federation. General requirements to space assets on mitigation of near-Earth space pollution with man made space debris, GOST-P-52925-2008, 2008.

[48] Jizhang Sang and James C. Bennett. Achievable debris orbit prediction accuracy using laser ranging data from a single station. *Advances in Space Research*, 54(1):119 – 124, 2014.

[49] Jeffrey D. Scargle. Studies in astronomical time series analysis. ii-statistical aspects of spectral analysis of unevenly spaced data. *The Astrophysical Journal*, 263:835–853, 1982.

[50] Pranab Kumar Sen. Estimates of the regression coefficient based on Kendall's tau. *Journal of the American statistical association*, 63(324):1379–1389, 1968.

[51] Andrew F. Siegel. Robust regression using repeated medians. *Biometrika*, 69(1):242–244, 1982.

[52] Space-Track. Basic description of the two line element (TLE) format. https://www.space-track.org/documentation. Accessed on: 2020-03-26.

[53] Henri Theil. A rank-invariant method of linear and polynomial regression analysis, 3; confidence regions for the parameters of polynomial regression equations. *Indagationes Mathematicae*, 1(2):467–482, 1950.

[54] R.H.D. Townsend. Fast calculation of the lomb-scargle periodogram using graphics processing units. *The Astrophysical Journal Supplement Series*, 191(2):247, 2010.

[55] United Nations. International cooperation in the peaceful uses of outer space, resolution a/res/62/217 adopted by the general assembly. *Proceedings of the 62nd Session, Agenda Item 31*, 2007.

[56] United Nations. General Assembly. Committee on the Peaceful Uses of Outer Space. *Report of the Committee on the Peaceful Uses of Outer Space*. Number (A/62/20). United Nations Publications, 2007.

[57] David A. Vallado. *Fundamentals of astrodynamics and applications*, volume 12. Springer Science & Business Media, 2001.

[58] David A. Vallado, Paul Crawford, Ricahrd Hujsak, and T.S. Kelso. Revisiting spacetrack report# 3. In *AIAA/AAS Astrodynamics Specialist Conference and Exhibit*, page 6753, 2006.

[59] Vivek Vittaldev, Erwin Mooij, and Marc Naeije. Unified state model theory and application in astrodynamics. *Celestial Mechanics and Dynamical Astronomy*, 112, 03 2012.

[60] Karel F. Wakker. *Fundamentals of astrodynamics*. TU Delft Library, 2015.

[61] Brian Weeden and Kevin Shortt. Development of an architecture of sun-synchronous orbital slots to minimize conjunctions. In *Advanced Maui Optical and Space Surveillance Technologies Conference*, page E72, 2008.

[62] James R. Wertz. Orbit & constellation design & management, second printing ed. El Segundo, 2009.